

Air Force Institute of Technology

AFIT Scholar

Theses and Dissertations

Student Graduate Works

3-1996

Structural Damage Identification from Limited Measurement Data

Richard G. Cobb

Air Force Institute of Technology

Follow this and additional works at: <https://scholar.afit.edu/etd>



Part of the [Aerospace Engineering Commons](#), and the [Structural Materials Commons](#)

Recommended Citation

Cobb, Richard G., "Structural Damage Identification from Limited Measurement Data" (1996). *Theses and Dissertations*. 6073.

<https://scholar.afit.edu/etd/6073>

This Dissertation is brought to you for free and open access by the Student Graduate Works at AFIT Scholar. It has been accepted for inclusion in Theses and Dissertations by an authorized administrator of AFIT Scholar. For more information, please contact AFIT.ENWL.Repository@us.af.mil.

AFIT/DS/ENY/96-3

STRUCTURAL DAMAGE IDENTIFICATION FROM LIMITED MEASUREMENT DATA

DISSERTATION

Richard G. Cobb
Captain, USAF

AFIT/DS/ENY/96-3

Approved for public release; distribution unlimited

AFIT/DS/ENY/96-3

STRUCTURAL DAMAGE IDENTIFICATION FROM LIMITED MEASUREMENT
DATA

DISSERTATION

Presented to the Faculty of the School of Engineering
of the Air Force Institute of Technology
Air Education and Training Command
In Partial Fulfillment of the
Requirements for the Degree of
Doctor of Philosophy

Richard G. Cobb, B.S., M.S.
Captain, USAF

Sponsored by the Phillips Laboratory, KAFB, NM.

March, 1996

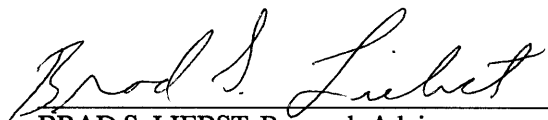
Approved for public release; distribution unlimited

STRUCTURAL DAMAGE IDENTIFICATION FROM LIMITED MEASUREMENT
DATA

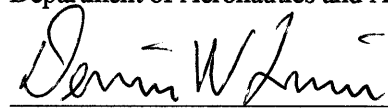
Richard G. Cobb, B.S., M.S.

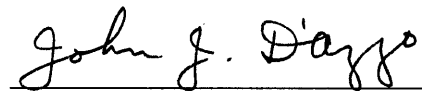
Captain, USAF

Approved:

 22 Feb 96
BRAD S. LIEBST, Research Advisor
Associate Professor of Aerospace Engineering
Department of Aeronautics and Astronautics

 22 Feb 96
ROBERT A. CANFIELD, Committee Member
Major, USAF
Assistant Professor of Aerospace Engineering
Department of Aeronautics and Astronautics

 22 Feb 96
DENNIS W. QUINN, Committee Member
Professor of Mathematics
Department of Mathematics and Statistics

 22 Feb 96
JOHN J. D'AZZO, Dean's Representative
Professor of Electrical Engineering
Department of Electrical and Computer Engineering

 27 Feb 97
Robert A. Calico, Jr.
Dean, Graduate School of Engineering

Acknowledgements

It is difficult to put down on a single page my appreciation of all those who have influenced my life and contributed to the success of my research over the last three years. However, I'd like to attempt to thank those individuals whose contributions to the research were indispensable.

First and foremost I'd like to thank my research advisor Dr. Brad Liebster, to whom I am most indebted. Dr. Liebster was always willing to discuss problems, offer suggestions, and remain focused on the task. He became my mentor and my friend, and challenged me throughout the research both academically and on the racquetball court. His enthusiasm for the research was contagious, which led to many late nights during the experimental work. It is rare to work with an advisor who is not afraid to be seen working in the laboratory, for which I am most grateful.

I would like to acknowledge the members of my research committee, which provided both breadth and depth of expertise and enhanced the research work. Major Robert Canfield's expertise with ASTROS was crucial. Without his suggestions and guidance, the use of ASTROS-ID would not have been possible. I'd also like to thank Dr. Dennis Quinn and my Dean's representative, Dr. John D'Azzo for their technical review of the manuscript. The committee's insightful comments and suggestions helped me to better express my ideas and results, which significantly improved the dissertation.

I'd also like to thank Mr. Jay Anderson and Mr. Andy Pitts for their help during the experimental portion of the research. They provided and maintained all the equipment and were always willing to fix any problems without hesitation. Additionally, I'd like to thank Mr. Robert Gordon from Wright Laboratories who donated the experimental truss and measurement equipment. I'm also indebted to Dr. Tom Kashangaki who provided the data on the NASA truss.

Thanks especially to my friends, Major Jim Greer and Captain Jim Solti. They kept the research fun by providing a much needed diversion during lunch.

Most of all, I'd like to thank my wife Lisa and my sons Greg and Ryan. Even before I began the research, they had no doubt I would be successful. They gave me the strength and desire to finish the task. I love them all dearly.

Richard G. Cobb

Table of Contents

	Page
Acknowledgements	iii
List of Figures	viii
List of Tables	xi
List of Symbols	xii
List of Acronymns	xv
Abstract	xvi
I. Introduction	1-1
II. Background	2-1
2.1 Motivation	2-1
2.2 System Identification Techniques	2-1
2.2.1 Time Domain	2-3
2.2.2 Frequency Domain	2-5
2.3 Model Tuning Techniques	2-7
2.3.1 Sensitivity Based	2-8
2.3.2 Orthogonality Based	2-8
2.3.3 Connectivity Based	2-11
2.3.4 Residual Force Based	2-12
2.3.5 Assigned Eigenstructure Based	2-14
2.3.6 Realization Theory Based	2-18
2.4 Summary	2-18

	Page
III. Damage Identification Methodology	3-1
3.1 Identification of Modal Parameters from Measured Data	3-2
3.2 Model Tuning	3-3
3.3 Damage Identification Using Assigned Partial Eigenstructure	3-3
3.4 Sensor Prioritization and Damage Localization	3-4
3.5 Summary	3-4
IV. Identification of Modal Parameters from Measured Data	4-1
4.1 Overview	4-1
4.2 Obtaining Measured Data	4-1
4.3 Eigensystem Realization Algorithm	4-2
4.4 Software Implementation	4-4
4.5 An Analytical Example	4-5
4.6 Summary	4-8
V. Model Tuning Using ASTROS-ID	5-1
5.1 Overview	5-1
5.2 Theory	5-2
5.2.1 Eigenvalue Sensitivity	5-2
5.2.2 Eigenvector Sensitivity and Normalization	5-3
5.2.3 Mode Switch Detection	5-6
5.3 Software Implementation	5-6
5.4 Selection of Tuning Parameters	5-8
5.5 An Analytical Example	5-8
5.6 Summary	5-10
VI. Damage Identification Using Assigned Partial Eigenstructure	6-1
6.1 Overview	6-1
6.2 Theory	6-1

	Page
6.3 Software Implementation	6-9
6.4 An Analytical Example	6-12
6.5 Summary	6-16
VII. Sensor Prioritization and Damage Localization	7-1
7.1 Overview	7-1
7.2 Theory	7-2
7.2.1 Sensor Location Prioritization	7-5
7.2.2 Damage Localization	7-7
7.3 Software Implementation	7-8
7.4 An Analytical Example	7-9
7.5 Summary	7-12
VIII. Experimental Validation of Theory	8-1
8.1 Test Objective	8-1
8.2 NASA Test Data Analysis	8-1
8.2.1 Hardware	8-1
8.2.2 Model Tuning	8-1
8.2.3 Sensor Prioritization and Damage Localization Analysis	8-6
8.2.4 Damage Identification Results	8-7
8.3 Flexible Truss Experiment	8-10
8.3.1 Hardware	8-10
8.3.2 Model Tuning	8-14
8.3.3 Damage Localization Analysis	8-22
8.3.4 Damage Identification Results	8-23
8.4 Summary	8-26
IX. Conclusions and Recommendations	9-1
9.1 Research Conclusions	9-1
9.2 Recommendations for Additional Research	9-2

	Page
Appendix A. ASTROS-ID Software Modules	A-1
A.1 Modified Software Modules	A-1
A.2 New Software Modules	A-2
Appendix B. APEWARE: Damage Identification Integrated Software	B-1
B.1 System Identification	B-5
B.2 Model Tuning	B-7
B.3 Sensitivity Analysis	B-10
B.4 Damage Identification	B-15
B.5 Model File Requirements	B-15
B.5.1 Utilities	B-17
Bibliography	BIB-1
Vita	VITA-1

List of Figures

Figure	Page
1.1. On-orbit configuration of International Space Station Alpha.	1-2
1.2. Solar array sub-assembly from International Space Station Alpha.	1-2
4.1. Sequence of events for identification of modal parameters.	4-6
4.2. 41-element free-free planar truss example showing degree-of-freedom numbering.	4-6
4.3. 41-element free-free planar truss example showing element numbering.	4-6
4.4. Effect of sample size and measurement noise on the ability to extract eigendata using ERA.	4-9
5.1. ASTROS-ID decision flow.	5-7
6.1. Example two degree-of-freedom system.	6-3
6.2. Assigned partial eigenstructure decision flow.	6-9
6.3. 41-element free-free planar truss showing element and degree-of-freedom numbering.	6-12
6.4. Change in frequencies and shapes due to structural damage for the first three flexible modes.	6-14
6.5. Change in frequencies and shapes due to structural damage for the fourth and fifth flexible modes.	6-15
7.1. Damage localization decision flow.	7-10
7.2. 41-element free-free truss showing degree-of-freedom and element numbering. . .	7-10
8.1. Joint construction for the NASA 8-bay truss experiment.	8-2
8.2. Measured frequency response function for the NASA truss.	8-3
8.3. Damage configurations for the NASA truss, cases A, B, and C.	8-3
8.4. Damage configurations for the NASA truss, cases D, E, and F.	8-4
8.5. Damage configurations for the NASA truss, cases G, H, and I.	8-4
8.6. Prioritized sensor locations for the NASA truss.	8-7

Figure	Page
8.7. Six-Meter Flexible Truss Experiment, showing initial sensor locations.	8-12
8.8. Joint construction for the FTE.	8-12
8.9. Linear actuators for the FTE.	8-13
8.10. Low frequency mode shapes for the FTE.	8-14
8.11. Comparison of bending and torsional excitation on the FTE.	8-16
8.12. Prioritized sensor locations on the FTE.	8-17
8.13. Analytical and measured mode shapes before de-coupling, Case 2.	8-19
8.14. Analytical and measured mode shapes after de-coupling, Case 2.	8-19
8.15. Comparison of initial analytical model and measured frequency response.	8-20
8.16. Comparison of the tuned analytical model and measured frequency response.	8-22
8.17. APE identified damage regions on the FTE.	8-25
8.18. Effect of structural damage on the measured response.	8-26
B.1. Software opening menu.	B-1
B.2. APE control menu.	B-2
B.3. Geometry display screen.	B-3
B.4. Manual input dialogue box.	B-3
B.5. Sample graphical sensor selection window.	B-4
B.6. Sample 3-D view selection control.	B-5
B.7. Tolerance menu.	B-6
B.8. ERA control menu.	B-8
B.9. ERA parameters control panel.	B-8
B.10. ERA help menu dialogue box.	B-9
B.11. Sample frequency response showing measured data and simulated data from an ERA identified model.	B-9
B.12. Control panel to extract measured modes.	B-10
B.13. Mode viewer control panel.	B-11
B.14. Sample display of deformed geometry.	B-11

Figure	Page
B.15. Sample line plot of a partial measured eigenvector corresponding to the sensor points only.	B-12
B.16. Sample line plot of a full eigenvector.	B-12
B.17. Sample sensor location gradient information.	B-13
B.18. Sample sensor location prioritized list.	B-14
B.19. Sample damage localization gradient results.	B-14
B.20. Sample damage localization analysis results.	B-15
B.21. Sample damage identification numerical results.	B-16
B.22. Sample damage identification graphical results.	B-16

List of Tables

Table	Page
4.1. 41-element free-free planar truss eigenvalues.	4-8
5.1. Frequency values for the tuned 41-element free-free planar truss.	5-9
5.2. Design variable values for the tuned 41-element free-free planar truss.	5-10
6.1. Damage identification results on the 41-element free-free planar truss.	6-13
7.1. Damage localization results for a 41-element free-free planar truss.	7-11
7.2. Damage localization for different sensor locations for a 41-element free-free planar truss.	7-11
7.3. Damage localization based on eigenvalue sensitivity using the first 5 flexible modes, for the 41-element free-free planar truss.	7-12
8.1. Measured natural frequencies of NASA’s 8-bay truss.	8-5
8.2. Changes in natural frequencies from damage on the NASA truss.	8-6
8.3. Damage localization results for the NASA 8-bay truss.	8-8
8.4. Element numbering and descriptions for the NASA 8-bay truss.	8-8
8.5. APE identification results on the NASA truss.	8-10
8.6. ASTROS-ID identification results on the NASA truss.	8-11
8.7. Design variable values in the FTE finite element model.	8-21
8.8. Analytical and measured natural frequencies of the FTE.	8-23
8.9. Damage localization results for the FTE.	8-24
8.10. Element numbering and descriptions for the FTE.	8-24
8.11. APE damage identification results on the FTE.	8-25

List of Symbols

To minimize multiple definitions, symbol definitions for the background development in Chapter II are not included. Symbols are listed in order of first appearance.

Symbol	Page
M ··· $n \times n$ mass matrix	3-2
K ··· $n \times n$ stiffness matrix	3-2
x ··· state vector	3-2
$\bar{\lambda}_i$ ··· measured eigenvalue	3-2
$\bar{\phi}_i$ ··· measured partial eigenvector	3-2
ϕ_i ··· partial eigenvector	3-2
Φ_i ··· i^{th} eigenvector from the modal matrix	3-2
C ··· mapping between full and partial eigenvectors	3-2
ϕ ··· partial modal matrix	3-2
J ··· scalar cost function	3-2
λ_i ··· eigenvalue for the i^{th} mode	3-2
ϕ_{ij} ··· j^{th} eigenvector component for the i^{th} mode	3-2
Φ ··· modal matrix	3-2
a_i ··· weighting coefficient for the i^{th} eigenvalue	3-2
b_{ij} ··· weighting coefficient for the j^{th} component of the i^{th} eigenvector	3-2
r ··· number of measured eigenvalues	3-2
s ··· number of measured eigenvector components	3-2
$u(t)$ ··· measured input signal	4-1
$y(t)$ ··· measured output signal	4-1
T ··· sample period of measurements	4-1
$\Psi_{uu}(k)$ ··· discrete auto spectra	4-1
$\Psi_{uy}(k)$ ··· discrete cross spectra	4-1

Symbol	Page
N ··· number of sample points	4-1
N ··· number of sample points	4-1
$U(k)$ ··· discrete Fourier transform of input signal	4-1
$Y(k)$ ··· discrete Fourier transform of output signal	4-1
$\Psi_{uy}(k)$ ··· averaged spectral estimates	4-1
m ··· number of samples in average	4-2
$H_{uy}(k)$ ··· averaged frequency response functions	4-2
$h(i)$ ··· discrete impulse response sequence	4-2
(A, B, C, D) ··· state-space system matrices	4-2
$H(k)$ ··· block Hankel matrix	4-3
n_r ··· number of rows in the block Hankel matrix	4-3
n_c ··· number of columns in the block Hankel matrix	4-3
Δg ··· vector of design variable values	5-2
$\nabla \lambda_i$ ··· eigenvalue gradient vector for the i^{th} mode	5-3
$\nabla^2 \lambda_i$ ··· eigenvalue Hessian matrix for the i^{th} mode	5-3
$\nabla \Phi_i$ ··· eigenvector gradient vector for the i^{th} mode	5-3
$\Phi_{i,j}$ ··· derivative of the i^{th} eigenvector with respect to the j^{th} design variable	5-4
S_i ··· eigenvector normalization matrix for the i^{th} eigenvector	5-5
$V_{i,j}$ ··· particular solution vector for $\Phi_{i,j}$ used in Nelson's method	5-5
O ··· cross orthogonality matrix	5-6
ΔK ··· perturbation in stiffness matrix resulting from structural damage	6-2
B ··· structural influence matrix	6-2
G ··· diagonal matrix containing damage fractions	6-2
p ··· number of structural elements used in construction of B	6-4
A_i ··· cross sectional area of i^{th} element	6-4
E_i ··· elastic modulus of i^{th} element	6-4
L_i ··· length of i^{th} element	6-4

Symbol	Page
g_i ··· damage fraction for i^{th} element	6-4
R_i ··· rotation matrix for i^{th} element	6-4
I_1 ··· inertia properties in the 1 direction	6-4
I_2 ··· inertia properties in the 2 direction	6-4
μ_i ··· Poisson’s ratio for the i^{th} element	6-4
j_i ··· torsional stiffness of i^{th} element	6-4
J_i ··· appended cost function for the i^{th} mode	6-5
$\tilde{P}(\alpha, \beta)$ ··· matrix operator	6-6
N ··· LHS matrix for assigned partial eigenstructure	6-7
D_ϕ ··· eigenvector detectability metric	7-6
S_ϕ ··· eigenvector colinearity metric	7-6
D_λ ··· eigenvalue detectability metric	7-7
S_λ ··· eigenvalue colinearity metric	7-7

List of Acronymns

Acronymn	Page
FEM ··· finite element method	1-3
ERA ··· eigensystem realization algorithm	2-5
MIMO ··· multi-input/multi-output	2-5
ASTROS-ID ··· Automated Structural Optimization System-Identification	3-3
APE ··· assigned partial eigenstructure	3-3
FRF ··· frequency response function	4-2
RMS ··· root mean square	4-7
ASTROS ··· Automated Structural Optimization System	5-1
MAPOL ··· Matrix Analysis Problem Oriented Language	5-6
FTE ··· Flexible Truss Experiment	8-10

Abstract

The research focused on the development of a new method to identify damaged structural elements from a large flexible space structure on-orbit, using limited measured modal data. Limited measured modal data is loosely defined as measured data containing only a few modal frequencies and less than 10% of the total structural degrees-of-freedom. This effort was decomposed into four specific tasks. The first is the identification of partial modal properties from measured data of the nominal space structure. Second, the finite element model must be adjusted to match the measured nominal partial data. The third task is an analysis of the extent to which structural damage can be localized to individual structural elements using the measured data. In conjunction with this task is the determination of where to best place the limited number of sensors on the structure. Lastly, the identification of structural damage must be performed using the limited measured modal data from a damaged space structure.

Identification of the modal parameters was accomplished using the Eigensystem Realization Algorithm, a time domain based method, adopted for use with averaged measured frequency response functions. Model tuning was performed using the Automated Structural Optimization Software package, adapted for model tuning. The method minimizes a cost function based on the mismatch between the measured and analytical eigenstructure. The minimization is solved using the eigenvalue and eigenvector sensitivities at each iteration step. The determination of prioritized sensor locations and damage localization is performed using the eigenvalue and eigenvector sensitivities. Damage identification is performed using a newly developed assigned partial eigenstructure method, which determines required stiffness changes, consistent with the finite element formulation to achieve the measured data.

The theory for each task is presented and illustrated on an analytical example of a 41-element free-free planar truss. Two experimental demonstrations were performed and the results reported. The first was a cantilevered truss modeled with 104 rod elements with a total of 96 degrees-of-freedom. The measured data consisted of the first five flexible modal frequencies, and only eight components of the five corresponding eigenvectors. The second experiment was a cantilevered frame assembly modeled with 96 beam elements with a total of 192 degrees-of-freedom. The measured data consisted of the first eight flexible modal frequencies, and only eight components of the eight corresponding eigenvectors.

The research showed that in each test case, the structural damage could successfully be localized to a small portion of the structure. The extent to which damage can be localized was limited by both model fidelity and accuracy of the measured modes.

STRUCTURAL DAMAGE IDENTIFICATION FROM LIMITED MEASUREMENT DATA

I. Introduction

Over the past decade, both the size and complexity of military and civilian spacecraft have increased considerably. Future Air Force space systems will continue to increase in size due to mission requirements, while minimizing weight to remain within launch constraints of the booster inventory. In addition to the size and complexity increase, the on-orbit lifetime has increased as a result of new advances in solar power generation and battery storage devices. These advances coupled with NASA's demonstrated ability to perform on-orbit repair and replacement of flight critical items, further extend a satellite's usable lifetime. As a result, future large flexible space structures will have an unprecedented requirement for verifying the structural integrity of such space structures on orbit, on a periodic basis over the lifetime of the space system. The potential degradation of structural components from long term exposure to the space environment was documented with the retrieval of NASA's Long Duration Exposure Facility.^[44] Additional damage is also possible due to loads introduced during orbital maneuvers, spacecraft docking operations, and from collisions with space debris. NORAD currently tracks over 5000 objects 10 centimeters in size or larger in low Earth orbit.^[2] Information on both the location and extent of structural damage will be critical in assessing required in-space repair missions and/or deviations from the planned mission profiles. The current configuration of the International Space Station Alpha is shown in Figure 1.1.^[27] This research focuses on identification of damage to structural sub-assemblies typical of large orbiting space platforms. The truss-like structure of International Space Station Alpha's solar array sub-assembly is depicted in Figure 1.2.^[28]

One method of structural verification is visual inspection, however this method may be impractical due to the extra-vehicular activity man-hours required, or impossible as in the case of unmanned and high altitude missions. Thus an alternative solution to visual inspection is desired, and is the main focus of this research. Two current disciplines, closely related to this topic, are system identification theory and analytical model tuning from experimental data. These two disciplines will be briefly reviewed, and their correlation to structural damage identification will be highlighted.

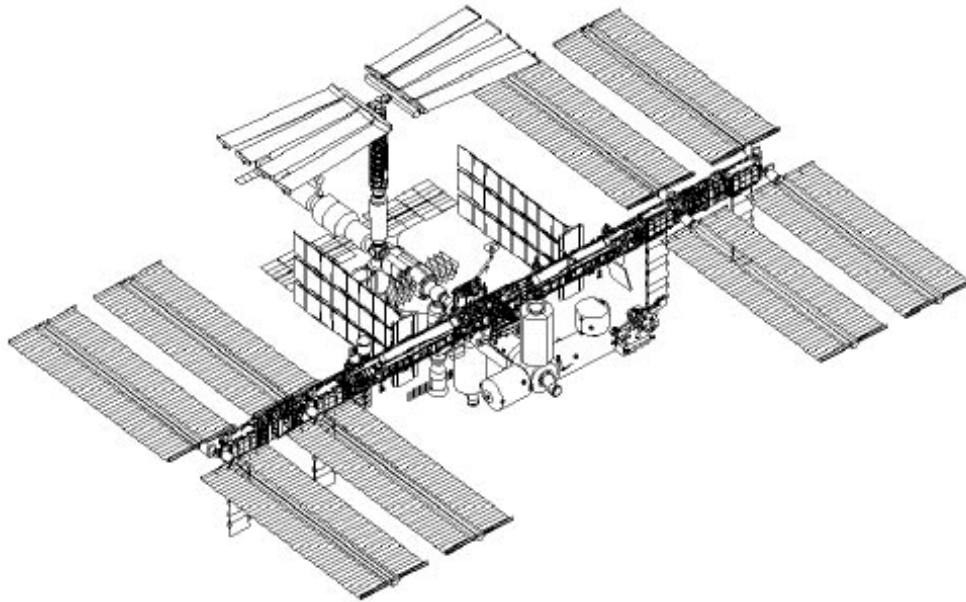


Figure 1.1 On-orbit configuration of International Space Station Alpha.

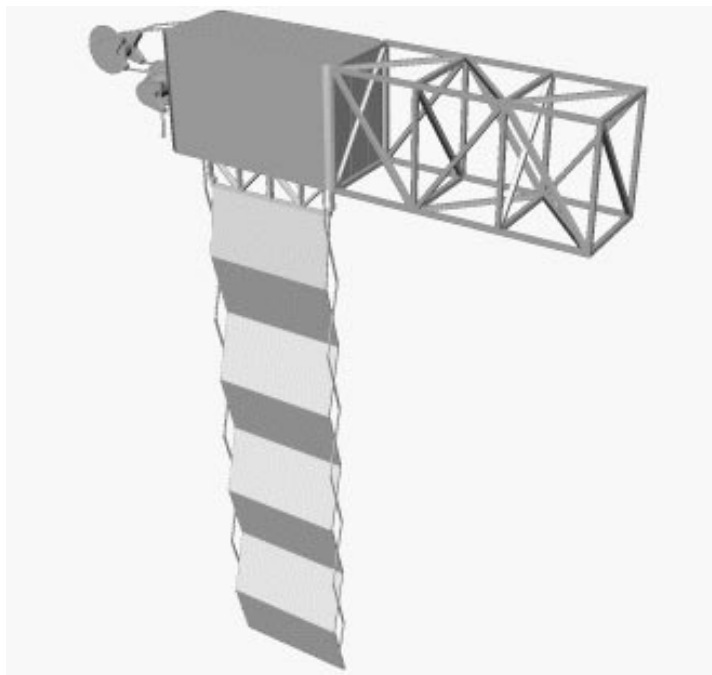


Figure 1.2 Solar array sub-assembly from International Space Station Alpha.

Vibration testing has been used extensively in industry to monitor rotating machinery. From observations of input/output relationships, the frequency signature of a system can be used to detect failures. Identifying specific failure modes can then be accomplished by a comparison of the frequency signature to that of a predetermined set for each failure mode. For a large system, this failure mode set may be impractical to produce or store and interpolation is not necessarily possible between failure modes. Thus an alternative to searching a frequency signature database is sought. One alternative is the use of a system identification algorithm.

System identification techniques are based on determining the underlying physical system from a given set of input/output relationships. For non-parametric system identification, the physical system can be viewed as a 'black box' and thus no inherent knowledge of the structure of the system is required. The primary measure of the effectiveness of the system identification is in how well the identified mathematical model produces an output which matches the measured output for a given input signal. Since there is a direct relationship between the time and frequency domain through the Fourier transform, the identification can be accomplished in either domain. System identification methods have been shown to be very effective in producing models which exactly (theoretically) or closely match (to within the experimental error) the true system; however, they typically do not directly give information about the physical structure of the system. For structural damage identification, the system identification techniques are useful in obtaining the eigenstructure of the physical system, which will be shown to be sufficient to determine structural damage. The feasibility of identifying modal frequencies, damping ratios and shapes from on-orbit testing has been addressed in previous studies.^[43]

Unlike the non-parametric identification, model tuning is a parametric approach to system identification which includes a detailed physical model with well defined parameters of uncertain values. Model tuning attempts to match the input/output relationships of an analytical model and the physical system by varying parameters in the mathematical model. Differences in model tuning methods depend on the assumptions made on how to vary these parameters. For physical structures, one approach is to vary the material properties of the elements in the model. This is typically done by adjusting the stiffness and mass and/or damping matrices of the model. This method assumes the existence of a finite element method (FEM) model which produces simulated output which is reasonably close to experimental measurements. To exactly match experimental data, only small perturbations to the model matrices are required. Model tuning can then be approached as an optimization problem.

For a given input, a minimization on the difference between the model output and the measured output can be performed through the use of an appropriate metric, while iterating on the perturbation of the matrices. The key distinction between different model tuning methods, important to structural damage identification, is whether or not the physical connectivity of the structure is retained. Clearly, to correctly determine a change in a structural element, the tuned model must not remove load paths or introduce load paths not present in the physical structure.

An additional complexity with model tuning algorithms is in obtaining complete experimental information. A typical FEM model of a large flexible space structure will include hundreds or thousands of nodes with as many as six degrees-of-freedom at each node. In contrast, typical experimental data will include accurate information on only the lower frequency modes of vibrations, taken at only a small subset of the nodes in the FEM model. Furthermore, typically only translational degrees-of-freedom are measured which further reduces the available data. Thus an additional distinguishing feature between model tuning algorithms is in how to incorporate the reduced experimental data sets into the model. Several model reduction/expansion algorithms have been used to correlate the model to experimental data.^[25, 29, 63] A common attribute of these methods is the use of the nominal FEM model to obtain the unmeasured degrees-of-freedom. For damage detection however, the FEM model is the unknown and hence cannot be used as the basis for the reduction/expansion.

Having briefly motivated the problem of on-orbit damage identification, along with introducing the concepts of system identification and model tuning, a statement of the research objective can now be given. The research focused on the development of a new method to identify damaged structural elements from a large flexible space structure on-orbit, using limited measured modal data. This effort was decomposed into four specific tasks. The first is the identification of partial modal properties from measured data of the nominal (i.e. undamaged) space structure. Second, the FEM model must be adjusted to match the measured nominal partial data. The third task is an analysis of the extent to which structural damage can be localized to individual structural elements using the measured data. In conjunction with this task is the determination of where to best place the limited number of available sensors on the structure. Lastly, the identification of structural damage must be performed using the measured data from a damaged space structure.

This chapter briefly introduced the research effort and outlined some of the related work in this area. Chapter II presents a background of related work in system identification and model tuning and

discusses the relevance to damage identification. The subsequent chapters develop the four tasks of the on-orbit damage identification problem in detail, beginning with an overview of the methodology for each task in Chapter III. The four tasks were integrated into a single software package which is presented Appendix B. Lastly, validation of the research effort was performed using laboratory experiments which exhibit the same dynamic properties as large flexible space structures, and is presented in Chapter VIII.

II. Background

2.1 Motivation

The problem of producing analytical models capable of predicting dynamic responses has been widely studied. While these solution methods may result in analytical models which match (typically in a weighted least squares sense) experimental data, they most often do not directly address the problem of relating perturbations of the analytical model to changes in the physical parameters of the structure. Direct identification of failed structural components is exactly the information required to adjust mission profiles to minimize structural dynamic loading and to enable development of repair missions where possible. Thus a method which directly identifies damaged structural members from experimental data is highly desirable. Due to the similarities among damage identification, system identification and model tuning, an overview of existing methods for system identification and model tuning will be presented as well as current methods of damage identification.

2.2 System Identification Techniques

The problem associated with system identification is: given the measured response to a known input, determine a mathematical representation of the system which reproduces the output sequence given the input sequence. Differences in algorithms are based on the assumptions of the underlying system, which then establishes the structure of the analytical model. For large flexible space structures, a finite-dimensional linear time-invariant model can adequately represent the dynamics of the structure and hence will be the subject of this investigation. In general system identification theory, such a restrictive assumption need not be imposed.

To illustrate the general approach to system identification, a sampled data single-input single-output system will be considered. This presentation is based on work by Ljung.^[49] Given an input sequence $u(t)$ and an output sequence $y(t)$ where $t = (0, 1, \dots, N - 1)$, the discrete-time system can be represented as:

$$y(t) = G(z)u(t) + v(t) \tag{2.1}$$

with $G(z)u(t)$ representing the convolution summation of the system's impulse response sequence $g(t)$ with the input sequence $u(t)$, and is given by:

$$G(z)u(t) = \sum_{k=0}^{\infty} g(k)u(t-k) \quad (2.2)$$

The function $v(t)$ represents the measurement noise (uncertainty) associated with obtaining the output sequence. The term $G(z)$ represents the system's transfer function and is defined as:

$$G(z) = \sum_{t=0}^{\infty} g(t)z^{-t} \quad (2.3)$$

where z represents the time-shift operator such that:

$$z^{-1}y(t) = y(t-1) \quad (2.4)$$

A parametric approach to system identification is then confined to the determination of a set of parameters which fully describe $G(z)$. To illustrate the different approaches, a more general form of Equation (2.1) is used to form a general parametric model given as the following convolution:

$$A(z)y(t) = \frac{B(z)}{F(z)}u(t) + \frac{C(z)}{D(z)}e(t) \quad (2.5)$$

where $A(z)$, $B(z)$, $C(z)$, $D(z)$, and $F(z)$ are polynomials in the time shift operator z as follows:

$$A(z) = 1 + a_1z^{-1} + \dots + a_{na}z^{-na} \quad (2.6)$$

and similarly for the remaining four polynomials. The order of the polynomials is given by na , nb , nc , nd and nf respectively. The sequence $e(t)$ is assumed to be a white noise sequence and is shaped by $\frac{C(z)}{A(z)D(z)}$ to produce the measurement noise $v(t)$ of Equation (2.1). The commonly used linear models are all special cases of the general form of Equation (2.5). The autoregressor with exogenous input model is obtained by setting $nc = nd = nf = 0$. Similarly, the autoregressor with moving average and exogenous input is obtained by setting $nf = nd = 0$. The output error model corresponds to $na = nc = nd = 0$, while the Box-Jenkins model is obtained by setting $na = 0$. A large set of models can thus be obtained from the general form given in Equation (2.5).

Although the above development was in transfer function form, an equivalent state-space representation is also possible. The state-space representation of Equation (2.5) is given as:

$$x(t + 1) = Ax(t) + Bu(t) \quad (2.7)$$

$$y(t) = Cx(t) + Du(t) + v(t) \quad (2.8)$$

where A , B , C , and D are redefined as constant matrices. Equation (2.7) can be rewritten in terms of the time shift operator as:

$$zx(t) = Ax(t) + Bu(t) \quad (2.9)$$

Solving for $x(t)$ yields:

$$x(t) = (zI - A)^{-1} Bu(t) \quad (2.10)$$

Substituting this result into Equation (2.8) yields the convolution:

$$y(t) = [C(zI - A)^{-1} B + D] u(t) + v(t) \quad (2.11)$$

Thus the transfer function is directly related to the state-space quadruple (A, B, C, D) by:

$$G(z) = C[zI - A]^{-1} B + D \quad (2.12)$$

Hence the system identification problem is equivalent to determining the constant matrices of the quadruple (A, B, C, D) which accurately reproduces a given measured response from a known input. A further distinction between techniques involves whether the input $u(t)$ and output $y(t)$ are represented in the time or frequency domain. The foundation of these two methods will be briefly discussed.

2.2.1 Time Domain. System identification in the time domain seeks to reconstruct the transfer function based on identification of the system's impulse response function. For the scalar case, if the input is a pulse defined as:

$$u(t) = \begin{cases} a & t = 0 \\ 0 & t \neq 0 \end{cases} \quad (2.13)$$

then the output $y(t)$ becomes:

$$y(t) = ag(t) + v(t) \quad (2.14)$$

where $g(t)$ is the unit-impulse response sequence and $v(t)$ is the measurement noise. If the signal to noise ratio is high, then $v(t) \ll ag(t)$ and can be neglected. An estimate of the impulse response is then simply:

$$g(t) = \frac{y(t)}{a} \quad (2.15)$$

with an error of $\frac{v(t)}{a}$. An estimate of the transfer function can then be determined directly from the estimated impulse response.

$$G(z) = \sum_{t=0}^{\infty} g(t)z^{-t} \quad (2.16)$$

A disadvantage with the above method is the requirement to excite the system with an impulse. This can be approximated with a finite pulse input, but may be impractical to implement on certain systems, and it may be difficult to obtain response levels which are significantly above the measurement noise levels. An alternative procedure known as correlation analysis overcomes this shortcoming by requiring the input is a zero-mean white noise sequence, i.e. its auto-correlation function is given as:

$$R_{uu}(\tau) = \begin{cases} \lambda & \tau = 0 \\ 0 & \tau \neq 0 \end{cases} \quad (2.17)$$

Then, from Equation (2.1) the cross-correlation between the input and output is given as:

$$R_{yu}(\tau) = \lambda g(\tau) \quad (2.18)$$

where $g(\tau)$ is the desired impulse response sequence. By definition,^[50] the cross-correlation between two zero-mean sequences is given as:

$$R_{yu}(\tau) = \lim_{N \rightarrow \infty} \frac{1}{N} \sum_{t=0}^{N-1} y(t)u(t - \tau) \quad (2.19)$$

where it is assumed that the limit exists. An estimate of the correlation is then obtained by selecting N sufficiently large. Thus the correlation estimate is defined as:

$$R_{yu}(\tau) \equiv \frac{1}{N} \sum_{t=0}^{N-1} y(t)u(t - \tau) \quad (2.20)$$

Using the estimated correlation, an estimate of $g(\tau)$ can then be obtained from the input and output sequences using Equations (2.18) and (2.20).

$$g(\tau) = \frac{1}{\lambda N} \sum_{t=0}^{N-1} y(t)u(t-\tau) \quad (2.21)$$

Although the assumption was made that the input $u(t)$ was white noise, this is not a restrictive assumption since a shaping filter can always be constructed to produce the actual sequence $u(t)$.^[53] The output sequence can then be filtered through this same filter and the estimate is computed using Equation (2.21) with filtered data. Although presented here for the scalar case, the method is applicable to multiple input/output combinations.

Based on these concepts, a vast array of system identification methods have been studied and presented in the literature. From these methods, the eigensystem realization algorithm (ERA) was singled out as one which has demonstrated its ability to accurately produce a minimum system realization from multi-input/multi-output (MIMO) experimental data typical of large flexible space structures.^[32] The ERA method is presented in Chapter IV.

2.2.2 Frequency Domain. The aforementioned methods were based on reconstruction of the impulse response in the time domain. An alternative method is identification of the system's transfer function in the frequency domain. This method is commonly referred to as spectral analysis and is included here for completeness.

The frequency response function of the system in Equation (2.1) is found by evaluating the transfer function $G(z)$ on the unit circle $z = e^{j\omega}$. Furthermore, the noise sequence $v(t)$ can be described in terms of its power spectral density $\Phi_{vv}(\omega)$, where the power spectral density function is defined as the Fourier transform of the autocorrelation function. Thus the input output relationship of Equation (2.1) is completely specified from knowledge of $G(\omega)$ and $\Phi_{vv}(\omega)$. If initially we assume the measurement noise is negligible, the frequency response function can be found from sine-dwell testing. In this method, the system is given a known sinusoidal input.

$$u(t) = a \sin(\omega t) \quad (2.22)$$

For a linear time-invariant system, it is well known that the steady-state output response after the transients die out is given by:^[62]

$$y_{ss}(t) = a |G(\omega)| \sin(\omega t + \phi) + v(t) \quad (2.23)$$

where ϕ is given by the phase angle of $G(\omega)$. In this way, an estimate of the transfer function can be found by repeated application of the input sinusoid at frequencies of interest and measuring the magnitude and phase of the response. A reconstruction of the transfer function from the data can then be performed.

In the preceding analysis it was assumed that the measurement noise was small and hence was neglected from the analysis. A less restrictive assumption is to assume $u(t)$ and $v(t)$ are independent, but $v(t)$ not necessarily negligible. The relationship between input and output given in Equation (2.1) corresponds to a relationship between the power spectra of:

$$\Phi_{yy}(\omega) = |G(\omega)|^2 \Phi_{uu}(\omega) + \Phi_{vv}(\omega) \quad (2.24)$$

and

$$\Phi_{yu}(\omega) = G(\omega)\Phi_{uu}(\omega) \quad (2.25)$$

Estimates of the frequency response function and the noise power spectrum are obtained by computing the appropriate estimates of the correlation functions using Equation (2.20) and their corresponding power spectra (by Fourier transformation).

$$G(\omega) = \frac{\Phi_{yu}(\omega)}{\Phi_{uu}(\omega)} \quad (2.26a)$$

$$\Phi_{vv}(\omega) = \Phi_{yy}(\omega) - \frac{|\Phi_{yu}(\omega)|^2}{\Phi_{uu}(\omega)} \quad (2.26b)$$

The above highlights the general aspects of spectral analysis. A more complete derivation of spectral analysis is contained in Newland.^[57] The preceding material was based on a discrete time analysis, since this is the form of measured data. The material presented in the remainder of this chapter and all subsequent chapters is based on a continuous time analysis unless otherwise stated.

2.3 Model Tuning Techniques

As opposed to system identification techniques where no *a priori* model is required to perform the identification, model tuning assumes the existence of an analytical model. For flexible structures, the model can be written as:

$$Mx + Cx + Kx = Ff \quad (2.27)$$

where M, C, K represent the mass, damping, and stiffness matrices respectively for the degree-of-freedom vector x . The matrix F represents the influence matrix to a given input vector f . This analytical model is the result of an application of Newton's second law, and most likely produced as the output of a FEM program and used to simulate the dynamic response of the actual structure. Note that the matrices M, C, K, F of the second-order Equation (2.27) can be related to the first-order quadruple (A, B, C, D) as given in Equations (2.7) and (2.8). The transformation from second-order to first-order form for a state vector $[x, \dot{x}]^T$ is given by:

$$A = \begin{bmatrix} 0 & I \\ -M^{-1}K & -M^{-1}C \end{bmatrix} \quad (2.28a)$$

$$B = \begin{bmatrix} 0 \\ M^{-1}F \end{bmatrix} \quad (2.28b)$$

$$C = [I \quad 0] \quad (2.28c)$$

$$D = [0] \quad (2.28d)$$

Due to violation of modeling assumptions and to inherent uncertainties in material properties, joint properties, boundary conditions, etc. in developing the analytical model, there will exist an imperfect correlation between the experimental and analytical results. If the correlation results are unsatisfactory, an adjustment to the finite element model is necessary. The common attribute of model tuning techniques is that they attempt to minimize the required modification to the matrices, assuming the FEM model is a reasonable approximation to the physical structure. Additionally, for realistic structures, the FEM model will include a large number of degrees-of-freedom (dimension of x) of which only a small subset will be measured. The differences in the techniques stem from how to incorporate the reduced data set and on what restrictions to make on the set of allowable perturbations to the existing matrices as well as the selection of what error metric is to be minimized. Further classifications can

be made on whether damping is considered in both the model and the measurements. For cases where damping is neglected, $C = 0$ in Equation (2.27), the distinction is whether adjustments are made to the mass matrix, stiffness matrix, or both. The adjustments are the result of the solution of eigenvalue problems, orthogonality relationships, and eigenstructure assignment techniques. Several relevant techniques will now be reviewed.

2.3.1 Sensitivity Based. A straightforward approach to adjusting the matrices in Equation (2.27) is to establish an objective function which is a measure of the difference between the experimental and analytical model data.^[66] The eigenstructure (eigenvalues and eigenvectors) has been widely accepted as an acceptable method of measuring correspondence between models.^[70] This is due to the fact that the eigenstructure is invariant under a state transformation and thus allows direct comparisons of different realizations. Sensitivity is the quantification of changes in the objective function due to changes in the design variables. The sensitivity of the objective function with respect to the design parameters is determined for each parameter in the matrices. A numerical optimization problem is then solved by searching over the entire parameter space using the sensitivity information to determine search directions. An advantage of this method is that the updated models are consistent with the FEM formulation and thus the connectivity is preserved.

While this method can yield acceptable results for small problems, the major drawback is the large number of design parameters contained in the search space.^[9,21] For larger problems, the selection of a suitable set of parameters to search over may not be intuitive. Its advantage in structural damage identification, however, is that a set of parameters can be chosen that reflect physical failure modes, such as searching over an elastic modulus value or the cross-sectional area of each member. Preliminary knowledge of the damage location may be required for large structures to minimize the required search space. Hemez and Farhat applied this procedure to damage detection.^[14,24] Success of the detection algorithm relied on the extent of the damage and the sensitivity to the chosen design variables.

2.3.2 Orthogonality Based. If the underlying physical system is assumed to be linear and either undamped or proportionally damped, then the mode shapes of the structure will be orthogonal with respect to the mass matrix.^[5,7] Modal orthogonality can then be represented as:

$$\Phi^T M \Phi = I \quad (2.29)$$

where Φ is the matrix composed of the measured eigenvectors (mode shapes). Using this orthogonality requirement, small adjustments can then be made to the mass matrix M to force the orthogonality requirement. Note that confidence in the analytical mass matrix is assumed higher than the confidence in the stiffness matrix. For the undamped structure, the corresponding eigenvalue problem can then be written as:

$$\Phi^T K \Phi = \Lambda \quad (2.30)$$

Adjustments to the stiffness matrix are then made such that Equation (2.30) is satisfied. In Equations (2.29) and (2.30), both Φ and Λ are required to have the same dimension as the analytical model. As previously discussed, the sets of measured eigendata will be much smaller than the number of degrees-of-freedom in the analytical model. Thus, to apply the orthogonality equations, either a modal expansion on the measured data or a modal reduction on the analytical model must be performed. As presented by Berman, a modal expansion can be performed on the test data as follows.^[7] The analytical matrices are first ordered such that the coordinates associated with the measured degrees-of-freedom are ordered above the remaining coordinates. The eigenvalue problem for each mode can then be written as:

$$[K - \lambda_i M] \Phi_i = 0 \quad (2.31)$$

This equation can then be partitioned as:

$$\left\{ \begin{bmatrix} k_1 & k_2 \\ k_2^T & k_4 \end{bmatrix} - \lambda_i \begin{bmatrix} m_1 & m_2 \\ m_2^T & m_4 \end{bmatrix} \right\} \begin{Bmatrix} \phi_{1i} \\ \phi_{2i} \end{Bmatrix} = 0 \quad (2.32)$$

The unknown lower partition of the eigenvector can then be solved using the following:

$$\phi_{2i} = -(k_4 - \lambda_i m_4)^{-1} (k_2^T - \lambda_i m_2^T) \phi_{1i} \quad (2.33)$$

This result is repeated for each measured mode. This method represents an interpolation of the measured modes at the unmeasured degrees-of-freedom. The accuracy of this technique is clearly dependent on how accurately the analytical model represented the physical structure. It should be noted that if the frequency dependence in the above equation were ignored, this would result in the standard Guyan reduction relationship.

Having obtained full-length eigenvectors, the adjusted mass matrix is then formed from the solution of a constrained minimization problem.^[7] An objective function of the form:

$$J = \left\| M_a^{-1/2} (M - M_a) M_a^{-1/2} \right\| \quad (2.34)$$

is used which penalizes deviations from the analytical model. In the original work the Frobenius norm was chosen. The subscript a denotes the analytical model. The orthogonality constraint is then appended with Lagrange multipliers as follows:

$$L = J + \sum_{i=1}^n \sum_{j=1}^n \nu_{ij} (\Phi^T M \Phi - I)_{ij} \quad (2.35)$$

Differentiating L with respect to M and setting derivatives equal to zero yields a solution to the adjusted mass matrix which now satisfies the orthogonality relationships and has minimized deviations from the analytical mass matrix according to the applied norm in the objective function. The corrected mass matrix is given by:

$$M = M_a \Phi m^{-1} (I - m) m^{-1} \Phi^T M_a \quad (2.36)$$

with m defined as:

$$m = \Phi^T M_a \Phi \quad (2.37)$$

Although not presented in the original work, an iterative scheme could be used because the interpolated value of Φ will change for the adjusted M . Having obtained the adjusted mass matrix, the stiffness matrix is then obtained in a similar manner. The objective function is formed as an appropriate weighted norm on the difference between the analytical and adjusted stiffness matrices. In Berman's work which was an extension of the stiffness matrix adjustment method of Baruch,^[5] the analytical mass matrix was chosen as the appropriate weighting function for the individual elements. This seems appropriate only when elemental stiffness values are directly related to the mass of each element. Certainly, there are structures which contain mass elements which do not contribute to the overall stiffness of the structure. With the norm chosen, the eigenvalue equation is then appended as a constraint with Lagrange multipliers. An additional constraint to ensure symmetry of the stiffness matrix is also appended. The adjusted stiffness matrix is then found from a differentiation with respect to the elements of K_a and

setting them equal to zero. The resulting adjusted stiffness matrix is given as:

$$K = K_a + \Delta + \Delta^T \quad (2.38)$$

where

$$\Delta = \frac{1}{2} (M\Phi(\Phi^T K_a \Phi + \Lambda)\Phi^T M) - K_a \Phi \Phi^T M \quad (2.39)$$

Although the presentation above based on the work of Berman and Baruch did not consider damping, it could be expanded to include the proportional damping case. The advantage of this method is the straightforward mathematical formulation of the adjusted matrices. Furthermore, this method will result in a tuned analytic model which exactly reproduces the experimental data. Its shortcoming is that it does not guarantee the closeness to unmeasured modes not used in the tuning process. This is a result of potentially unrealistic changes in the stiffness matrix such as the introduction of load paths which physically do not exist. The introduction of fictitious load paths is undesirable when identifying damaged elements since the stiffness changes can not be directly related to physical elements.

The orthogonality based approach described above is essentially a matrix update approach in which perturbation mass, damping, or stiffness matrices are determined that, when added to the analytical matrices, reproduces the measured result. Brock originally examined this problem while enforcing symmetry and positive-definiteness of the solution.^[8] Success of this method is dependent on the ability to accurately measure or reconstruct the modal matrix Φ . When using limited measurements, an accurate Φ matrix is not a realistic expectation.

2.3.3 Connectivity Based. To overcome some of the shortcomings of Baruch's method of stiffness matrix adjustments, Kabe introduced an objective function which ensures stiffness terms are corrected in a relative manner such that the connectivity of the analytical model is preserved.^[35,37] This method was also expanded to include a weighting function which assigns a confidence level to each term in the stiffness matrix. Kabe's algorithm uses a percent change in stiffness value cost function and then appends a constraint on the sparsity pattern of the stiffness matrix to preserve the original load paths. The addition of the structural connectivity information enables Kabe's method to identify stiffness changes exactly in some cases, even when only a limited number of measurements were used.

A mathematically equivalent but more intuitive method was developed by Kammer using an alternative matrix minimization formula. Similar work has been investigated by Smith and Beattie.^[64]

In all of these methods, the minimization of a matrix norm (typically the Frobenius norm) of the difference between the measured and analytical models can be justified when the goal is model refinement. This method tends to make small changes across all the matrix elements, whereas damage to a structural element will create a large localized change.

2.3.4 Residual Force Based. Another approach which has been applied to both model tuning and damage identification is the residual force approach. This technique, developed by Chen and Garba, is based on computation of a residual force vector which represents the mismatch between the analytical model and the modal data.^[10] For simplicity, assume an undamped structure. The solution to the second-order homogeneous equation:

$$Mx + Kx = 0 \quad (2.40)$$

is given by the eigenvalues and eigenvectors (λ_i, Φ_i) in Equation (2.31). If the mass matrix M is assumed correct, and the stiffness matrix K is written as:

$$K = K_o + \Delta K \quad (2.41)$$

then substitution of Equation (2.41) into Equation (2.31) yields:

$$\Delta K \Phi_i = (\lambda_i M - K_o) \Phi_i \quad (2.42)$$

The residual force vector $\Delta K \Phi_i$ is essentially equivalent to the modal force error proposed by Ojalvo.^[59] The residual force vector for the i^{th} mode can then be written in terms of the unknown elements of the stiffness matrix Δk_{ij} and the connectivity matrix C_i for the i^{th} mode. Construction of C_i is based on nodal geometry, elemental physical properties, and the measured eigenvector for the i^{th} mode. An example construction of C_i is given in Reference 10. Equating the result to the residual force vector yields:

$$\Delta K \Phi_i = C_i \Delta k_{ij} \quad (2.43)$$

The length of the residual force vector corresponds to the number of degrees-of-freedom of the system, while Δk_{ij} is a vector whose length is equal to the number of independent elements in the stiffness matrix. A least squares solution to Δk_{ij} is found using:

$$\Delta k_{ij} = C_i^{\#} \Delta K \Phi_i \quad (2.44)$$

The $(\bullet)^{\#}$ notation denotes the pseudoinverse operation. If multiple modes are used, the equations are stacked so that:

$$\Delta k_{ij} = \begin{bmatrix} C_1 \\ C_2 \\ \vdots \end{bmatrix}^{\#} \begin{bmatrix} \Delta K \Phi_1 \\ \Delta K \Phi_2 \\ \vdots \end{bmatrix} \quad (2.45)$$

Advantages of this method include its ability to handle a subset of the total number of modes of the system. However, when forming the least squares solution without a full set of eigendata, there is no guarantee that a realistic Δk_{ij} will result. This method was demonstrated using a FEM model of a 78 element triangular truss. The author used 3 iterations and constrained Δk_{ij} values to lie between 0 and 100% stiffness reduction from the unbroken values. The use of a reduced length eigenvector (when the number of sensors is less than the degrees of freedom) was not addressed.

The residual force vector in Equation (2.42) was also investigated by Kaouk and Zimmerman.^[38,39] Using this method, the problem is approached in a decoupled fashion, using the residual force vector to localize the damage and then using the minimum rank update to determine the extent of damage. This method works well when all the degrees-of-freedom can be measured, but degrades rapidly when the size of the measurement set is reduced. The determination of the extent of damage varied, depending on which modes were used in the algorithm. Best results were obtained using only modes with significant changes from their nominal values.

Additional work on establishing which modes to use in damage identification algorithms has been presented by Kashangaki.^[42] In this work, calculation of the strain energy associated with each mode in each member is performed using the analytical model. It is assumed that elements which are highly strained in a given mode will be more readily identified using the eigendata for that particular mode. This information could easily be incorporated into Chen's work once an assessment of initial damage location was performed.

2.3.5 *Assigned Eigenstructure Based.* An alternative approach to model tuning, more frequently formulated in a controls setting, is through eigenstructure assignment. With this technique, a set of desired eigenvalues/eigenvectors is achieved in closed-loop manner by the selection of a proper set of feedback gains. The following paragraphs discuss some general results for eigenstructure assignment, along with a closed form solution for obtaining the desired eigenstructure.

Consider a linear time-invariant system represented as:

$$\dot{x} = Ax + Bu \quad (2.46a)$$

$$y = Cx \quad (2.46b)$$

$$u = Ky \quad (2.46c)$$

The dimensions of the state, control, and output vectors x , u and y are of dimension n , m and r respectively. If the system is both controllable and observable, and the matrices B and C are full rank, then the following results can be proven^[4]:

1. The position of $\max(m, r)$ closed-loop eigenvalues can be arbitrarily assigned, with the stipulation that complex eigenvalues must be assigned in complex conjugate pairs.
2. A total of $\min(m, r)$ elements of the closed-loop eigenvectors can be assigned, with the same complex conjugate stipulation.
3. The assigned eigenvector associated with the assigned eigenvalue λ_i , must lie in the subspace spanned by $(\lambda_i I - A)^{-1}B$.

As applied to structural damage identification, the matrix A is obtained from the analytical mass and stiffness matrices of the tuned finite element model, as given in Equation (2.28a). The matrix B , which represents the control influence matrix, can be constructed from the connectivity matrix of the structure. For realistic structures this matrix can always be chosen to be full rank from proper selection of the structural elements. The rank of the measurement matrix C will primarily depend on the number of sensors chosen. As will be shown, this will be a critical factor in obtaining the desired eigenstructure from condition 2 above.

A closed-form solution to the eigenstructure assignment problem has been developed by Liebst and Garrard.^[45] The solution involves determination of a feedback gain matrix G , such that for all desired closed-loop eigenvalue/eigenvector pairs (λ_i, Φ_i) , the following relation holds.

$$(A + BKC)\Phi_i = \lambda_i\Phi_i \quad (2.47)$$

This is equivalently written as finding the vectors w_i such that:

$$(\lambda_i I - A)\Phi_i = Bw_i \quad (2.48)$$

Determination of the gain matrix G once the w_i 's have all been calculated is:

$$G = W[C\Phi]^{-1} \quad (2.49)$$

where $W = [w_1 w_2 \dots]$ and assuming the matrix product $C\Phi$ is non-singular.

In general, the desired eigenvectors may not be achievable. In this case, it is desirable to select the w_i 's such that a minimization between the desired and achievable eigenvectors is obtained. For the minimization, a weighted cost function is established as:

$$J_i = (\Phi_i - \Phi_i^d)^* P_i (\Phi_i - \Phi_i^d) \quad (2.50)$$

The achievable and desired closed-loop eigenvectors are denoted by Φ_i and Φ_i^d respectively. The $(\bullet)^*$ notation denotes the complex conjugate operation. The positive definite symmetric weighting matrix P_i can be chosen to weight certain elements of the vector of differences in the desired and achievable eigenvectors more heavily than others. Thus for a given desired eigenvalue λ_i , it is desirable to minimize J_i subject to Equation (2.48). The solution is found by appending Equation (2.48) to Equation (2.50) with a Lagrange multiplier ν_i .

$$J_i = \frac{1}{2}(\Phi_i - \Phi_i^d)^* P_i (\Phi_i - \Phi_i^d) + \nu_i^* [(\lambda_i I - A)\Phi_i - Bw_i] \quad (2.51)$$

The cost J_i is minimized in equation 2.50 when:

$$\frac{\partial J_i}{\partial w_i} = -\nu_i^* B = 0 \quad (2.52)$$

$$\frac{\partial J_i}{\partial \Phi_i} = (\Phi_i - \Phi_i^d)^* P_i + \nu_i^* (\lambda_i I - A) = 0 \quad (2.53)$$

Writing equations 2.48, 2.52, and 2.53 in matrix form yields:

$$\begin{bmatrix} (\lambda_i I - A) & -B & 0 \\ 0 & 0 & B^T \\ P_i & 0 & (\lambda_i I - A)^* \end{bmatrix} \begin{bmatrix} \Phi_i \\ w_i \\ \nu_i \end{bmatrix} = \begin{bmatrix} 0 \\ 0 \\ P_i \Phi_i^d \end{bmatrix} \quad (2.54)$$

or equivalently,

$$N_i \begin{bmatrix} \Phi_i \\ w_i \\ \nu_i \end{bmatrix} = \begin{bmatrix} 0 \\ 0 \\ P_i \Phi_i^d \end{bmatrix} \quad (2.55)$$

The obtainable λ_i and w_i are then given by:

$$\begin{bmatrix} \Phi_i \\ w_i \\ \nu_i \end{bmatrix} = N_i^{-1} \begin{bmatrix} 0 \\ 0 \\ P_i \Phi_i^d \end{bmatrix} \quad (2.56)$$

It can be shown that N_i is always non-singular with positive definite P_i and B full rank, even if λ_i is not moved from its open-loop value. If an eigenvalue/vector pair (λ_i, Φ_i) is not to be altered, setting the corresponding $w_i = 0$ assures that the open-loop values are retained. As developed above, this algorithm requires the selection of a set of desired eigenvalues/vectors. Since in general when performing modal tests on a structure, only eigenvector elements corresponding to the instrumented degrees-of-freedom are identified, the technique as presented is not suitable for damage detection. The eigenvector expansion method presented in Equation (2.33) is not suitable to use with damage detection since it requires knowledge of the damaged mass and stiffness matrices which are unknown.

Using the basic concepts of eigenstructure assignment, a method for correcting FEM models using eigenstructure assignment was developed by Zimmerman and Widengren.^[70] Their solution method is based on a symmetric eigenstructure assignment technique in which the symmetry (not necessarily the connectivity) of the change in the stiffness matrix is preserved. A standard output

feedback assignment^[65] is used, but a set of pseudosensors C and pseudoactuators B are judiciously chosen to yield a symmetric feedback matrix. The pseudoactuator matrix is chosen such that the measured eigenvectors lie in the achievable eigenvector subspace. Thus each mode has its own corresponding pseudoactuator matrix. For a given B , the corresponding C is found from the solution of a generalized algebraic Riccati equation. Since there will exist a set of non-unique real solutions, this set must be evaluated for one which yields the ‘best’ adjusted stiffness matrix. In the solution technique, only necessary (but not sufficient) conditions are used and hence some solutions will be asymmetric and can be immediately discarded.

Again, the assignment algorithm requires full length eigenvectors. The eigenvector elements corresponding to the unmeasured degrees-of-freedom are obtained using an optimal least-squares expansion into the achievable eigenvector subspace. An alternative to the least squares expansion has also been developed by posing it as an orthogonal Procrustes problem which yields similar, but computationally more efficient results.^[39]

Using the symmetric eigenstructure assignment technique does not preserve the load paths. An iterative scheme was introduced to zero out stiffness matrix elements which were zero in the analytical stiffness matrix. The disadvantage of this method is the requirement to solve the generalized algebraic Riccati equation and then sort through the potential solution sets in an iterative fashion.

An alternative to the symmetric eigenstructure assignment is presented by Lindner.^[47] In this method, eigenstructure assignment is performed for each element of the truss, using the elemental stiffness value as the pseudocontrol variable. Location of the damaged element is based on the assumption that for each eigenvalue and eigenvector pair (λ_i, Φ_i) assigned, only the assignment using the damaged element will consistently return the same required stiffness change to assign each (λ_i, Φ_i) pair. Hence this algorithm requires a complete search over all the elements, but in a non-iterative fashion. A full set of sensor information (full length eigenvectors) was assumed in this work. An advantage of this approach is that it does not require the inverse connectivity problem, i.e. finding the element(s) corresponding to the change in the stiffness matrix. This is done initially in the problem formulation. A disadvantage in the detection scheme is that an increasing number of experimental modes are required to better assess which element is the actual damaged element. The method is also unsuitable for multiple element failures, since each eigenstructure assignment uses only a single pseudocontrol variable.

2.3.6 Realization Theory Based. A conceptually straightforward approach to damage detection would be to simply compare the first-order matrices of the analytical model to those obtained using an identification algorithm. A direct comparison however, is only possible when the two systems are represented using the same state-space realization. An algorithm developed by Alvin and Park called the common basis-normalized structural identification procedure performs this transformation.^[3] This procedure requires the identified model to be the same order as the analytical model, which may be difficult to obtain. When smaller realizations are identified, a reduced order model is obtained. A reduction of the analytical model will destroy the connectivity information and make damage detection difficult. In subsequent work by the same authors, this technique was applied to an eight-bay truss structure, instrumented with three degree-of-freedom sensors at each node.^[60] The use of a complete set of sensors at each node allowed a post analysis to determine individual element damage. This method was also shown to be very sensitive to experimental imprecision.

As previously mentioned, when performing model reduction the sparsity of the stiffness matrix and hence connectivity information is not preserved. The advantage of the reduced model is that the number of sensors can correspond directly to the degrees-of-freedom of the model. A compromise solution was developed by Kim in which an intermediate set of coordinates is chosen, greater than the number of measurements but less than the number in the analytical model.^[43] The experimental modes were expanded using a modal expansion technique, and the analytical model was reduced using a standard model reduction algorithm. Using this intermediate coordinate set, an optimal matrix update was performed as developed by Baruch.^[6] Using this intermediate set, the location of the damage can be localized, but can no longer be determined to within an individual element.

2.4 Summary

A large collection of techniques for system identification, model tuning and damage detection have been presented. For system identification, the ERA method was singled out as the method of choice for obtaining the modal parameters from the measured response data. Common to most model tuning techniques was the minimization of a matrix norm on the perturbation to the stiffness matrix required to match experimental data. For damage detection, a matrix norm minimization is not necessarily desirable. Additionally, several approaches to the damage detection problem have been reviewed. All approaches require full-length eigenvectors (or construction thereof) in their formulation.

Of the methods presented, it is the author's opinion that the assigned eigenstructure based approach has the best potential to be computationally efficient, but must be adapted to handle limited measurement data. Using the desirable aspects of each method, such as load path preservation and computational efficiency, a solution was formulated in the subsequent chapters which specifically addresses damage identification when only a minimal number of sensors are used.

III. Damage Identification Methodology

The terms damage detection and damage identification appear frequently in the literature. In this work, the term detection applies to the process of monitoring, typically on line, the measured response of the system. From the response, a decision is made as to whether or not ‘damage’ has occurred. Damage can be defined as a failed sensor or actuator, or an actual change in the dynamics of the structure. In contrast to detection, structural damage identification, as used herein, refers to the off-line analysis of the measured response to determine damage to individual structural elements. Clearly damage detection must occur to begin the damage identification phase. Current fault detection schemes include monitoring residuals in an on-line estimator.^[30,31] The residual is the difference between the measured output and the predicted output of an on-line estimator such as a Kalman filter. A fault is indicated by the residual level rising above some predetermined threshold. Different threshold levels are investigated in Faitakis.^[15] Furthermore, since the residual using a properly tuned estimator should appear as white noise, additional research has focused on monitoring the ‘whiteness’ of the residuals.^[22,68] In this research effort, it was assumed that a suitable damage detection algorithm is available and thus was not further investigated. Each reported test case began with the assumption that damage had already been detected. The research focused on the identification of damaged element(s), using the measured data.

Once damage has been detected, the off-line damage identification process is initiated. The identification process can be divided into four main tasks: (1) identification of partial modal properties from measured data of the nominal space structure, (2) adjusting the FEM model to match the measured nominal partial data, (3) analyzing the extent to which structural damage can be localized to individual structural elements using the measured data, and finally (4) the identification of structural damage using measured partial modal data from a damaged space structure. The methodology for each task is overviewed in the subsequent sections of this chapter, while the mathematical development is deferred to later chapters. The four tasks are based on a FEM model of the space structure where structural damping is assumed negligible and is omitted from the analysis for simplicity. The free vibration of the undamaged structure is modeled as:

$$Mx + Kx = 0 \quad (3.1)$$

with the symmetric mass and stiffness matrices M and $K \in \mathfrak{R}^{n \times n}$, x representing the state vector and \ddot{x} denoting a double time differentiation on x . The eigenvalue and eigenvector for the i^{th} mode of Equation (3.1) is given as (λ_i, Φ_i) whereas the measured eigenvalue and partial eigenvector for the same mode is represented as $(\bar{\lambda}_i, \bar{\phi}_i)$. The relationship between the n dimensional eigenvectors Φ_i and the s dimensional partial eigenvectors ϕ_i is $\phi_i = C \Phi_i$. The matrix $C \in \mathfrak{R}^{s \times n}$ maps the full length eigenvectors into the partial eigenvectors corresponding to the measured degrees-of-freedom, $\phi = C \Phi$. With minimal sensor information available, a natural cost function representing the mismatch between the eigenstructure of the finite element model and the measured eigendata is:

$$J = \sum_{i=1}^r a_i \left(\frac{\lambda_i}{\bar{\lambda}_i} - 1 \right)^2 + \sum_{i=1}^r \sum_{j=1}^s b_{ij} (\phi_{ij} - \bar{\phi}_{ij})^2 \quad (3.2)$$

where the analytical eigenvalue for the i^{th} mode is denoted as λ_i and ϕ_{ij} denotes the j^{th} element of the i^{th} eigenvector from the analytical modal matrix Φ . The overbar indicates a measured quantity. The positive coefficients a_i and b_{ij} allow for individual weightings in the objective function. The summation upper limits r and s represent the number of eigenvalues/eigenvectors, and elements of the eigenvectors, respectively, from the measured data. With the objective function defined, each task can now be discussed by examining its relation to Equation (3.2).

3.1 Identification of Modal Parameters from Measured Data

The first task is the extraction of the system parameters $(\bar{\lambda}_i, \bar{\phi}_{ij})$ from the measured response data. This is accomplished through the use of the ERA method. ERA is a time domain approach based on the system's impulse response functions. On orbit, there are several difficulties associated with directly measuring impulse response functions. It is both difficult to apply the impulse, and difficult to obtain adequate signal/noise levels without imparting physical damage. An alternative method is to measure frequency response functions, and then perform an inverse Fourier transform to obtain the impulse response functions. The frequency response functions are averaged before performing the inverse operation to minimize the effect of noise corruption. Additionally, since acceleration measurements are used, a time integration (a division by $j\omega$ in the frequency domain) is used to obtain velocity measurements, and a second integration for displacements. The ERA method is then applied to the impulse data to determine a discrete-time state-space realization. This realization is then converted

to a continuous model and the modal properties determined via an eigenanalysis. The identified modal properties are used in the evaluation of Equation (3.2) either initially to tune the baseline FEM model or subsequently to identify damage.

3.2 *Model Tuning*

The objective of model tuning is the determination of small adjustments to the matrices in Equation (3.1) such that Equation (3.2) is minimized. An additional requirement is placed on the tuning method not to add or delete load paths in the model. This is imposed for two reasons. The first is so the model will correlate well with measured data of the damaged structure when the model is used to simulate a damaged configuration. The second is to ensure that changes in the matrices can be directly related to physical elements of the structure. The model tuning task was accomplished using ASTROS-ID, an automated multidisciplinary software package.^[18] The method employed uses a mathematical optimization strategy to minimize deviations between measured and analytical modal frequencies and partial mode shapes. Search directions are determined based on eigenvalue and eigenvector sensitivities to design variables. A mode tracking algorithm is also incorporated to identify and account for mode switching during the optimization process. It will be demonstrated in Sections 6.4 and 8.2.4 that ASTROS-ID can also be utilized for damage identification by restricting the allowable changes to the matrices in Equation (3.1), only allowing changes which are consistent with structural damage.

3.3 *Damage Identification Using Assigned Partial Eigenstructure*

An alternative to the sensitivity based approach to the minimization of Equation (3.2) is achieved through the use of an assigned partial eigenstructure (APE) method. Using the identified eigenstructure of the damaged structure $(\bar{\lambda}_i, \bar{\phi}_i)$, and the tuned FEM model (M, K) , the APE method is applied to determine the magnitude of the combinations of the fictitious actuators required to match the measured data. For damage identification, it is assumed that the damage is confined to changes in the stiffness matrix (K) of the FEM model which are consistent with the FEM formulation. Additionally, only decreases in the stiffness matrix are permitted. The results of a damage localization analysis is used to establish the initial search space for the given measured data. The minimization of Equation (3.2) is accomplished by appending the eigenstructure constraint of Equation (3.1) along with the structural constraint to form the Lagrangian, which is then differentiated to determine the necessary conditions.

When only a subset of the total degrees-of-freedom are measured, an iterative scheme is required to solve the necessary conditions.

3.4 *Sensor Prioritization and Damage Localization*

With only minimal sensor information available, two questions naturally arise: (1) at which locations should the sensors be placed, and (2) to what extent can damage be identified with the selected sensor locations? An eigenstructure sensitivity based method is presented to answer these questions. The method presented is based on examining the first-order partial eigenstructure sensitivity to changes in the structural stiffness of each element of a finite element model. No *a priori* knowledge of the damage location is assumed. Two aspects of the partial eigenstructure sensitivity are explored. First is the amount by which variations of the elemental stiffness values change the measured partial eigenstructure. Independent of the damage detection scheme used, elements which produce little or no change in the measured data, and consequently in the cost function J of Equation (3.2), will be difficult or impossible to detect when damaged. Second is the direction of change in the partial eigenstructure. Elements which produce similar or identical changes in the partial eigenstructure will be difficult or impossible to distinguish between when damaged. Therefore, sensor locations are chosen so that the change in the measured partial eigenstructure due to damage is maximized. Localization of the damage to an element(s) is based on both the amount and direction of change to the partial eigendata for the chosen sensor locations.

3.5 *Summary*

This chapter provided an overview of the four tasks associated with damage identification and presented the methodology that will be used to accomplish each task. In the following chapters, the mathematical basis for each task will be presented along with a description of how this was implemented in software. An analytical example using a 41-element 8-bay planar free-free truss is presented to illustrate each task.

IV. Identification of Modal Parameters from Measured Data

4.1 Overview

Independent of the damage identification or model tuning method used is the requirement to measure modal data $(\bar{\lambda}_i, \bar{\phi}_i)$. System identification using ERA reconstructs the transfer functions based on identification of the system's impulse-response functions. A disadvantage with this method is the requirement to excite the system with an impulse. This may be impractical to implement on certain systems, and it may be difficult to obtain response levels which are significantly above the measurement noise levels. An alternative procedure is obtained using time-averaged frequency response functions to obtain the impulse response functions, as discussed next.

4.2 Obtaining Measured Data

It is assumed that the flexible space structure is equipped with at least one disturbance actuator (input) and is instrumented with at least one accelerometer (output). From random vibration testing, the averaged frequency response functions are computed for each input/output combination. This is done by exciting the structure with a band-limited pseudo-random noise sequence applied to each actuator. The method below details the computations for a single applied input series $u(t)$ and a single measured output series $y(t)$. The extension to the MIMO case is simply a matter of subscripting the input/output pairs. The definition of the discrete Fourier transform of each measured input and output time series $u(t)$ and $y(t)$, consisting of N points sampled with sample period T is given as:

$$U(k) = \sum_{i=0}^{N-1} u(i) e^{-j \frac{2\pi i k}{N}} \quad k = 0, 1, \dots, N-1 \quad (4.1)$$

From this, the auto spectra $\Psi_{uu}(k)$ and cross spectra $\Psi_{uy}(k)$ are computed using:

$$\Psi_{uu}(k) = \frac{T}{N} U(k)^* U(k) \quad k = 0, 1, \dots, N/2 - 1 \quad (4.2)$$

and

$$\Psi_{uy}(k) = \frac{T}{N} U(k)^* Y(k) \quad k = 0, 1, \dots, N/2 - 1 \quad (4.3)$$

where $(\bullet)^*$ represents the complex conjugate operation and $U(k)$ and $Y(k)$ are the discrete Fourier transforms of the sampled input/output time series. Averaged spectral estimates $\Psi_{uy}(k)$, are then

obtained from m sample sets by:

$$\Psi_{uy}(k) = \frac{1}{m} \sum_{p=1}^m \Psi_{uyp}(k) \quad k = 0, 1, \dots, N/2 - 1 \quad (4.4)$$

The averaged frequency response functions (FRF) denoted as $H_{uy}(k)$, are then obtained from:

$$H_{uy}(k) = \frac{\Psi_{uy}(k)}{\Psi_{uu}(k)} \quad k = 0, 1, \dots, N/2 - 1 \quad (4.5)$$

The impulse response function $h(i)$, is computed for each input/output combination from the definition of the inverse Fourier transform, given as:

$$h(i) = \sum_{k=0}^{N-1} H_{uy}(k) e^{-j \frac{2\pi i k}{N}} \quad i = 0, 1, \dots, N - 1 \quad (4.6)$$

This “averaged” impulse response function can then be used as an input to a time domain identification algorithm such as the ERA.

4.3 Eigensystem Realization Algorithm (ERA)

ERA is based on the singular value decomposition of the block Hankel matrix.^[62] Consider the MIMO discrete-time linear system described by:

$$x(k+1) = Ax(k) + Bu(k) \quad (4.7a)$$

$$y(k) = Cx(k) + Du(k) \quad (4.7b)$$

where (A, B, C, D) are of dimension $(n \times n)$, $(n \times p)$, $(q \times n)$, and $(q \times p)$ respectively. A solution to the Markov parameters * is determined from a unit impulse response Y as:

$$Y(k) = CA^{k-1}B \quad (4.8)$$

*The discrete impulse sequence is commonly referred to in the literature as the Markov parameters.^[32]

The ERA method determines the Markov parameters by forming the block Hankel matrix $H(k)$, composed of the sampled unit impulse response.

$$H(k-1) = \begin{bmatrix} Y(k) & \cdots & Y(k+n_c) \\ \vdots & \ddots & \vdots \\ Y(k+n_r) & \cdots & Y(k+n_r+n_c) \end{bmatrix} \quad (4.9)$$

where n_r and n_c are arbitrary integers satisfying the inequalities $qn_r \geq n$ and $pn_c \geq n$. The singular value decomposition of H evaluated at $k = 1$ is expressed as:

$$H(0) = PDQ^T \quad (4.10)$$

The matrices P and Q contain the left and right singular vectors respectively, and D is a diagonal matrix containing the singular values. The discrete-time minimum-order model is then computed from the decomposition as:

$$A_d = D_n^{-1/2} P_n^T H(1) Q_n D_n^{-1/2} \quad (4.11a)$$

$$B_d = D_n^{1/2} Q_n^T E_p \quad (4.11b)$$

$$C_d = E_q^T P_n D_n^{1/2} \quad (4.11c)$$

$$D_d = Y(0) \quad (4.11d)$$

The subscript n represents the first n columns of P and Q . The matrix D_n is a diagonal matrix composed of the n non-zero singular values. E_p^T is $[I_p, 0]$, and E_q^T is $[I_q, 0]$ where I_p and I_q are identity matrices of order p and q respectively and 0 is the zero matrix. A transformation from the z -plane to the s -plane based on the sample rate of the impulse data, can then be performed if a continuous model is desired. The original development of the ERA algorithm is given in Juang and Pappa.^[32] The condensed derivation presented above was based on work by Crassidas *et al.*^[12] Determining D_n from D in Equation (4.10) when using noise corrupted data may be difficult since there are no longer only n non-zero singular values. The effects of noise on the sampled data is presented in subsequent papers by Juang and Pappa^[33], and Akers and Bernstein.^[11] Alternative strategies have been investigated to handle noisy measurements and are found in the literature.^[26,34,54]

The ERA identified quadruple (A_d, B_d, C_d, D_d) is used as the basis for the identified eigenstructure. However, when comparing eigenvectors as in Equation (3.2), it is required that the components of the eigenvectors represent the same coordinates for a meaningful comparison. Clearly the eigenvectors of the A_d matrix will vary depending upon the realization used. The ERA method produces an equivalent (from the input/output point of view) but different state-space realization. Although the full-length state vector can never be recovered if only limited sensors are used, the measured partial eigenvector can be directly related to the instrumented degrees-of-freedom through the transformation:

$$\bar{\phi}_i = C_d \bar{\Phi}_{c_i} \quad (4.12)$$

The matrix C_d is the output matrix determined by ERA. The vector $\bar{\Phi}_{c_i}$ is the i^{th} eigenvector of the matrix A_c . The matrix A_c is the state-space A_d matrix from ERA after a conversion from the discrete to the continuous domain based on the sample rate. The relationship between continuous and discrete time is given as:

$$A_d = e^{A_c T} \quad (4.13a)$$

$$B_d = \int_0^T e^{A_c \tau} B_c d\tau \quad (4.13b)$$

$$C_d = C_c \quad (4.13c)$$

$$D_d = D_c \quad (4.13d)$$

This assumes a zero-order hold on inputs over the sample period T . The subscripts c and d denote continuous and discrete respectively.

4.4 Software Implementation

When using experimental frequency response data obtained from accelerometer measurements, some pre-processing of the frequency response measurements is required. The first is a double time integration to obtain displacement measurements. This enables the identification of strictly proper transfer functions. This also results in compatible data between the measured and FEM data, since the FEM eigenvector data represents nodal displacement and rotation information. The time integration is accomplished efficiently by a division of the frequency response function by the complex number $j\omega$

where ω is the frequency in radians corresponding to each data bin. For the double time integration, the divisor is simply $-\omega^2$. Next, to avoid the consequence of dividing by zero, the first few data points in the frequency response function are artificially set to zero and no division is performed. This is equivalent to removing any bias from the measurements. The first few bins represent the steady-state component. Typically, the accuracy of the accelerometers for very low frequencies is poor, and therefore no valuable data is lost by zeroing out this portion. Lastly, for the particular analyzer used in this experiment (see Hardware Section 8.3.1), only data corresponding to 0 - 80% of the Nyquist^[17] frequency of the complex frequency response is output for analysis. Thus, before an inverse Fourier transform can be performed, the data is padded with zeros (acting as low pass filter) up to the Nyquist frequency, and then reflected about the real and imaginary axes to obtain the full symmetric spectrum. For example, data consisting of 4096 real sampled time points, results in 2048 unique complex points. Of the 2048 complex points, only 1601 are statistically reliable due to aliasing effects, and thus this is all that is available for analysis. To obtain a discrete-time model based on the same sample rate as the recorded data it is necessary to use the full 4096 point symmetric spectrum for use in Equation (4.6). To achieve this, the 1601 complex points are expanded to 2048 points by padding with zeros, and then the symmetric portion is reconstructed to achieve the full 4096 complex points. This reconstructed set of 4096 points is used in the computation of the impulse response function as given in Equation (4.6). This is repeated for each measured frequency response function.

From the impulse response functions, the block Hankel matrix is constructed according to Equation (4.9), using the results of Equation (4.6). The size of the block Hankel matrix is chosen based on the desired number of modes to be identified and is selectable as a parameter in the software. In general, the block Hankel matrix is not square, unless there are an equal number of inputs and outputs. For computational efficiency only the singular values and vectors corresponding to the smaller dimension need be computed. The state-space representation is found from the singular value decomposition using Equations (4.11). After a conversion from discrete to continuous time using MATLAB[®]'s **d2cm** algorithm, the measured frequencies and shapes are obtained from an eigenanalysis of the matrix A_c and Equation (4.12) to obtain $(\bar{\lambda}_i, \bar{\phi}_i)$. The sequence of events required for the identification of the modal parameters is depicted in Figure 4.1.

4.5 An Analytical Example

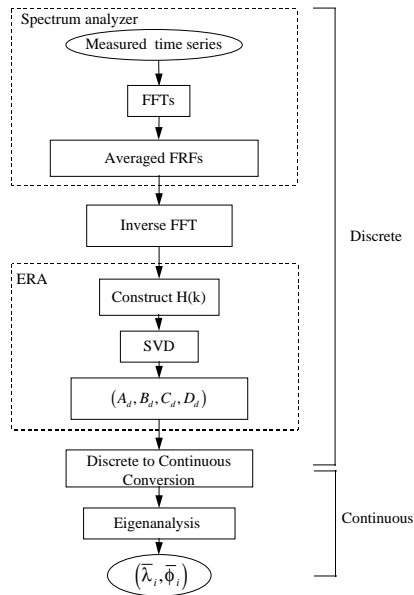


Figure 4.1 Sequence of events for identification of modal parameters.

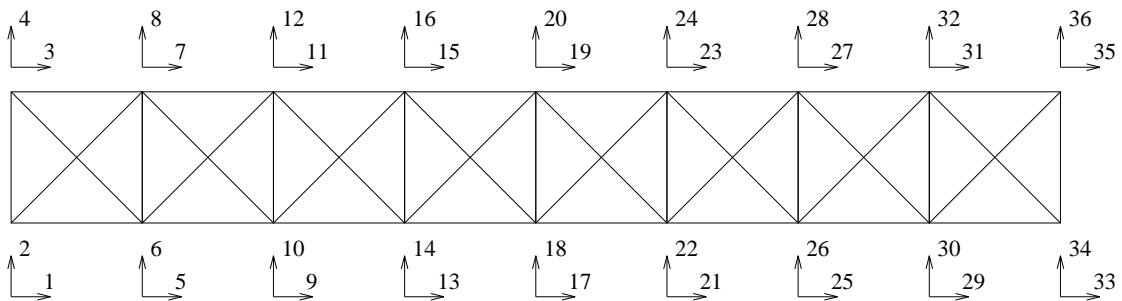


Figure 4.2 41-element free-free planar truss example showing degree-of-freedom numbering.

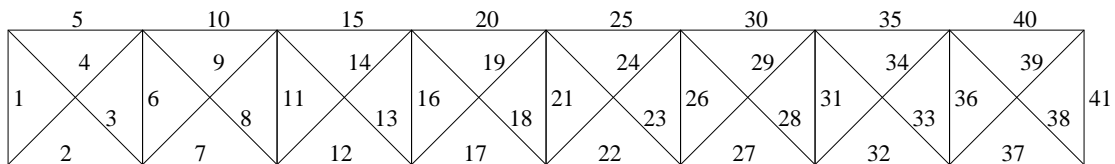


Figure 4.3 41-element free-free planar truss example showing element numbering.

To illustrate the contribution of each of the four tasks to the damage identification problem, a 41-element 8-bay planar free-free truss was chosen, which is the planar analogue of the Flexible Truss Experiment described in Section 8.3. The truss was modeled using forty-one rod elements, with two translational degrees-of-freedom per node. The vertical and horizontal members were constructed of aluminum with a cross-sectional area of 0.373 square inches and thirty inches in length. The diagonal members were modeled as Lexan (polycarbonate), with a cross-sectional area of 0.540 square inches, an elastic modulus 20 times less stiff than aluminum and 70% percent less dense. The density of all members was equally scaled to produce natural frequencies for the first few flexible modes on the order of 10 Hertz. This configuration was also chosen because it exhibits attributes common to on-orbit flexible structures which include: a low fundamental frequency, rigid body motion, minimal structural damping, and structural symmetry. Redundant diagonal members were included in each bay to help illustrate the concept of damage localization. Figure 4.2 shows the degree-of-freedom numbering scheme and Figure 4.3 show the element numbering scheme. An excitation actuator was simulated at degree-of-freedom # 2 for vibration testing. Four accelerometers were placed at degree-of-freedom numbers 2, 10, 18, and 26.

To test the ERA method, a simulation of the measured data was performed. The analytical model was used to generate four sampled-data time series at the instrumented degrees-of-freedom to a random input sequence. A second random sequence was added to each output time series to simulate the effect of noise corruption. A metric of the root-mean-square (RMS) value of the noise signal divided by the RMS value of the original signal was used to define the noise corruption level. Fourier transforms of these simulated signals were computed and averaged to compute the averaged frequency response functions as described in Section 4.2. The data was sampled at a 100 Hz rate using 1024 sample points and 25 averages. One percent of critical damping for all modes was included in the analytical model to ensure the response functions were bounded. Using these simulated frequency response functions, the ERA identified eigenvalues and eigenvectors were computed and compared to the FEM results. The results are tabulated in Table 4.1 for the first five flexible modes.

A study was conducted to illustrate the effect of both the noise level on the measurements as well as the selected size of the block Hankel matrix. The number of sample points used in the construction of the block Hankel matrix for a fixed number of inputs/outputs (1/4) was varied, as well as the measurement noise level. Increasing the number of sample points increases the computation

Table 4.1 41-element free-free planar truss eigenvalues.

Mode #	True Frequency (Hz)	ERA (Hz) [†]	
		clean	10% noise
1	5.90	5.90	5.90
2	10.59	10.59	10.59
3	15.67	15.67	15.67
4	20.35	20.35	20.34
5	25.14	25.14	25.13

[†]Data presented for 75 sample points used in construction of the Hankel matrix.

time required to decompose the block Hankel matrix. The results shown in Figure 4.4 illustrate that, for an increase in noise, a larger number of sample points is required to achieve the same relative error in the measured eigendata. The identification error was the value of J as defined in Equation (3.2) with unity weightings. For the actual test configuration, the number of sensors available and the noise level are predetermined quantities. Thus, in the determination of $(\bar{\lambda}_i, \bar{\phi}_i)$, it is desirable to use as many sample points as computationally feasible in the construction of the block Hankel matrix. All subsequent identification using ERA will adopt this approach.

In general, a similar study can be performed to illustrate the effect of adding additional inputs or outputs to extract the modal quantities. This is particularly important when there are modes which are either uncontrollable or undetectable from the chosen input/output set. For this analytical example however, the first five flexible modes are both controllable and observable from the input/output set, and thus no further ERA analysis on this model was performed. In a separate study, this software was applied to an experimental large, lightly damped space structure to produce a state-space representation. The results are reported in Reference 69.

4.6 Summary

The identification of modal parameters from measured frequency response functions was presented using the ERA method. Averaging in the frequency domain was performed to mitigate noise effects. A description of how this algorithm is implemented in software was presented along with the results of the method applied to an analytical example. The identified $(\bar{\lambda}_i, \bar{\phi}_i)$ pairs can then be used either to tune the FEM model as described in Chapter V, or identify structural damage as described in Chapter VI.

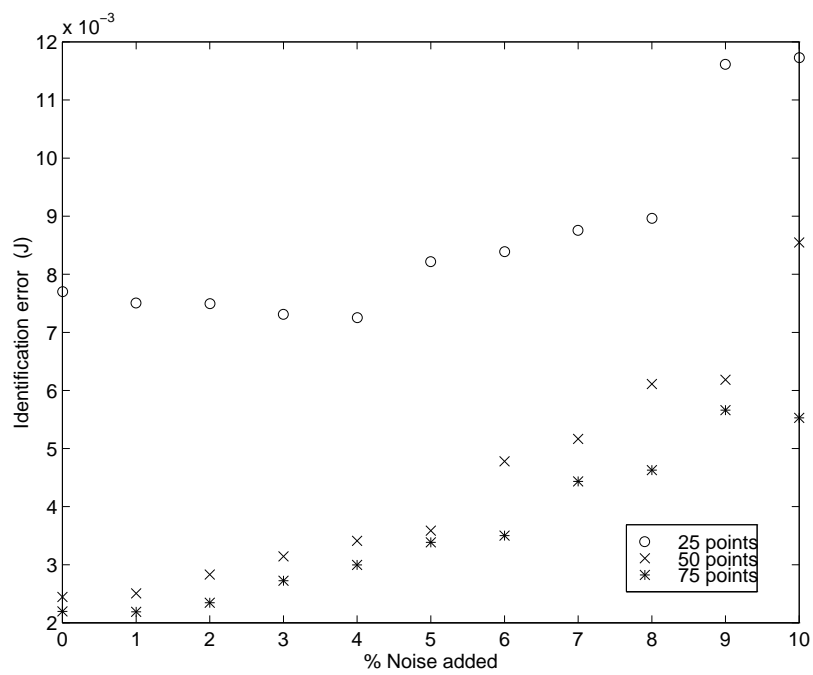


Figure 4.4 Effect of sample size and measurement noise on the ability to extract eigendata using ERA.

V. Model Tuning Using ASTROS-ID

5.1 Overview

Accurate prediction and simulation of the dynamic behavior of large flexible space structures require analytical models which agree with measured data. Unfortunately, uncertainty in a finite element model (FEM) implies less than perfect correlation between analytical and measured data. When the disagreement is deemed unacceptable, it is necessary for the design engineer to make adjustments to the FEM. For large problems the number of potential parameters to adjust, such as elemental areas, elastic moduli, inertia moments, etc., quickly becomes overwhelming. Thus a systematic method is required to ensure that the adjustments produce the desired results. To this end, a method is introduced which poses a numerical optimization problem. Namely, given a set of measured eigenvalues and partial eigenvectors, determine the values of selected physical parameters of the model which minimize the weighted deviations from the analytical eigenvalues and eigenvectors.

ASTROS-ID represents an automated method of adjusting analytical finite element models to measured data. The algorithm uses a mathematical optimization strategy to minimize deviations between measured and analytical modal frequencies and partial mode shapes. A mode tracking algorithm is used to identify and account for mode switching during the optimization process.

A critical aspect to any model tuning algorithm is its practical implementation. Key advantages to the method presented herein include its ability to handle a small subset of the total eigenstructure of the system without using an eigenvector expansion method, and the ability to track mode switches during the tuning process. This optimization strategy was implemented using the Automated Structural Optimization System (ASTROS) software package, developed by Wright Laboratory.^[58] The present research work is an extension to the work begun by Gibson on the software modules ASTROS-ID, an enhancement to ASTROS to incorporate system identification.^[18] The overall intent of this software enhancement is to enable the user to input a set of desired modal frequencies and partial modal vectors and then iterate on a set of structural parameters to minimize deviations between analytical and experimental measurements.

5.2 Theory

Model tuning is performed by minimizing an objective function based on a weighted sum of deviations from measured eigenvalues and partial eigenvectors. The free vibration of the structure is modeled as:

$$Mx + Kx = 0 \quad (3.1)$$

Assuming real eigenvalues and eigenvectors, the objective function as previously defined is given as:

$$J = \sum_{i=1}^r a_i \left(\frac{\lambda_i}{\bar{\lambda}_i} - 1 \right)^2 + \sum_{i=1}^r \sum_{j=1}^s b_{ij} \left(\phi_{ij} - \bar{\phi}_{ij} \right)^2 \quad (3.2)$$

The summation upper limits r and s represent the number of eigenvalues/eigenvectors, and elements of the eigenvectors, respectively, chosen to be tuned. The minimization of the objective function J is carried out in an inner and outer loop fashion. The outer loop consists of performing the eigenanalysis, normalizing and matching analytical and measured modes, calculating design parameter sensitivities, updating design variables, and detecting solution convergence. The inner loop solves an approximate optimization problem after each outer-loop eigenanalysis using the new design variable sensitivity information. The inner loop is an approximate solution because the sensitivity information is used to project new values of the analytical eigenvalues and eigenvectors for given changes in the design variables without recomputing the eigenanalysis. Once the approximate problem is solved by a general constrained optimization method, control is passed to the outer loop where the variables are updated and a new eigenanalysis is performed. The details of computing the sensitivity information as well as the mode normalization and tracking is discussed next. The problem considered herein assumes a real eigenanalysis with unique eigenvalues, and for simplicity is not developed for the case where damping is included in the finite element formulation.

5.2.1 Eigenvalue Sensitivity. A second-order Taylor series expansion is used to project new eigenvalue values to given design variable changes contained in the vector Δg . The expansion is given as:

$$\lambda_i \cong \lambda_{oi} + \nabla \lambda_i^T \Delta g + \frac{1}{2} \Delta g^T (\nabla^2 \lambda_i) \Delta g \quad (5.1)$$

where λ_{oi} denotes the initial eigenvalue resulting from the eigenanalysis. The j^{th} element of the eigenvalue gradient vector $\nabla \lambda_i$ is given as:^[61]

$$\lambda_{i,j} = \frac{\Phi_i^T [K_{,j} - \lambda_i M_{,j}] \Phi_i}{\Phi_i^T M \Phi_i} \quad (5.2)$$

where a comma denotes differentiation with respect to a design variable. The elements of the Hessian matrix $\nabla^2 \lambda_i$ are given as:

$$\lambda_{i,jk} = \frac{\Phi_i^T [F_{i,j} \Phi_{i,k} + F_{i,k} \Phi_{i,j}] - [\lambda_{i,j} \Phi_i^T M_{,k} \Phi_i + \lambda_{i,k} \Phi_i^T M_{,j} \Phi_i]}{\Phi_i^T M \Phi_i} \quad (5.3)$$

with $F_{i,j}$ defined as:

$$F_{i,j} \equiv K_{,j} - \lambda_i M_{,j} - \lambda_{i,j} M \quad (5.4)$$

The notation $(\bullet)_{i,j}$ represents differentiation with respect to the j^{th} design variable of some quantity (\bullet) , associated with the i^{th} mode. The decision to include a second-order approximation, rather than only a first order, was due to the fact that the terms appearing in the second-order eigenvalue gradient are already computed when calculating the first-order eigenvector gradients. Equations (5.2) and (5.3) include the scalar normalization term $\Phi_i^T M \Phi_i$. Thus the eigenvector normalization will scale the eigenvalue gradients. Proper choice of eigenvector normalization is addressed in the next section. Design sensitivities of the mass and stiffness matrices M and K are known explicitly from the finite element formulation, and can thus be computed using either analytical derivatives or finite-difference methods. Eigenvalue sensitivity for each mode included in the objective function is computed according to Equations (5.2) and (5.3). The eigenvector derivatives in Equation (5.3) can be computed by a modal expansion^[16] or more efficiently by Nelson's method^[56] when only a subset of eigenvectors are involved, as explained next.

5.2.2 Eigenvector Sensitivity and Normalization. A first-order Taylor series expansion is used to project the new value of the eigenvector based on the current eigenvector value Φ_{oi} and the eigenvector gradient $\nabla \Phi_i$. The expansion is computed for each degree-of-freedom in the eigenvector set. The expansion of the k^{th} term of the eigenvector for the i^{th} mode is given as:

$$\phi_{ik} \cong \phi_{oik} + \nabla \phi_{ik}^T \Delta g \quad (5.5)$$

The eigenvector gradient is found by first differentiating the eigenvalue equation for each mode with respect to each design variable:

$$[K - \lambda_i M] \Phi_{i,j} = [\lambda_{i,j} M + \lambda_i M_{,j} - K_{,j}] \Phi_i \quad (5.6)$$

Since the bracketed term on the left hand side is necessarily singular by definition, the solution to $\Phi_{i,j}$ is found by employing Nelson's method. The problem is solved by separating $\Phi_{i,j}$ into the sum of a particular and homogeneous solution given as:

$$\Phi_{i,j} = c_{ij} \Phi_i + V_{ij} \quad (5.7)$$

Assuming there are no repeated roots, and $[K - \lambda_i M]$ is an $(n \times n)$ matrix, then its rank is $n - 1$. Thus the homogeneous solution is found by eliminating a row and column and then performing the inverse.

$$\tilde{V}_{ij} = [\tilde{K} - \lambda_i \tilde{M}]^{-1} [\lambda_{i,j} \tilde{M} + \lambda_i \tilde{M}_{,j} - \tilde{K}_{,j}] \tilde{\Phi}_i \quad (5.8)$$

and

$$V_{ij} = [\tilde{V}_{1j}, \dots, \tilde{V}_{(l-1)j}, 0, \tilde{V}_{lj}, \dots, \tilde{V}_{(n-1)j}]^T \quad (5.9)$$

The $(\tilde{\bullet})$ notation denotes matrices reduced by one row and column, or vectors reduced by one element. Nelson's method removes the row and column corresponding to the maximum entry in Φ_i . Equation (5.9) shows the expansion of \tilde{V}_{ij} to V_{ij} for the maximum entry occurring in the l^{th} entry. Note that the matrix inverse in Equation (5.8) need not be explicitly calculated. Rather, the reduced matrices can be used in Equation (5.6) and solved through matrix decomposition followed by forward and back substitution. To solve for the unknown scalar constant c_{ij} in Equation (5.7), a normalization constraint must be applied. The objective of the optimization is to minimize differences between measured and analytical modes, which clearly can only be computed when the eigenvectors are normalized in the same manner. To achieve this objective, a point normalization scheme is used in which eigenvectors are normalized such that the degree-of-freedom with maximum amplitude in the measurement set is set to unity. Presumably, this would also correspond to a degree-of-freedom in which there was high measurement confidence (i.e., high signal/noise ratio). This is important because the analytic gradient of this degree-of-freedom will be identically zero. It is not practical nor useful for

optimization to normalize eigenvectors based on the analytical model, such as by mass normalization, since the analytical matrices are the unknowns in the optimization routine. However, mass normalized analytical eigenvectors are useful in detecting mode switches as discussed in the next section. After each eigenanalysis in the outer loop, the eigenvectors used in the objective function must be point normalized per the measurement data. Having chosen the degree-of-freedom normalization point for each mode, the normalization constraint for each mode can be expressed as:

$$\Phi_i^T S_i \Phi_i = 1 \quad (5.10)$$

where the matrix S_i contains only one non-zero entry, a one in the row and column corresponding to the normalization point for the i^{th} mode. Differentiating the constraint Equation (5.10) with respect to each design variable and substituting the result from Equation (5.7) yields:

$$\Phi_i^T S_i [c_{ij} \Phi_i + V_{ij}] = 0 \quad (5.11)$$

Due to the special form of the matrix S_i Equation (5.11) simplifies to:

$$c_{ij} = -(V_{ij})_{norm.pt.} \quad (5.12)$$

which is the negative of the element in vector V_{ij} corresponding to the normalization point for the i^{th} mode. The point normalized eigenvectors must be used in calculating the term $\Phi_i^T M \Phi_i$ in Equations (5.2) and (5.3) to ensure proper scaling of the eigenvalue and eigenvector sensitivities. The eigenvector sensitivity is computed for each mode included in the objective function. For measured modes where only frequency information (not shape) is available, a first-order Taylor series expansion is used in lieu of Equation (5.1).

The assumption of $[K - \lambda_i M]$ having no repeated roots for use in Equation (5.8) can potentially cause difficulties for structures with closely spaced modes. However, no difficulty was observed for the models tuned during this research effort, even though they contained closely spaced modes. An examination of the effects of repeated roots, and the required extension to Nelson's method to handle this case, is a recommended topic of future research.

5.2.3 *Mode Switch Detection.* For convenience, the engineer typically will assign a numbering scheme to the set of measured modes from an experimental analysis. It is imperative that the same numbering scheme be employed when comparing measured modes to analytical modes. Prior to the start of the optimization, this numbering scheme is most easily facilitated through the use of computer aided software capable of displaying mode shapes. At this point, the designer can pair up measured and analytical modes. Once the optimization starts however, it is necessary for the software to track the analytical mode sequencing. As the design variables change it is highly likely that mode switching will occur. Without mode tracking, an optimization scheme would become hopelessly lost trying to match bending modes to torsion modes, for example, and vice-versa. Mode tracking can be performed using cross orthogonality checking.^[18] If the eigenvectors are mass normalized, mode tracking can be accomplished by computing the modal correlation coefficient matrix between successive eigenanalysis solutions. The cross orthogonality matrix is given as:

$$O = \Phi^{(n-1)T} M^{(n)} \Phi^{(n)} \quad (5.13)$$

The modal matrix Φ includes only the eigenvectors computed in the eigenanalysis. The superscript n denotes the iteration number. Assuming mass orthonormalization, near unity values in O indicate high correlation between modes. Mode tracking is accomplished by searching over O successively for the largest absolute value. If the entry is in a diagonal location, this mode has not changed between iterations. An absolute maximum in a non-diagonal entry indicates the mode number switch between two iterations by its row and column position. After each mode is paired, the corresponding row and column are eliminated from O , and the search for the next pair is accomplished on the reduced matrix until all modal pairs are found. As discussed previously, mode switch detection is done in the outer optimization loop, just prior to point normalization and eigensensitivity calculations.

5.3 *Software Implementation*

This model tuning technique was implemented using the structural design software ASTROS. This software uses an executive control sequence called MAPOL (Matrix Analysis Problem Oriented Language) to develop the solution sequence. MAPOL allows the user to incorporate custom software modules into the solution sequence while maintaining full access to the ASTROS solution modules.

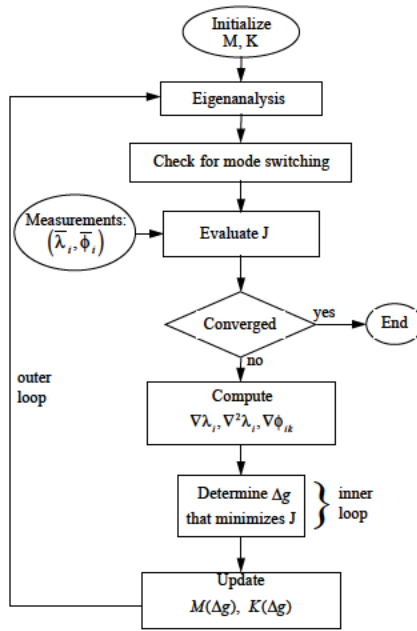


Figure 5.1 ASTROS-ID decision flow.

For the problem at hand, software modules written in FORTRAN 77 were developed (or modified from Gibson's original work) for eigenvector normalization, mode switch testing, eigenvalue and eigenvector sensitivities, objective function evaluation, and processing data to and from the optimization module. A small section of MAPOL code is then inserted into the standard ASTROS solution sequence to control the calling of these new modules. Tuning information (desired frequencies, mode shapes and the corresponding weighting values) are appended to the standard bulk data input. It should be noted that the actual software implementation was less restrictive than that given in Equation (3.2), in that it allowed for a different number of measured components for each mode if desired. This is applicable in situations where numerous frequencies can be measured, but only a few shapes. Additional information on the use of ASTROS as a multidisciplinary design tool can be found in References 55 and 51. The decision chart for ASTROS-ID is shown in Figure 5.1. A brief description of modifications to the original software modules along with a description of new modules is contained in Appendix A.

5.4 Selection of Tuning Parameters

Before the optimization can be performed, the designer must choose a set of design variables. In ASTROS, the design variable for a beam element is the beam's cross-sectional area, because weight minimization is typically the overall objective. In model tuning however, other properties such as the elastic moduli, mass, or both may be the desired design variables. To accommodate the ability to tune more than one property of an element, superposition can be used. To illustrate this method, consider tuning the mass and elastic modulus of a beam between two nodes. Using two beam elements, one with the elastic modulus set to zero and a second with the density property set to zero, will have the combined effect of a single beam element. However, now both properties can be set as design variables. Note that adjusting the cross-sectional area of a beam with a zero elastic modulus is equivalent to adjusting the density property of that beam. A similar relation is true for the beam element with zero mass density. In a similar fashion, the torsional properties of the beam can be varied independently. Using this technique allows the user a wide choice of design variables.

Selection of which design variables to vary is dependent on the designer's objective and is problem dependent. If in the development of the finite element model some of the more complicated geometries were simplified using equivalent but uncertain parameters, then these parameters are the natural choice for the design variables. If however, the objective is damage identification, then design variables must be chosen which relate directly to damagable elements. Furthermore, a design variable may be associated with a group of elements. For tuning, it may be desirable to assign a single design variable to the elastic modulus of all the longitudinal elements. In this way, any symmetry present in the structure will be retained throughout the tuning process. For damage identification, it is required that a unique design variable be assigned to each element, in order to isolate the damage. In general, the search space (number of design variables) will be much larger for the damage identification problem than for model tuning. A method of reducing the initial search space is presented in Chapter VII on damage localization. A discussion of the choice of design variables is presented for the analytical example below, and for the experimental models in the Chapter VIII.

5.5 An Analytical Example

To illustrate the use of model tuning using ASTROS-ID, a 41-element free-free planar truss depicted in Figures 4.2 and 4.3 was modeled with the density of all the elements at 90% of the true

Table 5.1 Frequency values for the tuned 41-element free-free planar truss.

Mode #	Frequency (Hz)		
	True value	Initial value	Tuned value
1	5.90	6.51	5.90
2	10.59	12.01	10.59
3	15.67	17.89	15.67
4	20.35	23.37	20.35
5	25.14	28.90	25.14

value and the elastic modulus at 120% of the true value for the diagonal elements. The measured data $(\bar{\lambda}_i, \bar{\phi}_i)$ was taken to be that of the truss using the true density and stiffness values (see Table 4.1). The design variables were chosen as follows. Because the uncertainty in the density of all members was assumed equal, the density of all structural members was set to a single design variable. To account for the possible uncertainty in the joint connections, the elastic modulus of the vertical, horizontal, and diagonal members was chosen as three separate design variables. For this set of design variables, the elastic modulus of the different types of members could be varied independently, but all members of the same type (horizontal, vertical, diagonal) would vary simultaneously. Note that the selection of these four design variables was made only to illustrate the tuning method, and do not represent any true uncertainty in this theoretical model.

The measured data consisted of the first five flexible modes at the same four instrumented degrees-of-freedom (2, 10, 18, 26), as used in Chapter IV. Equal weighting was placed on all measured values in Equation (3.2). The results of the tuning are listed in Table 5.1 for the changes in the natural frequencies. The corresponding design variable changes are listed in Table 5.2. Three outer-loop iterations were required, which decreased the objective function seven orders of magnitude. To the numerical precision of the input data, the objective function was zero. As can be seen from the data in Table 5.1, the true values were not completely recovered, although the objective function was zero. This is a result of using only partial data in the objective function. The achieved solution is not necessarily unique. This is particularly true when both the mass and stiffness values are allowed to vary, as was the case for this example. For damage identification, variations will be confined to the stiffness matrix.

Table 5.2 Design variable values for the tuned 41-element free-free planar truss.

Design variable	True	Initial	Tuned
density (all)	1	.9	1.02
horizontal stiffness	1	1	1.02
vertical stiffness	1	1	1.00
diagonal stiffness	1	1.2	1.02
3 iterations in 46.5 seconds of cpu time.			

5.6 Summary

An algorithm was developed to tune finite element models to measured eigendata. Careful attention was placed on eigenvector normalization, and how the normalization relates to the computation of the eigenvalue and eigenvector sensitivities. Mode switches were successfully tracked through an analysis of the correlation coefficient matrix. Implementation of this algorithm in ASTROS makes this tuning procedure readily accessible to the design engineer during the finite element design phase. This level of experimentally validated automated tuning represents a substantial improvement over current capabilities. Natural applications of this algorithm include the identification of uncertain structural parameters, as well as the identification of damaged structural elements. This technique was successfully applied to an analytical model. Experimental results using ASTROS-ID for both model tuning and damage identification are contained in Chapter VIII.

ASTROS-ID requires an eigenanalysis and gradient evaluations at each outer-loop iteration, which can be computationally expensive. An alternative method to minimizing Equation (3.2) is pursued using an assigned eigenstructure method developed in the next chapter. Reduction of the initial search space, which will ease the computational burden, is presented in Chapter VII.

VI. Damage Identification Using Assigned Partial Eigenstructure

6.1 Overview

Presented is an algorithm to identify individual damaged structural elements of large flexible space structures using on-orbit data. Using measured partial eigendata, a control theoretic approach is applied in which fictitious actuators corresponding to each structural element are assumed. Using the identified partial eigenstructure $(\bar{\lambda}_i, \bar{\phi}_i)$ and these fictitious actuators, an assigned partial eigenstructure (APE) technique is employed on the analytical model of the undamaged structure. An identification of structural damage is obtained directly from the required control of the fictitious actuators (stiffness adjustment) to achieve the desired eigenstructure. This method represents an alternative to the gradient search technique using ASTROS-ID presented in Chapter V.

6.2 Theory

With minimal sensor information available, a natural cost function representing the mismatch between the eigenstructure of the finite element model and the measured eigendata is:

$$J = \sum_{i=1}^r a_i \left(\frac{\lambda_i}{\bar{\lambda}_i} - 1 \right)^2 + \sum_{i=1}^r \sum_{j=1}^s b_{ij} \left(\phi_{ij} - \bar{\phi}_{ij} \right)^2 \quad (3.2)$$

with all quantities as previously defined. A minimization of Equation (3.2) was developed in Chapter V to perform model updating using ASTROS-ID, in which the minimization is solved using the eigenvalue and eigenvector sensitivities at each iteration step. An alternative to computing these sensitivities (which still requires an eigenanalysis at each iteration step) is accomplished using APE, developed below.

The APE method is based on minimizing the same cost function given in Equation (3.2). Two initial assumptions are made. First, structural damage is confined only to changes in the stiffness properties of the structure. Second, structural damping is negligible. These two assumptions are consistent with most on-orbit damage scenarios of large flexible space structures. The free vibration of the undamaged structure is modeled as:

$$Mx + Kx = 0 \quad (3.1)$$

with the symmetric mass and stiffness matrices $M, K \in \mathfrak{R}^{n \times n}$, x representing the state vector and (\bullet) denoting a double time differentiation. With damage confined to the stiffness matrix, the damaged structure is modeled as:

$$Mx + (K - \Delta K)x = 0 \quad (6.1)$$

where ΔK represents an unknown perturbation to the stiffness as the result of structural damage. The eigenvalue and eigenvector for the i^{th} mode of Equation (6.1) is given as (λ_i, Φ_i) whereas the measured eigenvalue and partial eigenvector for the same mode is represented as $(\bar{\lambda}_i, \bar{\phi}_i)$. The relationship between the n dimensional eigenvector Φ_i and the partial eigenvector ϕ_i is $\phi_i = C\Phi_i$. The matrix $C \in \mathfrak{R}^{s \times n}$ maps the full length eigenvectors into the partial eigenvectors corresponding to the measured degrees-of-freedom. For the APE method, the cost function in Equation (3.2) based on the errors between the finite element model and the measured modes is rewritten in vector notation and is given as:

$$J = \frac{1}{2}(\lambda - \bar{\lambda})^T A(\lambda - \bar{\lambda}) + \frac{1}{2} \sum_{i=1}^r (\phi_i - \bar{\phi}_i)^T W_i (\phi_i - \bar{\phi}_i) \quad (6.2)$$

where $\lambda = [\lambda_1, \lambda_2, \dots, \lambda_r]$ for the r measured modes, with s degrees-of-freedom measured for each mode. The positive-definite constant matrices A and W can be used to weight the contribution of each term in the overall cost function. This cost function is then minimized subject to the eigenstructure constraint:

$$(-\lambda_i M + K - \Delta K)\Phi_i = 0 \quad (6.3)$$

where only r of the (λ_i, Φ_i) coupled with only s components of Φ_i are able to be measured. Additionally, to ensure ΔK is consistent with the finite element formulation, the structural constraint is represented as:

$$\Delta K = BGB^T \quad (6.4)$$

where B is constructed from the nodal connectivity information and the elemental parameters, and G is a diagonal matrix composed of the fraction of damage for each element. The parameterization of ΔK is best illustrated using a simple example. For a two degree-of-freedom spring mass system as shown in Figure 6.1, the equations-of-motion obtained from an application of Newton's second law are:

$$m_1 x_1 = -k_1 x_1 - k_2 (x_1 - x_2) \quad (6.5)$$

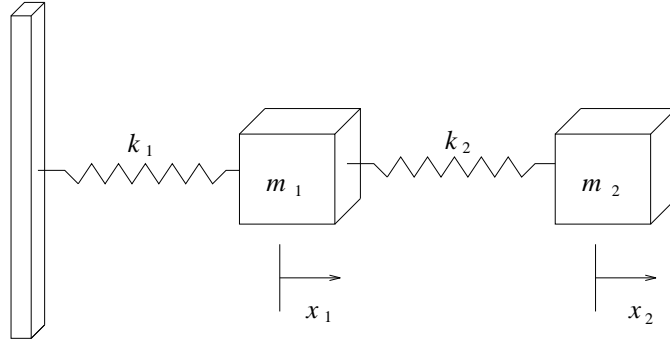


Figure 6.1 Example two degree-of-freedom system.

$$m_2 \ddot{x}_2 = -k_2(x_2 - x_1) \quad (6.6)$$

These equations can then be written in matrix form as:

$$\begin{bmatrix} m_1 & 0 \\ 0 & m_2 \end{bmatrix} \ddot{x} + \begin{bmatrix} k_1 + k_2 & -k_2 \\ -k_2 & k_2 \end{bmatrix} x = 0 \quad (6.7)$$

where the stiffness matrix K can then be written as:

$$K = \begin{bmatrix} k_1 + k_2 & -k_2 \\ -k_2 & k_2 \end{bmatrix} = \begin{bmatrix} 1 & -1 \\ 0 & 1 \end{bmatrix} \begin{bmatrix} k_1 & 0 \\ 0 & k_2 \end{bmatrix} \begin{bmatrix} 1 & -1 \\ 0 & 1 \end{bmatrix}^T \quad (6.8)$$

The matrix pre-multiplying the diagonal matrix in Equation (6.8) contains the structural connectivity information. For example, the first column corresponds to spring k_1 , which is connected only to degree-of-freedom x_1 , and hence has only a single non-zero entry in row one. The second column corresponds to spring k_2 , which is connected to both degree-of-freedom x_1 and x_2 , and hence both rows have non-zero entries. Direction cosines are used to determine the values of the non-zero entries, based on the relative position of the nodes. For this linear example, the direction cosines are plus and minus one. In the same fashion, the stiffness perturbation matrix ΔK can be expressed as:

$$\Delta K = \begin{bmatrix} \sqrt{k_1} & -\sqrt{k_2} \\ 0 & \sqrt{k_2} \end{bmatrix} \begin{bmatrix} g_1 & 0 \\ 0 & g_2 \end{bmatrix} \begin{bmatrix} \sqrt{k_1} & -\sqrt{k_2} \\ 0 & \sqrt{k_2} \end{bmatrix}^T = B G B^T \quad (6.9)$$

to a single design variable g_i ($g_i \cdot I_6$, where I_6 is the 6×6 identity matrix). Although developed explicitly herein only for rod and beam elements, any element's symmetric matrix ΔK_i can be written as BG_iB^T using the non-zero singular values and singular vectors of ΔK_i . The minimization of the cost function in Equation (6.2) is solved by forming the Lagrangian and establishing necessary conditions. The appended cost function J_i for the i^{th} mode is:

$$J_i = \frac{1}{2}a_i(\lambda_i - \bar{\lambda}_i)^2 + \frac{1}{2}(\phi_i - \bar{\phi}_i)^T W_i(\phi_i - \bar{\phi}_i) + \nu_i^T(-\lambda_i M + K - BGB^T)\Phi_i \quad (6.14)$$

where ν_i is a vector of Lagrange multipliers for the i^{th} mode. With $\phi_i = C\Phi_i$ this becomes:

$$J_i = \frac{1}{2}a_i(\lambda_i - \bar{\lambda}_i)^2 + \frac{1}{2}(\Phi_i - \bar{\Phi}_i)^T C^T W_i C(\Phi_i - \bar{\Phi}_i) + \nu_i^T(-\lambda_i M + K - BGB^T)\Phi_i \quad (6.15)$$

It is then assumed: $\exists G \ni \lambda_i = \bar{\lambda}_i$, $\forall i = 1, \dots, r$ implying there are sufficient design variables (structural elements) to achieve the measured eigenvalues. This is satisfied if the measured data is consistent with actual damage. For the case of noise corrupted measurements, $\lambda_i \approx \bar{\lambda}_i$, $\forall i = 1, \dots, r$, and is assumed to contribute negligibly to the cost function. With these assumptions, Equation (6.15) reduces to:

$$J_i = \frac{1}{2}(\Phi_i - \bar{\Phi}_i)^T C^T W_i C(\Phi_i - \bar{\Phi}_i) + \nu_i^T(-\bar{\lambda}_i M + K - BGB^T)\Phi_i \quad (6.16)$$

The necessary conditions for the minimization become:

$$\frac{\partial J_i}{\partial \nu_i} = (-\bar{\lambda}_i M + K - BGB^T)\Phi_i = 0 \quad (6.17)$$

$$\frac{\partial J_i}{\partial G} = \frac{\partial}{\partial G} (\nu_i^T BGB^T \Phi_i) = 0 \quad (6.18)$$

$$\frac{\partial J_i}{\partial \Phi_i} = C^T W_i C(\Phi_i - \bar{\Phi}_i) + [\nu_i^T(-\bar{\lambda}_i M + K - BGB^T)]^T = 0 \quad (6.19)$$

which can be rewritten as:

$$(-\bar{\lambda}_i M + K)\Phi_i - BGB^T \Phi_i = 0 \quad (6.20)$$

$$\frac{\partial}{\partial G} (\nu_i^T BGB^T \Phi_i) = 0 \quad (6.21)$$

$$C^T W_i C \Phi_i + (-\bar{\lambda}_i M + K) \nu_i - B G B^T \nu_i = C^T W_i \bar{\phi}_i \quad (6.22)$$

To pose this non-linear optimization problem as an approximate linear problem, it is necessary to introduce the matrix operator $\tilde{P}(\alpha, \beta)$. In the case where there is only one column of the matrix B associated with each design variable, such as for spring and rod elements as given in Equations (6.10 through 6.12), $\tilde{P}(\alpha, \beta)$ is defined as:

$$\tilde{P}(\alpha, \beta) \text{ with } \tilde{P} \text{ and } \beta \in \mathfrak{R}^{n \times p}, \alpha \in \mathfrak{R}^{n \times 1} \quad \tilde{P}_{ij} = \sum_{k=1}^n \alpha_k \beta_{ij} \beta_{kj} \quad (6.23)$$

where \tilde{P}_{ij} is the i^{th} row and the j^{th} column of the matrix \tilde{P} . In terms of the operator \tilde{P} , terms of the form $\beta \Gamma \beta^T \alpha$ can be written as:

$$\beta \Gamma \beta^T \alpha = \tilde{P}(\alpha, \beta) \gamma \quad \text{where } \gamma = \text{diag}(\Gamma) \text{ , } \Gamma \in \mathfrak{R}^{p \times p} (\text{diagonal}) \quad (6.24)$$

When there are multiple columns of B associated with a single design variable, such as given in Equation (6.13) for beam elements, an additional summation of the columns of \tilde{P} is required for each design variable. In the case where there are q columns of B for each design variable, $B \in \mathfrak{R}^{n \times pq}$, $G \in \mathfrak{R}^{pq \times pq}$ and hence $\tilde{P} \in \mathfrak{R}^{n \times pq}$ according to Equation (6.23). The summation is then defined as:

$$P = \left[\sum_{j=1}^q \tilde{P}_j \quad \sum_{j=q+1}^{2q} \tilde{P}_j \quad \cdots \quad \sum_{j=(p-1)q+1}^{pq} \tilde{P}_j \right] \text{ , } P \in \mathfrak{R}^{n \times p} \quad (6.25)$$

where \tilde{P}_j is the j^{th} column of \tilde{P} . Note that $P = \tilde{P}$ for the case where $q = 1$. Furthermore, constructing P from \tilde{P} gives the design engineer the ability to link multiple elements to a single design variable g_i as desired. In terms of the operator P , the following substitutions can be made in the necessary conditions:

$$B G B^T \Phi_i = P(\Phi_i, B) g \quad (6.26)$$

$$\frac{\partial}{\partial G} (\nu_i^T B G B^T \Phi_i) = P(\Phi_i, B)^T \nu_i \quad (6.27)$$

$$B G B^T \nu_i = P(\nu_i, B) g \quad (6.28)$$

The necessary conditions, with these substitutions become:

$$(-\bar{\lambda}_i M + K) \Phi_i - P(\Phi_i, B) g = 0 \quad (6.29)$$

$$P(\Phi_i, B)^T \nu_i = 0 \quad (6.30)$$

$$C^T W_i C \Phi_i + (-\bar{\lambda}_i M + K) \nu_i - P(\nu_i, B) g = C^T W_i \bar{\phi}_i \quad (6.31)$$

which can now be written in matrix form for the i^{th} mode as:

$$\begin{bmatrix} (-\bar{\lambda}_i M + K) & 0 & -P(\Phi_i, B) \\ 0 & P(\Phi_i, B)^T & 0 \\ C^T W_i C & (-\bar{\lambda}_i M + K) & -P(\nu_i, B) \end{bmatrix} \begin{bmatrix} \Phi_i \\ \nu_i \\ g \end{bmatrix} = \begin{bmatrix} 0 \\ 0 \\ C^T W_i \bar{\phi}_i \end{bmatrix} \quad (6.32)$$

Then since g , the vector of fractional structural damage for each element (g_i) is the same for each measured mode, the necessary conditions can be assembled as:

$$N \begin{bmatrix} \Phi_1 \\ \nu_1 \\ \vdots \\ \Phi_r \\ \nu_r \\ g \end{bmatrix} = \begin{bmatrix} 0 \\ 0 \\ C^T W_1 \bar{\phi}_1 \\ \vdots \\ 0 \\ 0 \\ C^T W_r \bar{\phi}_r \end{bmatrix} \quad (6.33)$$

where

$$N = \begin{bmatrix} (-\bar{\lambda}_1 M + K) & & & & & -P(\Phi_1, B) \\ & P(\Phi_1, B)^T & & & & \\ C^T W_1 C & (-\bar{\lambda}_1 M + K) & & & & -P(\nu_1, B) \\ & & \ddots & & & \vdots \\ & & & (-\bar{\lambda}_r M + K) & & -P(\Phi_r, B) \\ & & & & P(\Phi_r, B)^T & \\ & & & & C^T W_r C & (-\bar{\lambda}_r M + K) & -P(\nu_r, B) \end{bmatrix} \quad (6.34)$$

and $N \in \Re^{(2n+p) \times (2nr+p)}$, representing an over-determined set of linear equations whenever $r > 1$.

Only the non-zero entries are shown. The desired solution vector g is then found from a least squares solution to Equation (6.33) using a QR^[19] decomposition and back substitution. Since $N = N(\Phi_i, \nu_i)$, an iterative scheme is introduced updating (Φ_i, ν_i) with the results of the previous iteration. The initial

guess at (Φ_i, ν_i) is to use the nominal vector Φ_i from the undamaged model, with the measured $\bar{\phi}_i$ elements inserted at the measured degrees-of-freedom. It is assumed that structural damage did not result in catastrophic damage, and thus the nominal eigenvectors are a reasonable initial guess. Some typical deviations in the eigenvectors resulting from damage to a small number of structural elements are shown in Section 6.4. Vector normalization and sign convention is accounted for by setting $\|C\Phi_i\|_2 = \|\bar{\phi}_i\|_2 = 1$ and $(C\Phi_i)^T \cdot \bar{\phi}_i > 0$. The Lagrange multiplier vector ν_i is initially assumed to be zero. During the iteration process, values of the damage fraction g_i outside the allowable range are removed from subsequent iterations, further reducing the parameter search space. The weighting matrix W_i is nominally set to the identity matrix (scaled such that $\|W_i\| \approx \|K\|$) corresponding to the case where all measurements are assumed at the same level of uncertainty.

Having presented both the ASTROS-ID and the APE methodology for the minimization of Equation (3.2), a comparison can now be made, illustrating the different nature of the two solution techniques. Because the APE method assumes the eigenvalues can be achieved exactly, it is equivalent to placing a very high weighting on the eigenvalues. Additional design degrees-of-freedom are then used to achieve the desired eigenvector components. However, if the weighting on the eigenvalues in ASTROS-ID is too large as compared to the eigenvector weightings, then the eigenvector information is negligible in the cost function, and it is equivalent to only using the eigenvalue information. This tends to spread the assigned damage over several elements. Furthermore, since there are no constraints placed on the solution vector in the APE method until after the decomposition and back substitution is formed, unrealistic stiffness changes often result, which are then easily identified and removed from the search space. This establishes a natural and simple method to reduce the search space for subsequent iterations. No such search space reduction is currently available for ASTROS-ID, and is listed as a topic for future research. Note that in either case, convergence to the global minimum is not guaranteed.

Solution techniques used to minimize Equation (3.2) can be classified as either a mathematical programming approach or an optimality criterion approach. Mathematical programming, also referred to as a direct search method, is based on establishing search directions to arrive at the solution. This technique is used in ASTROS-ID. In contrast, optimality criteria methods seek to directly satisfy the optimality criteria, iteratively using a recursion formula. Satisfaction of Equation (6.33) is the optimality criterion used in APE. An overview of the two approaches as applied to structural optimization can be

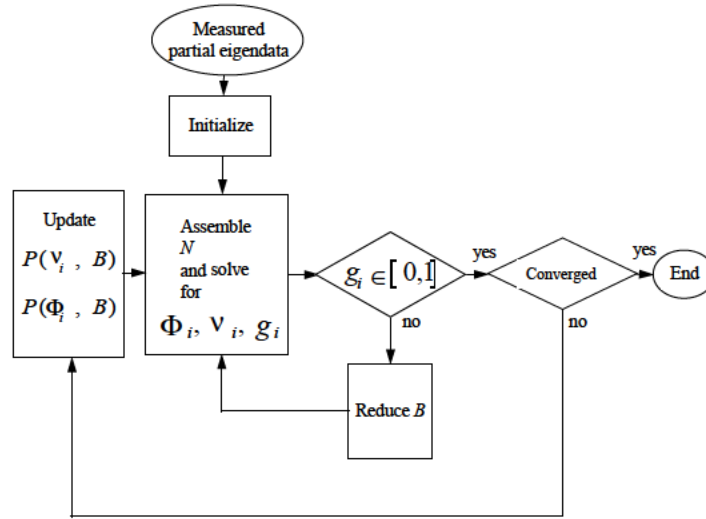


Figure 6.2 Assigned partial eigenstructure decision flow.

found in the text by Haftka and Gurdal.^[23] Additional work using optimality criteria is presented in the work by Venkayya.^[67]

6.3 Software Implementation

Structural damage detection using APE proceeds as follows. First, the matrix B is constructed according to Equation (6.11) for rod elements, or Equation (6.13) for beam elements. A B_i is constructed for each element in the search space. Next, using the mass and stiffness matrices M and K from a tuned finite element model (one in which the measured data of the undamaged structure correlates well with the model) and the measured eigendata of the damaged structure, Equation (6.33) is constructed. A QR decomposition and back-substitution is used to solve for the achievable eigenvectors Φ_i , the Lagrange multipliers ν_i , and the damage fractions g_i . Elements in g outside an allowable range (i.e., an increase in stiffness or negative stiffness) are removed from the search space by removing the corresponding columns of B . At each iteration step, the matrix N is updated using either the new (Φ_i, ν_i) solution pair or the new reduced B matrix. The solution sequence is repeated until convergence. The decision chart for this algorithm is shown in Figure 6.2.

For the initial construction of N using the measured $(\bar{\lambda}_i, \bar{\phi}_i)$ data, two preprocessing steps are required. The first is a pairing of the measured mode shapes with the nominal mode shapes. This is accomplished by normalizing the ∞ -norm of the partial mode shapes to unity and then checking the cross-orthogonality relation as given in the following:

$$O = \phi^T \bar{\phi} \quad , \quad \phi \text{ and } \bar{\phi} \in \mathfrak{R}^{s \times r} \quad (6.35)$$

Modes are paired based on the maximum values in the row and column positions of the matrix O . A second check is performed to verify the measured modal frequencies of the damaged structure are at or below the corresponding frequencies of the undamaged analytical model, i.e., $\bar{\lambda}_i \leq \lambda_i \forall i$. For each mode, measured frequencies above the analytical frequencies are set to the analytical values. Structural damage, when confined to decreases in the stiffness matrix, can only decrease the natural frequencies. This requirement can easily be shown by establishing the negative definiteness of changes in the eigenvalues to changes in the stiffness matrix. As will be developed in Chapter VII, these changes to first order can be expressed as:

$$\frac{\partial \lambda}{\partial g} = -\Phi^T P(\Phi, B) \quad (6.36)$$

For this first-order model, it is sufficient to show the negative definiteness of the i^{th} eigenvalue with respect to the j^{th} stiffness value change. This relationship is given as:

$$\frac{\partial \lambda_i}{\partial g_j} = -\Phi_i^T P(\Phi_i, B_j) \quad (6.37)$$

which, using the definition of P from Equation (6.23), valid for rod elements, and carrying out the vector multiplication yields:

$$\frac{\partial \lambda_i}{\partial g_j} = -\sum_{l=1}^n \sum_{k=1}^n \Phi_{li} \Phi_{ki} B_{lj} B_{kj} \quad (6.38)$$

Rearranging the summation yields:

$$\frac{\partial \lambda_i}{\partial g_j} = -\sum_{l=1}^n \Phi_{li} B_{lj} \sum_{k=1}^n \Phi_{ki} B_{kj} \quad (6.39)$$

which simplifies to:

$$\frac{\partial \lambda_i}{\partial g_j} = - \left(\sum_{l=1}^n \Phi_{li} B_{lj} \right)^2 \quad (6.40)$$

which is a negative definite quantity. If the more general definition of P is used as given in Equation (6.25), an additional summation is required over the corresponding columns of B associated with the j^{th} design variable. Again, this is a negative definite quantity since it is the sum of negative definite terms from Equation (6.40).

The APE iterative solution technique involves the least squares solution of the matrix N in Equation (6.34). This matrix is classified as a large sparse rectangular matrix which is possibly singular, and therefore the solution technique is tailored to this matrix classification. A sparse QR algorithm is used to decompose N and then a back-substitution to compute the solution vector. Due to the size of N , a sparse solver is required for all but small pedagogical problems. Column pivoting in the QR decomposition is not incorporated since pivoting does not preserve the matrix sparsity and increases the number of fill-ins. For the case when N is singular, the nature of the solution is different than that of the Moore-Penrose pseudo-inverse. The solution vector contains as many zero entries as the rank deficiency of N . This is a desirable attribute when determining damage detection, since typically damage is localized in the structure, and hence only a small number of elements have non-zero damage fractions. The APE algorithm was coded using MATLAB[®], with portions written in Fortran to handle the sparse matrix manipulations to speed processing time. MATLAB's **spqrmex** algorithm was used to perform the decomposition. In practice, the range of allowable damage fractions ($0 \leq g_i \leq 1$) was widened to ensure g_i 's were not discarded prematurely before convergence.

An additional consideration in damage detection algorithms is that of uniqueness. With only partial modal data available, the problem is generally ill-posed and hence there may exist multiple damage fractions which result in the same partial eigendata. This problem is exacerbated when noise corrupted measurements are used. The use of the structural constraint as given in Equation (6.4), combined with the restriction that the damage fraction g lie within an allowable range, helps to minimize the problem of non-uniqueness. For a given problem, solution uniqueness is dependent on the number of modes, the number of eigenvector components measured, the quality (signal/noise) of the measurements, the finite element model, and the numerical accuracies of the detection algorithm. To account for non-unique solutions in the APE algorithm, an off-line sensitivity analysis is performed

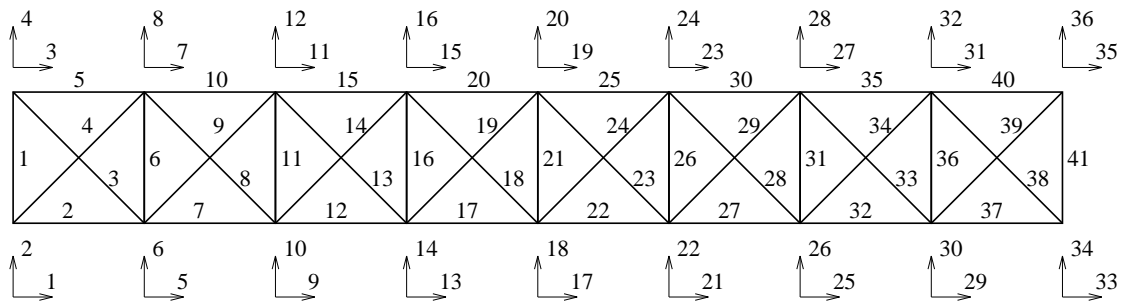


Figure 6.3 41-element free-free planar truss showing element and degree-of-freedom numbering.

once the size and quality of the measurement set has been determined. Using the results of this analysis, the parameter search space is confined to elements which produce unique and identifiable eigenstructures. Elements whose damage results in an identifiable change in the measured partial eigenstructure are defined as detectable. Next, APE symmetric elements are defined as damaged structural elements which produce the same measured partial eigenstructure. The results of the APE algorithm indicate damage fractions which are confined to an APE symmetric element set. Further refinement to an individual element within the set is not possible without additional or higher quality measurement data.

Numerous tests of the APE algorithm were conducted using finite element models of sizes ranging between 16 and 192 degrees-of-freedom constructed of 8 to 104 structural elements using either spring, rod, or beam elements. In all cases, when using analytical eigendata simulating both perfect measurements and model correlation, the APE algorithm converged to the correct damaged element(s), and indicated the correct percent of damage. In each case, less than ten percent of the total degrees-of-freedom were included in the measurement set, and only a small number of the natural frequencies. An additional attribute of the algorithm is that, in the case where the entire eigenvector can be measured exactly, the exact solution is obtained without iterating.

6.4 An Analytical Example

The APE method was applied to the 41-element free-free planar truss shown in Figure 6.3. Structural damage was arbitrarily defined as a 50% reduction in stiffness to element #7 and a 30% reduction to stiffness in element #18. An eigenanalysis of the FEM model using the reduced stiffness values produced the $(\bar{\lambda}_i, \bar{\phi}_i)$ measured data. The frequencies and partial shapes corresponding to

Table 6.1 Damage identification results on the 41-element free-free planar truss.

True		APE		ASTROS-ID	
element #	% damage	element #	% damage	element #	% damage
7	50	7	50.0	7	34.3
18	30	18	30.0	10	34.4
				18	19.1
				19	12.6
cpu time		14.6 (sec.)		540.2 (sec.)	

the same instrumented degrees-of-freedom (2, 10, 18, 26) as used in Chapter IV for the first five flexible modes were used. Figures 6.4 and 6.5 show the resulting change in modal frequency and shape from structural damage. The damaged configuration is plotted using dashed lines, while the nominal configuration is plotted using solid lines. As can be seen from the figures, the change in the shapes due to the damage is minimal, justifying the use of the nominal eigenvectors for the unmeasured degrees-of-freedom to initiate the APE algorithm. The 41 fictitious actuators corresponding to the 41 structural elements were used to construct B according to Equation (6.10).

The results of the APE method are listed in Table 6.1. Nineteen iterations were used in the solution process, starting from an initial search space of 41 elements. An analysis using ASTROS-ID with 41 design variables corresponding to the stiffness of the 41 elements was also performed. The results are listed in Table 6.1, along with the required CPU times for each method. Four outer-loop iterations were used in obtaining the ASTROS-ID results. Equal weighting on the eigenvalue and eigenvector components were used in the objective function, since all quantities are known exactly. Note that although both methods were run on the same CPU platform (Sparc-10 workstation), the methods were implemented in two different software environments. Because of this, there may be some small percentage of the CPU times reported that is associated with processing unique to the software environment and not the solution computation. Table 6.1 does illustrate the difference in the nature of the solutions. Using the APE method, the solution space is reduced to the fewest number of elements which can achieve the measured eigenstructure. Using ASTROS-ID, the damage is equally assigned between elements which have the same eigenvalue and eigenvector sensitivities. Elements number 7 and number 10 have exactly the same eigenvalue sensitivity and nearly the same eigenvector sensitivity to the measured data. The same is true for elements 18 and 19. In the case where uncertainty exists in the measured data, it becomes increasingly difficult, if not impossible to distinguish between

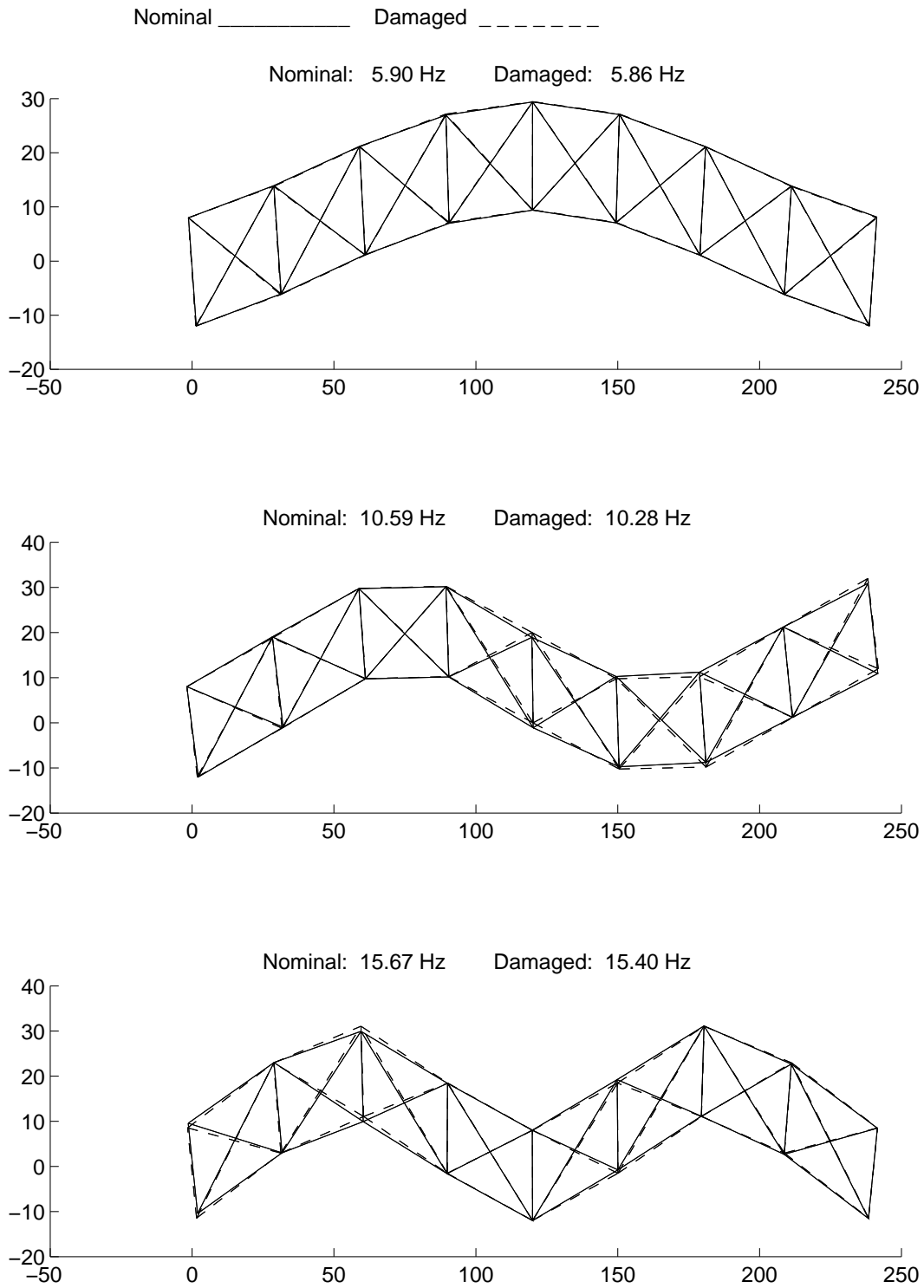


Figure 6.4 Change in frequencies and shapes due to structural damage for the first three flexible modes.

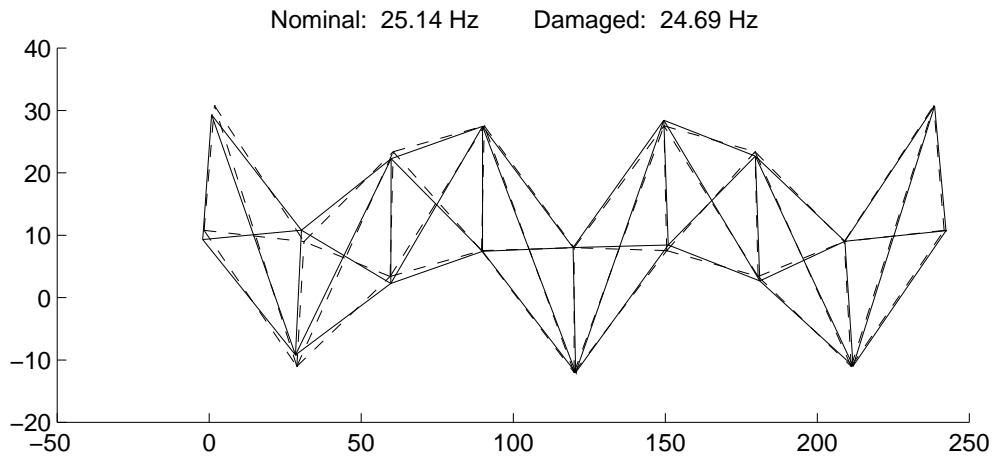
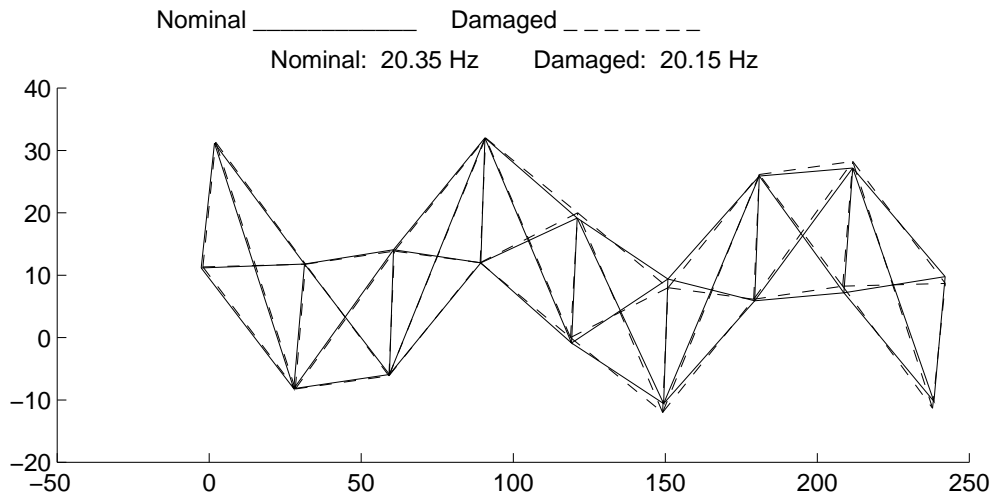


Figure 6.5 Change in frequencies and shapes due to structural damage for the fourth and fifth flexible modes.

which element to correctly assign the damaged value. A slight perturbation in the measured data can result in the APE method assigning a 50% damage to element 10 rather than element 7. The problem of distinguishing between elements with similar sensitivities is termed ‘damage localization’ and is discussed in Chapter VII.

6.5 *Summary*

A method was presented to achieve a set of measured eigenvalues and eigenvectors through changes in the stiffness matrix which are consistent with the finite element formulation. The method does not require the use of full-length eigenvectors in its formulation, and is suitable for use with minimally instrumented structures. The method was demonstrated on an analytical model, accurately identifying the damaged elements. A comparison between ASTROS-ID and APE was also performed. Common to both methods is the question of which degrees-of-freedom to instrument to facilitate damage identification, and to what extent can the damage be localized from the measured data. These two questions are addressed in Chapter VII.

VII. Sensor Prioritization and Damage Localization

7.1 Overview

For large space structures, practicality dictates that only partial modal data can be measured. With minimal sensor information, two questions naturally arise: at which locations should the sensors be placed, and to what extent can damage be identified with the selected sensor locations? An eigenstructure sensitivity based method is presented to answer these questions. While sensor placement methods have been presented by Lim ^[46], Kammer ^[36], and Liu and Tasker ^[48], they focused on maximizing either controllability or observability and not damage detection. Kashangaki ^[41] introduced a modal sensitivity parameter as a quantitative measure of the eigenvalue and eigenvector sensitivity, and used this to determine which modes should be used in a damage detection scheme. In practice however, for a given complex structure, only a few of the lower frequency global modes can be accurately identified. At higher frequencies, the separation of local and global modes becomes increasingly difficult, if not impossible. Furthermore, only a few degrees-of-freedom can be instrumented. Therefore, emphasis herein is placed on prioritizing sensor locations and on the ability to localize damage from partial eigendata for a given number of modes, and not on which modes to measure.

The method presented is based on examining the first-order partial eigenstructure sensitivity to changes in the structural stiffness of each element of a finite element model. No *a priori* knowledge of the damage location is assumed. Two aspects of the partial eigenstructure sensitivity are explored. First, is the amount by which variations of the elemental stiffness values change the measured partial eigenstructure. Independent of the damage detection scheme used, elements which produce little or no change in the measured data will be difficult or impossible to detect when damaged. Second, is the direction of change in the partial eigenstructure. Elements which produce similar or identical changes in the partial eigenstructure, will be difficult or impossible to distinguish between when damaged. Therefore, sensor locations are chosen so that the change in the measured partial eigenstructure due to damage is maximized. Localization of the damage to an element(s) is based on both the amount and direction of change to the partial eigendata for the chosen sensor locations.

7.2 Sensitivity Theory

Eigenvalue and eigenvector sensitivity to changes in structural elements will be based upon the finite element model of the structure. For on-orbit damage scenarios of large flexible space structures, two assumptions are made. First, structural damage is confined to changes in the stiffness properties of the structure. Second, structural damping is negligible. With these assumptions, the free vibration of the structure is modeled as:

$$Mx + (K - \Delta K)x = 0 \quad (6.1)$$

with all variables as previously defined. The eigenvalue and eigenvector for the i^{th} mode of Equation (6.1) is given as (λ_i, Φ_i) whereas the measured eigenvalue and partial eigenvector for the same mode is represented as $(\bar{\lambda}_i, \bar{\phi}_i)$. The relationship between the n dimensional eigenvectors Φ_i and the s dimensional partial eigenvectors ϕ_i is $\phi_i = C\Phi_i$. The matrix $C \in \mathbb{R}^{s \times n}$ maps the full length eigenvector into the partial eigenvector corresponding to the measured degrees-of-freedom. With minimal sensor information available, a natural cost function representing the mismatch between the eigenstructure of the finite element model and the measured eigendata is:

$$J = \sum_{i=1}^r a_i \left(\frac{\lambda_i}{\bar{\lambda}_i} - 1 \right)^2 + \sum_{i=1}^r \sum_{j=1}^s b_{ij} (\phi_{ij} - \bar{\phi}_{ij})^2 \quad (3.2)$$

Of interest for sensor location determination is how to choose the matrix C such that structural damage results in observable changes in $\bar{\lambda}_i$ and $\bar{\phi}_i$ and hence in J . Once C is determined, damage localization is concerned with the uniqueness of changes in $\bar{\lambda}_i$ and $\bar{\phi}_i$ for variations in the matrix ΔK . As developed in Chapter VI, the structural constraint can be imposed on ΔK by expressing it as:

$$\Delta K = BGB^T \quad (6.4)$$

where B is constructed from the nodal connectivity information and the elemental parameters. G is a diagonal matrix ($G = \text{diag}(g_1 \dots g_p)$) composed of the fraction of damage for each element (g_i). A value of $g_i = 0$ corresponds to an undamaged element whereas $g_i = 1$ corresponds to a complete loss of stiffness to the i^{th} element. The eigenvalue and eigenvector sensitivity to structural damage is computed based on the method presented by Fox and Kapoor.^[16] The sensitivity calculations are

consistent with the method presented in Chapter V, however with damage being confined to the stiffness matrix the calculations are further simplified. Furthermore, the matrix operator $P(\alpha, \beta)$ as defined in Chapter IV is used to develop the sensitivity equations. The eigenvalue equation is written as:

$$(-\lambda_i M + K - BGB^T)\Phi_i = 0 \quad (7.1)$$

With the assumption that changes from structural damage are confined to the perturbation matrix ΔK , Equation (7.1) is differentiated, which after simplifying results in:

$$M\Phi_i \frac{\partial \lambda_i}{\partial g} + \frac{\partial}{\partial g}(BGB^T \Phi_i) = 0 \quad (7.2)$$

As developed in Chapter VI, the matrix operator $P(\alpha, \beta)$ is defined as:

$$P(\alpha, \beta) \text{ with } P, \beta \in \mathfrak{R}^{n \times p}, \alpha \in \mathfrak{R}^{n \times 1}, P_{ij} = \sum_{k=1}^n \alpha_k \beta_{ij} \beta_{kj} \quad (6.23)$$

where P_{ij} is the i^{th} row and the j^{th} column of the matrix P . In terms of the operator P , the matrix product in parenthesis in Equation (7.2) can be written as:

$$BGB^T \Phi_i = P(\Phi_i, B)g \quad \text{where } g = \text{diag}(G), G \in \mathfrak{R}^{p \times p} \text{ (diagonal)} \quad (7.3)$$

Each eigenvector is normalized so that $\Phi_i^T M \Phi_i = 1$. Premultiplying Equation (7.2) by Φ_i^T and using the operator P , the eigenvalue sensitivity from Equation (7.2) can be written as:

$$\frac{\partial \lambda_i}{\partial g} = -\Phi_i^T P(\Phi_i, B), \quad \frac{\partial \lambda_i}{\partial g} \in \mathfrak{R}^{1 \times p} \quad (7.4)$$

In a similar fashion, eigenvector sensitivity is computed by differentiating Equation (7.1) and using the results of Equation (7.4). The eigenvector sensitivity for the i^{th} mode is:

$$[K - \lambda_i M - BGB^T] \frac{\partial \Phi_i}{\partial g} = [M \Phi_i \Phi_i^T + I] P(\Phi_i, B), \quad \frac{\partial \Phi_i}{\partial g} \in \mathfrak{R}^{n \times p} \quad (7.5)$$

The matrix I denotes the $n \times n$ identity matrix. The method introduced by Nelson^[56] is used to solve Equation (7.5). This is necessary due to the singularity of the matrix $[K - \lambda_i M - BGB^T]$. Assuming

no repeated roots, this method involves separating the solution into a particular and homogeneous solution, where:

$$\frac{\partial \Phi_i}{\partial g} = \Phi_i c_i + V_i \quad (7.6)$$

with:

$$\tilde{V}_i = \left[\tilde{K} - \lambda_i \tilde{M} - \tilde{B} \tilde{G} \tilde{B}^T \right]^{-1} \left[\tilde{M} \tilde{\Phi}_i \tilde{\Phi}_i^T + \tilde{I} \right] \tilde{P}(\Phi_i, B) \quad (7.7)$$

and

$$V_i = \left[\tilde{V}_{i1}, \dots, \tilde{V}_{il-1}, 0, \tilde{V}_{il}, \dots, \tilde{V}_{in-1} \right]^T \quad (7.8)$$

The $(\tilde{\bullet})$ notation represents matrices reduced by one row and one column, or vectors reduced by one element. Nelson's method removes the row and column corresponding to the maximum entry in Φ_i . Equation (7.8) corresponds to the maximum entry occurring at the l^{th} element. For computational efficiency, a decomposition and substitution is preferable to explicitly computing the inverse. The constant row vector c_i is given as:

$$c_i = -\Phi_i^T M V_i \quad (7.9)$$

With the first-order eigenvalue and eigenvector sensitivities defined, let $\nabla \lambda$ be the matrix whose i^{th} row and j^{th} column entry is defined as:

$$\nabla \lambda_{ij} = \frac{\partial \lambda_i}{\partial g_j} \cdot \frac{1}{\lambda_i} = -\frac{\Phi_i^T P(\Phi_i, B_j)}{\lambda_i} \quad (7.10)$$

The term λ_i is introduced to correct the scaling of the different modes. With this definition, each column of $\nabla \lambda$ corresponds to different structural elements and each row to a different mode. The eigenvalue change from changes in the structural elements $\Delta g \in \mathfrak{R}^{p \times 1}$, to first order, is given as:

$$\Delta \lambda = \nabla \lambda \Delta g \quad (7.11)$$

where

$$\Delta \lambda = [\Delta \lambda_1, \dots, \Delta \lambda_r]^T \quad \text{and} \quad \Delta \lambda_i = \frac{\lambda_i - \lambda_{oi}}{\lambda_{oi}}, \quad \forall i = 1, \dots, r \quad (7.12)$$

The vector $\Delta \lambda \in \mathfrak{R}^{r \times 1}$ consists of the fractional changes to the r measured eigenvalues of the structure due to damage. Similarly, the vector $\Delta \lambda_o \in \mathfrak{R}^{r \times 1}$ contains the eigenvalues of the structure evaluated

at BG_oB^T . For the undamaged structure, $BG_oB^T = 0$. Since Equation (7.11) is valid only for small changes of Δg , it is not possible to use it directly to determine damaged elements. However, for the purpose used herein, Equation (7.11) is adequate to examine the relationship between $\Delta \lambda$ and Δg . Information on the amount and direction of changes in $\Delta \lambda$ are contained in the matrix $\nabla \lambda$. With $\Delta g_i \in [0, 1]$, rows of $\nabla \lambda$ with negligible norms will contribute negligibly to changes in $\Delta \lambda$. Rows in $\nabla \lambda$ which are similar or identical to one another will have values of Δg_i that affect $\Delta \lambda$ similarly or identically, and hence will be indistinguishable from one another. For this analysis, it is assumed that $\|g\|_2$ is small and that, although individual elements in Δg may be close to unity, the overall effect on the global nature of the structure is small, i.e. no catastrophic failures.

Using the results from Equation (7.5), the partial eigenvector sensitivity for the i^{th} mode is defined as:

$$\nabla \phi_i = C \frac{\partial \Phi_i}{\partial g}, \quad \nabla \phi_i \in \mathbb{R}^{s \times p} \quad (7.13)$$

where C is determined from the measured degrees-of-freedom as previously defined. With this definition, changes in the partial eigenvector for the i^{th} mode, to first order in Δg , is given as:

$$\Delta \phi_i = \nabla \phi_i \Delta g \quad \text{where} \quad \Delta \phi_i = \phi_i - \phi_{i_o} \quad (7.14)$$

The vector $\phi_i \in \mathbb{R}^{s \times 1}$ is the partial eigenvector for the instrumented degrees-of-freedom, and $\phi_{i_o} \in \mathbb{R}^{s \times 1}$ contains the partial eigenvector of the finite element model evaluated at BG_oB^T . Similar to the eigenvalue case, information on the amount and direction of change of $\Delta \phi_i$ is contained in the matrix $\nabla \phi_i$. Note that there is one matrix $\nabla \phi_i$ for each measured mode. Information on which to base both sensor location and damage localization is contained in the matrices $\nabla \lambda$ and $\nabla \phi_i$. Two properties of these matrices are investigated, which are referred to as the detectability and colinearity. Detectability is a measure of the amount of change which occurs from changes in a design variable, whereas colinearity is a measure of the direction of change.

7.2.1 Sensor Location Prioritization. Initially with $C = I$, $\nabla \phi_i$ from Equation (7.13) contains information indicating which degrees-of-freedom to instrument. As previously discussed, on orbit only a few of the low frequency modes can be measured. Given this fact and the problem of solution non-uniqueness associated with using partial measurement data, it is assumed that any mode

which can be measured should be used in a damage detection scheme. Given then that there are r measured modes, the detectability in the measured eigenvectors at the l^{th} degree-of-freedom from changes in the p elements of the structure is defined as:

$$D_{\phi_l} = \sum_{k=1}^p \sum_{i=1}^r |\nabla \phi_i|_{lk} \quad (7.15)$$

The vector $D_\phi = [D_{\phi_1} \dots D_{\phi_n}]^T$ is then sorted in descending order, initially prioritizing the sensor locations based on detectability. A threshold is set based on the measurement uncertainty and the finite element modeling errors. Values of D_{ϕ_l} below this threshold indicate degrees-of-freedom which are unaffected by structural damage for the measured modes. Next, a colinearity check is made to determine degrees-of-freedom which yield similar information on the damaged elements. The colinearity, denoted S , between any two vectors α and β is defined as:

$$S_{\alpha\beta} = \alpha^T \beta \quad \|\alpha\|_2 = \|\beta\|_2 = 1 \quad (7.16)$$

which is simply the cosine of the angle between the two vectors. A value of $S_{\alpha\beta} = 1$ indicate perfect colinearity whereas $S_{\alpha\beta} = 0$ indicates orthogonal vectors. With this definition, the colinearity of the eigenvector sensitivity between measured degrees-of-freedom l and m is defined as:

$$S_{\phi_{lm}} = \left[\frac{1}{r} \sum_{i=1}^r [\nabla \phi_i \cdot \nabla \phi_i^T] \right]_{lm} \quad (7.17)$$

Again a threshold from unity is set based on the measurement uncertainty and the finite element modeling errors. Values in $S_\phi \in \Re^{n \times n}$ within this threshold are declared colinear, indicating that at these degrees-of-freedom for the r measured modes, the changes in the eigenvector are indistinguishable from one another to changes in the structural elements. Using this information, multiple colinear entries in vector D_ϕ are removed, leaving only one entry from each colinear grouping. The remaining first s elements of vector D_ϕ represent the prioritized s degrees-of-freedom to place sensors. With D_ϕ^s defined as the first s elements of the reduced and sorted vector D_ϕ , the matrix C is chosen such that $D_\phi^s = CD_\phi$ is satisfied. An analytical example is presented in a subsequent section, following the discussion of damage localization.

7.2.2 *Damage Localization.* Given the r modes measured at the s degrees-of-freedom as determined above, damage localization determines the extent to which damage can be isolated to individual elements. Similar detectability and colinearity metrics are used, which are now restricted to the instrumented degrees-of-freedom. The detectability in the measured eigenvalues from changes in the k^{th} structural element is defined as:

$$D_{\lambda_k} = \sum_{i=1}^r |\nabla \lambda_{ik}| \quad (7.18)$$

where $D_{\lambda} = [D_{\lambda_1} \dots D_{\lambda_r}]^T$. Eigenvalue colinearity information is contained in S_{λ} . The j^{th} row and k^{th} column of S_{λ} indicates the colinearity of the eigenvalue changes between the j^{th} and k^{th} structural elements and is defined as:

$$S_{\lambda_{jk}} = [\nabla \lambda^T \cdot \nabla \lambda]_{jk} \quad (7.19)$$

The eigenvalue colinearity is independent of the degree-of-freedom at which it is measured. Similarly, detectability in the measured eigenvectors from the k^{th} structural element is defined as:

$$D_{\phi_k} = \sum_{l=1}^s \sum_{i=1}^r |\nabla \phi_{li}| \quad (7.20)$$

where $D_{\phi} = [D_{\phi_1} \dots D_{\phi_p}]^T$. Eigenvector colinearity information is contained in S_{ϕ} . The j^{th} row and k^{th} column of S_{ϕ} indicates the colinearity of the eigenvector changes between the j^{th} and k^{th} structural elements and is defined as:

$$S_{\phi_{jk}} = \left[\frac{1}{r} \sum_{i=1}^r [\nabla \phi_i^T \cdot \nabla \phi_i] \right]_{jk} \quad (7.21)$$

Note the similarity between Equations (7.15) and (7.17) and Equations (7.20) and (7.21). For this reason, sensor prioritization and damage localization are considered dual problems, either of which can be determined with only a slight modification to the same algorithm. Notationally, detectability D and colinearity S were multiply defined, once for sensor prioritization and again for damage detection. It should be clear from the context of the problem which definition applies.

With these definitions, damage localization proceeds as follows. Elements in D_{λ} and D_{ϕ} which are below the modeling and measurement uncertainty threshold level are declared undetectable.

Damage in an undetectable element cannot be identified from the measured data. Of the remaining elements, colinear elements, as indicated by elements in S_λ and S_ϕ above the uncertainty level are indistinguishable from one another. From the measured data, structural damage can only be localized to a colinear group, and not to an individual element within the group. Elements contained in a colinear group are referred to as symmetric elements.

7.3 Software Implementation

The sensor prioritization and damage localization method was implemented using MATLAB[®] [52] software. For a given number of modes, the eigenvalue and eigenvector sensitivities are computed using Equations (7.4) and (7.6) respectively. From these, the detectability metrics D_λ and D_ϕ are computed using Equations (7.18) and (7.20). The colinearity metrics S_λ and S_ϕ are computed using either Equations (7.15) and (7.17) for sensor prioritization or using the transposes as given in Equations (7.19) and (7.21) for damage localization. These metrics are then compared against threshold values based on model and measurement uncertainty. The uncertainty is determined by how well the finite element model correlates to the measured data, for nominal as well as damage configurations. The detectability threshold was established as a percentage of the maximum element in the vector D . For colinearity the threshold was a percentage decrease from unity value. With the thresholds established, the elements of the structure are then classified as either undetectable (U) using D_λ and D_ϕ , symmetric (S), or identifiable (I). For computational efficiency, detectability is checked first. Any elements with values below the detectability threshold are classified as U and are removed from the sensitivity gradient matrices before forming the colinearity metrics. Colinearity groupings are then determined from the colinearity matrix by replacing the entries of the matrix with either ones or zeros based on being above or below the colinearity threshold. In this way, a nonzero entry in the i^{th} row and j^{th} column indicates symmetry between the i^{th} and j^{th} elements. Note that only the entries above the main diagonal need be computed. Based on these entries, the elements are classified as either S or I. For a colinear grouping of elements as determined by S_λ and S_ϕ , one element is classified as identifiable and the remaining as symmetric. The selection of the weighting between emphasis on S_λ and on S_ϕ is dependent on the damage identification scheme used. For damage identification based on the cost function minimization, such as given in Equation (3.2), the metric results should be combined consistently with the cost function weighting coefficients. For example, a high relative weighting on

the eigenvalues corresponds to an increased emphasis on the S_λ metric. A decision flow chart for the damage localization process as implemented for use with the APE method is shown in Figure 7.1. The decision chart reflects the emphasis the APE method places on eigenvalues over the eigenvectors.

Independent of the algorithm used for damage identification, the advantage of the U/S/I classification is apparent. It quickly indicates which damaged elements cannot be detected from the measured data. Furthermore, only elements in the I classification need be included in the search space. It has been observed that decreasing the search space precludes singularities of the N matrix in Equation (6.34) and significantly reduces the required solution time.

7.4 An Analytical Example

To demonstrate the use of the detectability and colinearity metrics, an analytical example of both the sensor prioritization and damage localization was performed using the same 41-element free-free planar truss assembly as shown in Figure 7.2 and described previously in Chapter IV.

The first analysis was an examination of the relationship between increasing the number of measured modes and increasing the number of sensors. Table 7.1 contains the tabulated results. The data clearly shows that, if possible, increasing the number of modes measured is preferable to increasing the number of sensors to enhance damage localization. For all cases, the threshold values were fixed at 10% for detectability and 5% colinearity. It should be noted that the tabulated results in some instances show that adding additional sensors had an adverse effect on identifiability. This trend is an artifact of using different length vectors, due to a different number of sensors, compared against a fixed threshold. The data as presented is intended only to show the overall trends.

To demonstrate sensor prioritization, the locations of three sensors were selected using a fixed number of modes and the same thresholds as stated above. As shown in Table 7.2, the prioritized locations increase the number of identifiable elements over two randomly chosen sensor locations.

A third analysis was performed to demonstrate the validity of using only first-order sensitivities, evaluated at the nominal configuration, over the range of Δg . Table 7.3 lists the symmetric elements as determined by S_λ for the first five flexible modes, for the same threshold values as used above and using a single sensor. As an example, the results indicate elements 8, 9, 33, and 34 are symmetric to the partial measured data, and thus only one element should be included in the damage detection search space.

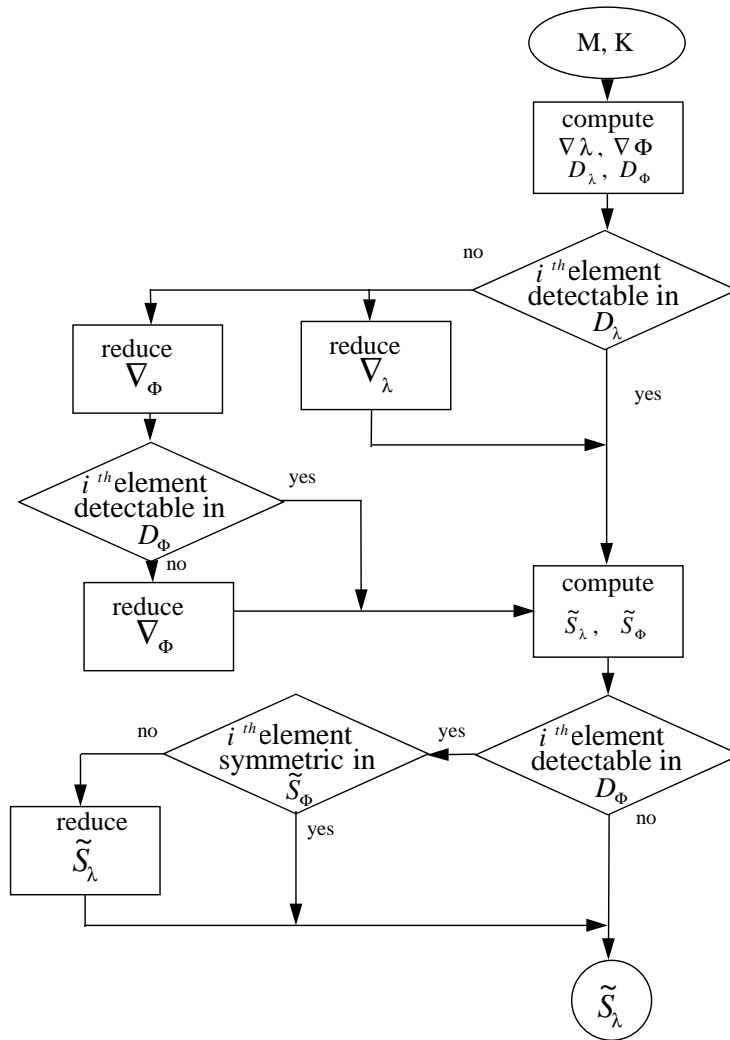


Figure 7.1 Damage localization decision flow.

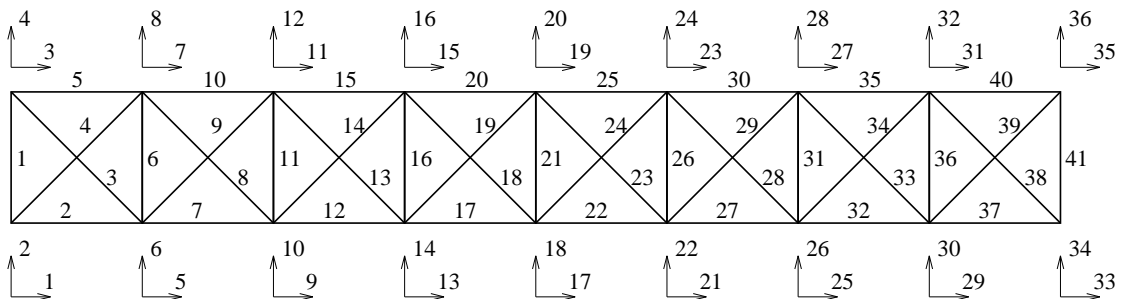


Figure 7.2 41-element free-free truss showing degree-of-freedom and element numbering.

Table 7.1 Damage localization results for a 41-element free-free planar truss.

# Sensors	Measured Flexible Modes				
	1	1,2	1,2,3	1,2,3,4	1,2,3,4,5
1	29/9/3 [†]	21/15/5	21/15/5	9/25/7	9/24/8
2	29/9/3	21/8/12	21/3/17	9/6/26	9/1/31
3	29/2/10	21/2/18	21/0/20	9/3/29	9/1/31
4	29/0/12	21/1/19	21/0/20	9/4/28	9/0/32
5	29/0/12	21/3/17	21/0/20	9/3/29	9/0/32
6	29/0/12	21/3/17	21/0/20	9/2/30	9/0/32
Locations [‡]	34,2,1,3,33,35	1,35,3,33,9,27	1,35,33,3,36,2	1,35,33,3,36,2	1,35,3,33,16,22

[†]Data presented in U/S/I format where U denotes the number of undetectable elements, S the number of symmetric elements, and I the number of identifiable elements. The sum of U, S, and I equals the total number of elements of the structure.

[‡]The locations of the sensors were chosen using the prioritization method presented and are reported by degree-of-freedom number in prioritized order.

Table 7.2 Damage localization for different sensor locations for a 41-element free-free planar truss.

Method	Sensor Location [†]	Damage Localization (U/S/I) [‡]
Prioritized	1,35,3	9/1/31
Random	3,11,19	9/5/27
Random	2,4,34	9/3/29

[†]Reported by degree-of-freedom number.

[‡]Based on measuring the first five flexible modes.

Table 7.3 Damage localization based on eigenvalue sensitivity using the first 5 flexible modes, for the 41-element free-free planar truss.

Element #	Equivalent Symmetric Elements (S_λ) [†]
2	5,37,40
3	4,38,39
7	10,32,35
8	9,33,34
12	15,27,30
13	14,28,29
17	20,22,25
18	19,23,24
Undetectable Elements	1,6,11,16,21,26,31,36,41

[†]Results are independent of selected sensor location.

The measured eigenvalues with damage to element 8, $g_8 \in [0, 1]$ corresponds to the same eigenvalues for an equivalent break in either elements 9, 33, or 34. For an example with multiple breaks, elements 8 and 30 were reduced by 70% and 50% respectively. Using any combination of two elements, selecting one element from the symmetric set (8,9,33,34), and one element from the symmetric set (12,15,27,30), reduced by 70% and 50% respectively, the changes in the measured eigenvalues were within 2% of each other. This is well within the uncertainty level established in the threshold for S_λ used to select the symmetric sets.

7.5 Summary

A method was presented which prioritizes the degrees-of-freedom to instrument when used to collect modal data for damage detection. It was shown that this method can also be used to determine the extent to which damage can be localized from these sensor locations. The method represents a computationally attractive alternative to an exhaustive search over the parameter space and is a valuable tool during the design phase to determine measurement and/or modeling accuracy requirements. An analytical example was presented which showed that the extent to which damage can be localized is limited by the amount and quality of the measured data. It was also shown that increasing the number of measured modes is of greater benefit than increasing the number of sensors.

Having developed the four tasks associated with damage identification, each task was combined into an integrated software package and programmed in MATLAB[®]. A description of this software

tool is provided in Appendix B. Using this software, the four tasks of damage identification were applied to experimental structures, the details of which are discussed in the Chapter VIII.

VIII. Experimental Validation of Theory

8.1 Test Objective

The test objective is the experimental demonstration of the ability to identify structural damage from a simulated damaged space truss using limited measurement data. In choosing an experimental apparatus to validate a new technique, it is important for the experiment to exhibit the common dynamic characteristics of the intended application. For large flexible space structures, these characteristics include a low fundamental frequency (on the order of 1 Hz) and high modal density at low frequencies with low modal damping ratios, and a truss-like structure. Furthermore, it is important that both the excitation actuator and measurement sensors be non-grounded since only these type devices are applicable to space-based applications. Lastly, to demonstrate the detection of actual damage, it is desirable to have a structure which contains structural elements which can easily be modified or removed to simulate a failure. Two different test beds were chosen to validate the theory. The first validation was through the use of experimental test data obtained from NASA's 8-bay truss test bed, and the second using AFIT's six-meter Flexible Truss Experiment.

8.2 NASA Test Data Analysis

8.2.1 Hardware. NASA's 8-bay truss test bed consisted of eight cubic bays of a hybrid space truss cantilevered from a rigid backstop plate. This configuration represents a scaled section of the proposed International Space Station. Each bay is a half meter in length, constructed of aluminum members. A typical joint configuration is shown in Figure 8.1. The truss was fully instrumented with one triaxial accelerometer at each of its 32 unconstrained nodes. Disturbance excitation was achieved using two ground-based dynamic shakers attached at two different node points. A complete description of the hardware and the testing procedure is contained in the work by Kashangaki.^[40]

8.2.2 Model Tuning. The NASA truss was modeled using 104 rod elements, with three translational degrees-of-freedom per node. The material properties of all elements were identical. Lumped masses were incorporated into the model to account for the mass of the node balls, standoffs, sleeves, collars, and instrumentation. The data received from NASA (T. Kashangaki) consisted of the identified natural frequencies and shapes for the first five flexible modes of the truss, for the nominal as well as several damage configurations. The first five modes in numerical order consisted of the

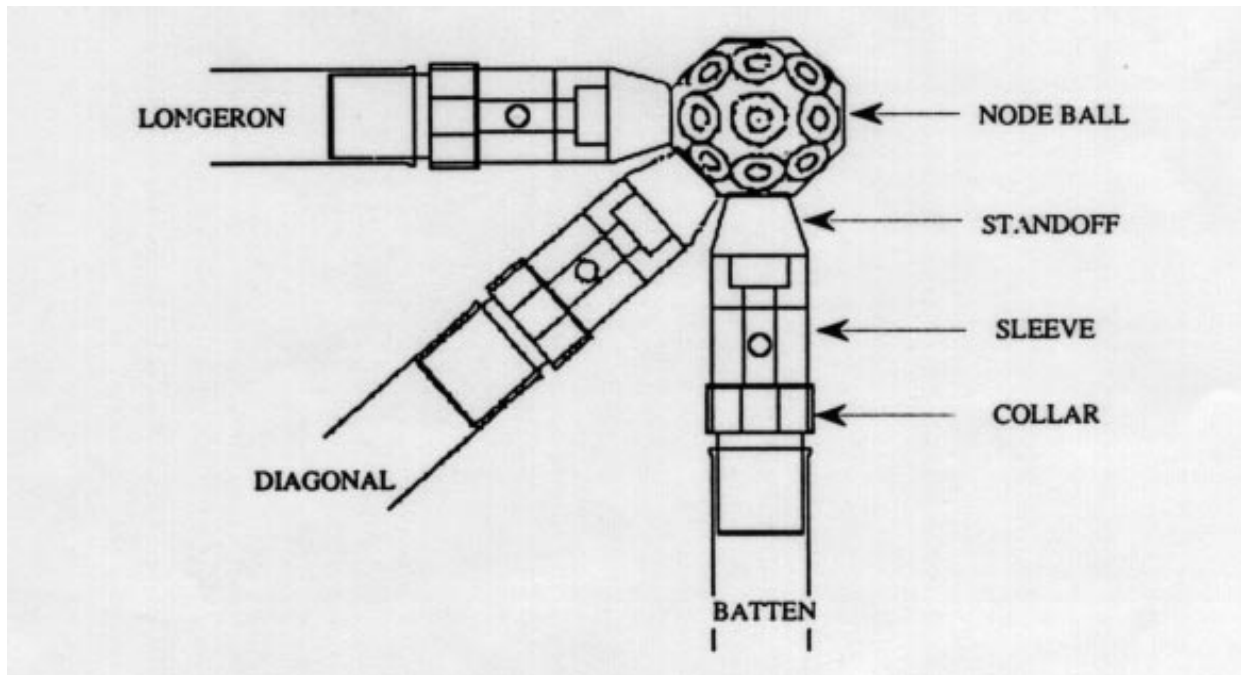


Figure 8.1 Joint construction for the NASA 8-bay truss experiment.

first bending modes about the 'X' and 'Z' axes, the first torsional mode about the 'Y' axis, and the second bending modes about the 'X' and 'Z' axes. A typical frequency response function is depicted in Figure 8.2, measured at the free end of the truss. Both the nominal and damaged measurements are shown. As can be seen in the figure, identification of global modes past 80 Hertz is difficult due to the presence of local element modes in this regime. Hence only the first five modes could be accurately measured. Also depicted in the frequency response functions is the effect of structural damage. For this particular damage case which corresponds to the removal of a longeron element at the cantilevered end, damage is manifest in the frequency response by a separation of the first two flexible modes only.

Nine damage cases were tested. The damage configurations were the full removal of one or two elements of the truss. The different damage configurations are shown in Figures 8.3, 8.4, and 8.5. For the nominal configuration, i.e. no damage, the results of the finite element analysis and the measured data are compared in Table 8.1. Although the FEM model is in fair agreement with the measured data, any disagreement will result in the damage identification method assigning a percentage of damage to an element(s) to account for the disagreement. Therefore, tuning was performed using ASTROS-ID to ensure the initial disagreement was as minimal as possible. A total of 110 design variables were

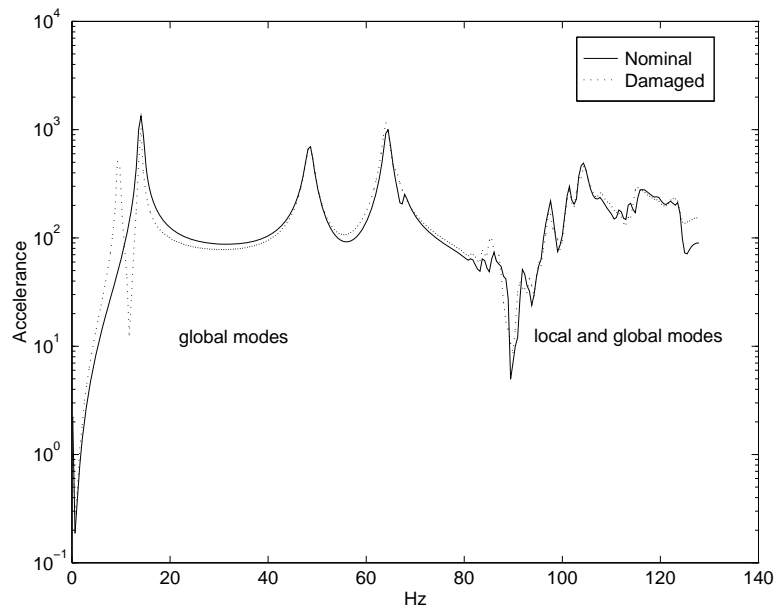


Figure 8.2 Measured frequency response function for the NASA truss.

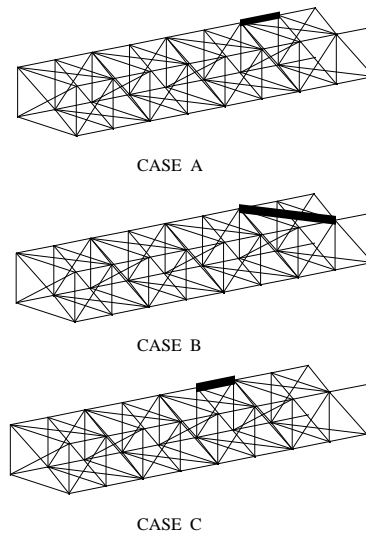
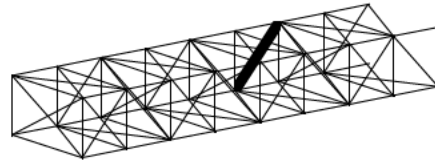
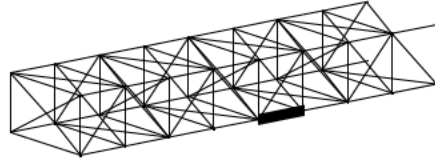


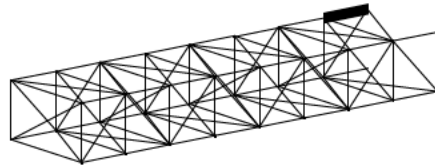
Figure 8.3 Damage configurations for the NASA truss, cases A, B, and C.



CASE D

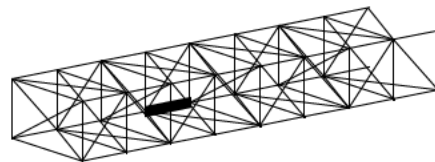


CASE E

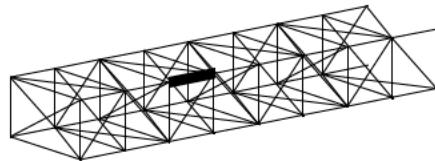


CASE F

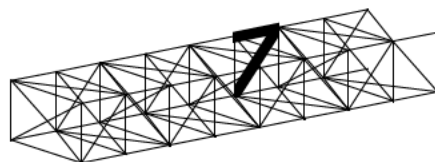
Figure 8.4 Damage configurations for the NASA truss, cases D, E, and F.



CASE G



CASE H



CASE I

Figure 8.5 Damage configurations for the NASA truss, cases G, H, and I.

Table 8.1 Measured natural frequencies of NASA's 8-bay truss.

Mode #	Frequency (Hz)			% difference	
	Measured	Initial	Tuned	Initial	Tuned
1	13.88	13.79	13.88	0.65	0.00
2	14.48	14.31	14.47	1.19	0.07
3	48.41	50.53	48.40	4.37	0.02
4	64.03	65.98	64.03	3.05	0.00
5	67.46	71.20	67.52	5.55	0.08

used to tune the model, which included the elastic modulus of the 104 rod elements. Two design variables were used for the mass of the rods, one for the half meter length rods and a second for the diagonal members ($1/\sqrt{2}$ in length). The remaining four design variables were used to adjust the mass properties of the lumped nodal masses. There were four different nodal configurations, depending on how many members were connected at a node point and whether or not an external shaker attachment was included. To tune the model, all five measured modes were used with equal weighting on all frequencies. Eigenvector information was not included in the tuning process for several reasons. First, the prioritized sensor locations were not chosen until after the model was tuned, and thus which elements of the eigenvector to include in the tuning process was yet unknown. (Eigenvalue information is independent of the sensor locations, assuming a sensor is not located at a node point for a particular mode.) Note that although the full length eigenvectors are available from the test data, this does not represent a realistic on-orbit capability and thus complete knowledge of the eigenvectors was not used. A second reason for not including eigenvector information was the desire to maintain the symmetry of the structure. With 110 design variables, there was adequate design freedom to nearly achieve any partial measured eigenvectors. Thus any measurement error in the partial vectors could alter the symmetry of the model. The result of the tuning is listed in Table 8.1. The tuning process required 23.4 minutes of CPU time for four outer-loop iterations, and resulted in a decrease in the objective function by four orders of magnitude. All design variables remained within 10% of their nominal values.

Using the tuned model, an eigenanalysis for each of the nine damage cases was performed. The results, along with the experimentally measured data from the damaged structure, is presented in Table 8.2 for comparison. In order for the objective function minimization to be successful, it is important that the analytical model with simulated damage correlate well with the measured data of the damaged structure. Unfortunately, tuning to the nominal as well as the damaged data is only possible

Table 8.2 Changes in natural frequencies from damage on the NASA truss.

Damage case	Frequency (Hz)				
	Mode #1	Mode #2	Mode #3	Mode #4	Mode #5
Nominal	13.88 / 13.88 [†]	14.48 / 14.47	48.41 / 48.40	64.03 / 64.03	67.46 / 67.52
A	13.94 / 13.88	9.50 / 9.43	48.52 / 48.40	64.16 / 64.03	65.91 / 64.98
B	13.47 / 13.16	14.12 / 14.25	35.65 / 34.25	60.18 / 59.06	65.86 / 65.90
C	13.97 / 13.88	11.39 / 11.29	48.53 / 48.40	64.50 / 64.03	59.90 / 58.51
D	13.21 / 13.16	14.44 / 14.24	36.68 / 35.92	61.35 / 61.20	66.95 / 65.97
E	13.96 / 13.88	11.42 / 11.30	48.57 / 48.40	64.61 / 64.03	59.91 / 58.60
F	13.94 / 13.88	9.50 / 9.42	48.50 / 48.40	64.08 / 64.03	65.80 / 64.91
G	12.29 / 12.26	14.50 / 14.47	48.67 / 48.40	50.65 / 48.60	67.76 / 67.52
H	13.73 / 13.70	14.55 / 14.47	48.68 / 48.40	54.76 / 54.30	67.71 / 67.52
I	13.74 / 13.58	9.86 / 9.74	36.66 / 35.89	63.35 / 62.56	58.86 / 57.46

[†]Data presented in (measured / FEM simulated) format, where the first number represents the measured frequency and the second is the result of an eigenanalysis on the FEM model with the damaged element(s) removed.

with *a priori* knowledge of the damage. An attempt to ensure the simulated damaged analytical model correlated well with the measured data was the rationale behind maintaining symmetry during the tuning process.

8.2.3 Sensor Prioritization and Damage Localization Analysis. After tuning the analytical model, a prioritization of the degrees-of-freedom to instrument was performed as developed in Chapter VII. To demonstrate the capabilities of the APE software, a small number of sensors (8) were chosen. Threshold values of 10% for detectability and 7% percent for colinearity were used for both the sensor prioritization and the damage localization method. These threshold values represent the assumed combined uncertainty in both the measurement error and the modeling error. These values were chosen by performing three analyses for threshold values of 5, 7, and 10%, and then comparing overall results against values in Table 8.2. The eight prioritized sensor locations are shown in Figure 8.6. These eight degree-of-freedom locations were used to construct the eight elements of the partial eigenvectors for the damage identification process.

Having identified the sensor locations, a damage localization analysis was performed. The results of this analysis are contained in Table 8.3, listing the undetectable, symmetric, and identifiable elements. Table 8.4 presents a description of the element numbering used. The results show that using only the first five modes and the 8 component eigenvectors, 64 of the elements are undetectable from the measured data. This indicates that changes in the measured data are insignificant from damage in these

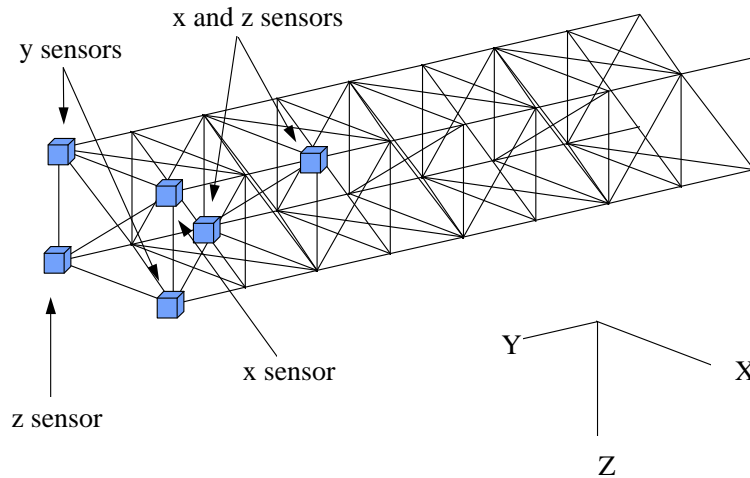


Figure 8.6 Prioritized sensor locations for the NASA truss.

elements. These results are consistent with a similar analysis on this truss presented by Kashangaki, Smith and Lim^[42] showing that 95% of the total strain energy associated with the first six modes was contained in only 40 elements. The unidentifiable elements are categorized as either battens, or elements located near the free end of the truss. The remaining 40 elements of the localization analysis are divided among 23 symmetric groupings containing one, two or four elements. One element from each of the 23 symmetric groups is used to define the initial search space for the identification process.

8.2.4 Damage Identification Results. Using the results of the sensor prioritization to define the measured data, the tuned analytical model, and the damage localization analysis to define the initial search space, damage identification using APE was performed. The results are contained in Table 8.5. On average, the results were achieved in one minute requiring 20 iterations. In six of the nine cases, the damage was localized to a single element or a single symmetric grouping. For Case D and Case E, a repeated use of the APE method using the results of the first identification application as the initial search space, was able to localize the damage down to the single correct element or

Table 8.3 Damage localization results for the NASA 8-bay truss.

Element #	Equivalent Symmetric Elements
32	36, 45, 49
34	38
47	51, 60, 64
58	62, 71, 75
59	
61	
63	
65	
72	
73	77, 86, 90
74	
76	
78	
84	88, 97, 101
85	
87	
89	
91	
98	
99	103
100	
102	
104	
Undetectable Elements	1-31,33,35,37,39-44,46,48,50,52-57,66-70,79-83,92-96

Table 8.4 Element numbering and descriptions for the NASA 8-bay truss.

Bay [†] #	Description		
	Longeron	Diagonal	Batten [‡]
1	6, 8, 10, 12	7, 9, 11, 13	1, 2, 3, 4, 5
2	19, 21, 23, 25	20, 22, 24, 26	14, 15, 16, 17, 18
3	32, 34, 36, 38	33, 35, 37, 39	27, 28, 29, 30, 31
4	45, 47, 49, 51	46, 48, 50, 52	40, 41, 42, 43, 44
5	58, 60, 62, 64	59, 61, 63, 65	53, 54, 55, 56, 57
6	71, 73, 75, 77	72, 74, 76, 78	66, 67, 68, 69, 70
7	84, 86, 88, 90	85, 87, 89, 91	79, 80, 81, 82, 83
8	97, 99, 101, 103	98, 100, 102, 104	92, 93, 94, 95, 96

[†]Bays are numbered consecutively starting from the free end.

[‡]Includes diagonal members in the batten plane.

single symmetric group. A capability could be incorporated into the APE algorithm to adaptively re-initialize the algorithm. Also noted in these two cases is assigned damage values which are greater than 100%. Unlike ASTROS-ID, the APE method cannot constrain the values of g_i to lie strictly within zero and one. These constraints can only be enforced by removing from the search space the corresponding elements with g_i 's outside the allowable range. As previously discussed in Chapter VI, to avoid prematurely discarding elements and allow for modeling error, the allowable range of g should be widened. For the results reported, the allowable range was set to $(0 \leq g_i \leq 2)$. An additional capability to slowly reduce the allowable range as the iteration progresses could be incorporated. The exact method to accomplish both the re-initialization and allowable range reduction are referred to as algorithm percolation methods, and is listed as a topic of future recommended research. For damage Case I, the compound break, damage to element #71 was not identified. Damage to element #71 (a longeron in the sixth bay) was assigned to a longeron in either bay three or four. This difficulty is in part due to the fact that the measured data for this damage case does not correlate well with the simulated damaged analytical model, as indicated by the values given in Table 8.2. The true culprit, modeling error or measurement error, cannot be determined from the known information. Anytime the simulated damage to the analytical model does not agree with the measured data for the same damage configuration, any method based on matching the partial measured data will have difficulty in obtaining the true solution.

For comparison purposes, ASTROS-ID was performed on Cases D, H, and I using the same 23 element initial search space as used for the APE method. The results are reported in Table 8.6. In the objective function, Equation (3.2), the eigenvalues were all assigned equal weighting of 100 for all five modes ($a_i = 100$), and all eigenvector components were assigned unity weighting ($b_{ij} = 1$). For Case D, ASTROS-ID identified damage to diagonal elements in the last four bays of the truss, but did not isolate it down to a single element. For Case H, damage was identified to longeron elements in the third and fourth bay of the truss. As for APE, ASTROS-ID could not correctly identify damage Case I, due to the measurement and/or modeling error as previously discussed. For Case I, both methods did identify damage in both longerons and diagonal elements.

Comparing the overall results, the ASTROS-ID method tended to spread the assigned damage over several elements, whereas the APE method typically assigned damage to a single element or symmetric group. This comparison illustrates the different nature of the two solution techniques, as

Table 8.5 APE identification results on the NASA truss.

Damage case	True damage		APE Identified		
	Element #	% damage	Element #	% damage	cpu time (sec.)
A	84	100	84(88,97,101) [†]	85	33
B	85	100	85	96	80
C	71	100	58(62,71,75)	94	65
D	78	100	78	98	76
			104	110	
E	62	100	58(62,71,75)	110	56
			32(36,45,49)	103	
F	97	100	84(88,97,101)	89	32
G	51	100	47(51,60,64)	88	85
H	34	100	34(38)	97	43
I	71	100	32(36,45,49)	80	63
	78	100	78	99	

[†]Data presented in I(S) format where I is the number of the identified element and S is the symmetric element numbers.

previously discussed in Section 6.2. Differences in the solutions are also in part due to the method used to establish the initial search space from the sensitivity analysis. Both methods used the results of the same damage localization analysis, however the analysis as described in Section 7.3 was tailored for the APE method. In general, an order of magnitude increase in CPU time was required for the ASTROS-ID solution.

8.3 Flexible Truss Experiment (FTE)

8.3.1 *Hardware.* The six-meter FTE was assembled at the Air Force Institute of Technology from excess hardware received from the Structural Dynamics Branch of Wright Laboratory after termination of the 12-Meter Truss Active Control Experiment.^[20] The hardware consists of the truss assembly, actuators and their power drivers, accelerometer sensors, and real-time digital control and signal processing equipment. As presented in the documentation on the 12-meter truss, there was considerable difficulty in obtaining a model of the 12-meter truss which correlated well with measured data. Although only half the structure is currently used due to physical space limitations, the difficulty in modeling the structure makes it ideally suited to use in validating a model tuning algorithm. It should also be noted that the experiment's name is somewhat of a misnomer. Although the word truss is used, the structure is actually a frame structure with rigid connections between members. The term truss typically is used for structures with pinned connections.

Table 8.6 ASTROS-ID identification results on the NASA truss.

Damage case	True damage		ASTROS-ID Identified		
	Element #	% damage	Element #	% damage	cpu time (sec.)
D	78	100	61	65	793
			63	36	
			65	93	
			76	15	
			78	88	
			91	64	
			104	24	
H	34	100	34(38)	96	602
			47(51,60,64)	73	
I	71	100	32(36,45,49)	40	541
	78	100	58(62,71,75)	83	
			61	84	
			63	50	
			65	94	
			78	90	
			84(88,97,101)	94	

8.3.1.1 *Truss Description.* The basic structure of the experiment is a lightly damped six-meter truss, cantilevered vertically from a rigid support base. The FTE is depicted in Figure 8.7. The truss is composed of two equal length frames of welded tubular aluminum alloy longerons and battens with bolt-in tubular Lexan diagonals in a back-to-back “K” pattern. A section of the FTE is depicted in Figure 8.8. The assembled truss has a square cross section of 20 inches on a side. The longerons are made from 6061-T6 aluminum alloy tubes with a 1.5-inch-square cross section and 0.065 inch wall thickness. The battens are 6061-T6 tubes with 0.5-inch-square cross section and 0.063 inch wall thickness. The diagonal members are Lexan tubing (270,000 psi elastic modulus) with a 1.5-inch-diameter circular cross section with 0.125-inch wall thickness. The diagonals have aluminum end fittings which are fastened to the truss with two bolts and a half-clevis joint at both ends. The truss has 4 bays in each of the two sections for a total of eight bays. The two sections are bolted together with two bolts at each longeron end. Four bolts at the base of each longeron secure the truss to a 1-inch thick aluminum plate which is securely bolted to the laboratory floor. The bolt-in diagonals allow quick structural modifications to simulate a damaged structure.

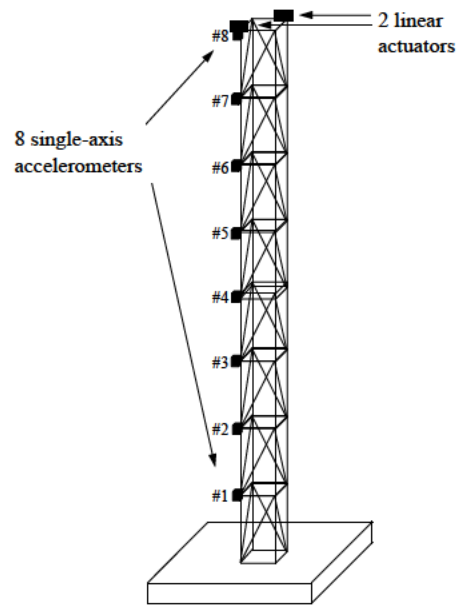


Figure 8.7 Six-Meter Flexible Truss Experiment, showing initial sensor locations.

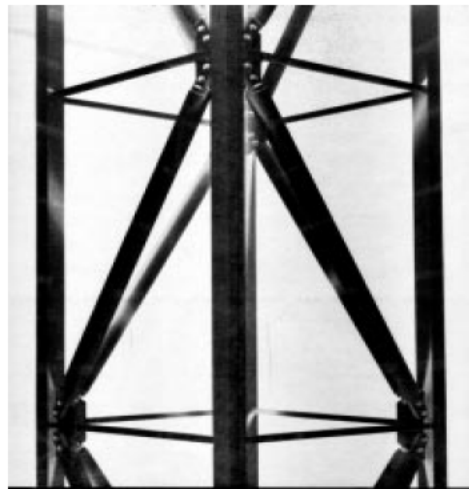


Figure 8.8 Joint construction for the FTE.

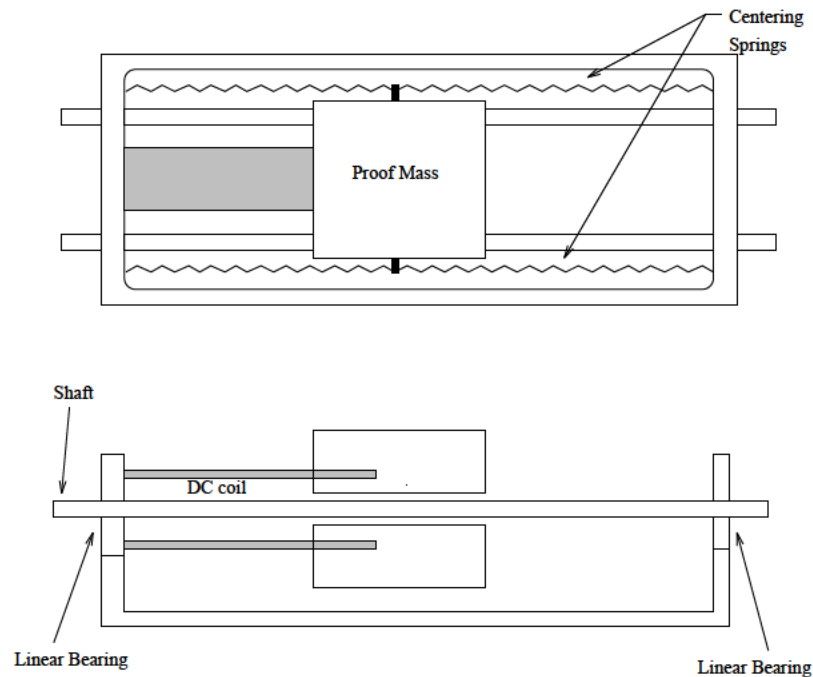


Figure 8.9 Linear actuators for the FTE.

8.3.1.2 *Actuators.* Input excitation to the truss for frequency response testing is provided through the use of two linear momentum exchange (reaction mass) actuators. Each actuator is capable of approximately 1-pound-force peak output. Power is provided to the actuators by individual current drive circuits. The actuators use a linear dc motor with the armature fixed to a base and the permanent magnetic field suspended on shafts and linear bearings. Two linear springs provide the centering force for the mass. The resonant frequency for each actuator is approximately 0.9 Hz, with an effective viscous damping ratio of approximately ten percent of critical. For comparison, the fundamental frequency of the truss is approximately 7 Hz. Mounting plates were fabricated to attach the actuators atop two longerons on the free-end of the truss. Driving the actuators in phase with one another excites the bending modes in one axis. The torsional modes are excited by driving the actuators 180 degrees out-of-phase. A sketch of the actuator is shown in Figure 8.9.

8.3.1.3 *Sensors and Supporting Equipment.* Acceleration measurements are made using eight Sunstrand QA-1400 single-axis inertial accelerometers. These accelerometers were chosen for their high sensitivity and low noise characteristics. Initially, the eight accelerometers were placed

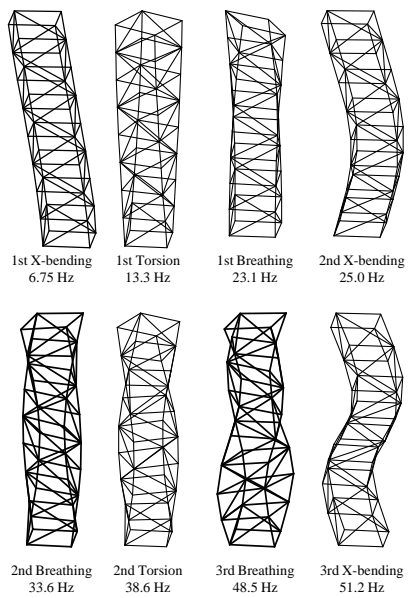


Figure 8.10 Low frequency mode shapes for the FTE.

along one longeron at the node location at each bay. For signal processing, a Tektronix 2642A Fourier Analyzer is used to measure and average the frequency response functions.

8.3.2 Model Tuning.

8.3.2.1 Finite Element Model. The FTE was modeled in ASTROS using five different types of beam elements for a total of 96 elements. The five types were: aluminum vertical longeron elements, aluminum horizontal batten elements, Lexan diagonal elements, aluminum horizontal mid-batten elements, and aluminum horizontal top-batten elements. The different batten configurations are due to the fact that the FTE is constructed of two 4-bay sections which can be bolted together. Lumped masses were included to account for the actuators, top-plates (actuator attach points), “K” brackets (used to secure the diagonal members) and mid-plates (bolt assemblies used to secure the two 4-bay sections together). Care was taken to accurately obtain the mass properties, area properties and moments of the structural elements. The elastic properties were determined from laboratory tests on individual elements. These parameters were all used to construct a baseline data deck for input into ASTROS. Using the results of the baseline finite element analysis along with software written in

MATLAB[®] to display and animate mode shapes, a characterization of the low frequency (below 70 Hz) behavior of the FTE was performed. Mode shapes were classified into four categories as: X-bending, Y-bending, torsion, and breathing. An illustration of these four different mode shapes are shown in Figure 8.10. Unlike the NASA truss, the FTE did not have diagonal members in the batten plane and thus exhibited a breathing mode. The breathing mode corresponds to an expansion and contraction of the truss in the batten plane, similar to the motion of the human rib cage. The diagonal battens in the NASA truss sufficiently stiffened the batten plane to preclude this type of motion at low frequencies. The presence of this fourth type of mode increased the modal density and consequently increased the difficulty in the modal parameter identification process. Due to the near symmetry, the Y-bending mode shapes are similar to the X-bending shapes and are not shown. Note that the frequencies appearing in the figure are for the analytical model prior to tuning. The next step was to compare the analytical results to measured data.

8.3.2.2 Testing Procedure. Experimental measurements were performed on the FTE using random vibration testing. Measured eigendata of the FTE were obtained from the 16 FRFs between the two linear actuators and eight single-axis accelerometers placed as shown in Figure 8.7. The input excitation to each actuator was a band limited (0 - 50 Hertz) pseudo-random signal. There were 4096 discrete sample points recorded by the spectrum analyzer, providing a frequency resolution of 0.031 Hertz. Frequency averaged transfer functions between the input excitation and the eight accelerometers were measured. The inverse discrete Fourier transforms of these transfer functions yielded the impulse response functions which were input into ERA to obtain measured modal frequencies and shapes, as described in Chapter IV. Distinguishing between bending modes and torsion modes was easily facilitated by exciting the structure in both bending (actuators in phase), and torsion (actuators 180 degrees out-of-phase). Figure 8.11 shows the resulting averaged FRF output at accelerometer #8 for the two different types of excitation, measured using a 100 Hz bandwidth.

8.3.2.3 Sensor Prioritization. The sensor prioritization method presented in Chapter VII was applied to the FTE to determine the prioritized location of the eight single-axis accelerometers for damage identification. During initial testing, it was determined that the initial locations of the eight sensors, along one longeron as was shown in Figure 8.7, was not a good choice. For these sensor locations, it was not possible to measure the Y-bending mode. Additionally, several of these

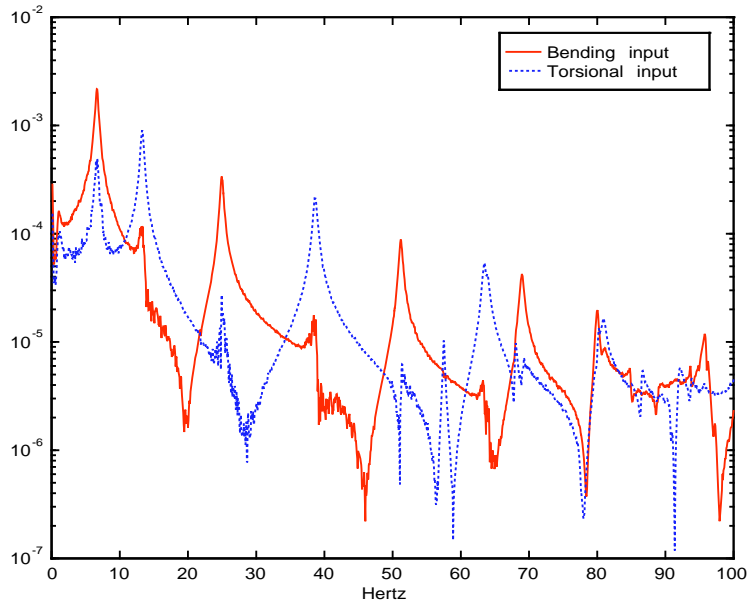


Figure 8.11 Comparison of bending and torsional excitation on the FTE.

locations yielded small gradient values as determined by the sensitivity analysis. For the analysis, the first eight modes were used, which represented all the global modes within the frequency band (0-50 Hz) measured. These modes were used to prioritize the eight sensor locations. The prioritized locations of the eight sensors are shown in Figure 8.12. The output of these eight sensors was used to obtain the partial mode shapes used in the tuning algorithm.

8.3.2.4 Measured Data. Numerous problems were encountered in obtaining the measured modal properties. The first was in the choice of the excitation. The original choice was to use the two actuators in-phase and out-of-phase as previously described. This presented a difficulty in measuring the breathing modes. Examination of the transfer functions depicted in Figure 8.11, illustrate the absence of the breathing modes (≈ 22 Hz, ≈ 34 Hz) in the measured transfer functions. Although ASTROS-ID does not require that all modes be included in the objective function, without inclusion of the breathing modes, numerous mode swaps occurred as the breathing modes “wandered” during the tuning process. For damage identification to be successful, it is important that the simulated analytical damage closely match the measured data of the damaged structure as previously discussed. This is best

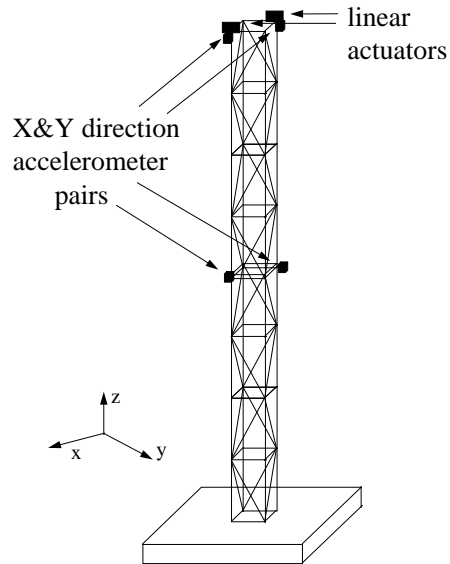


Figure 8.12 Prioritized sensor locations on the FTE.

accomplished by ensuring all modes including the breathing mode match the physical structure as best as possible. An additional discussion on this topic is contained in Reference 11.

To measure the breathing mode, the actuators atop the longerons were rotated ninety degrees. This allowed direct excitation of the breathing mode by exciting out-of-phase, and X-bending excitation by exciting in-phase. In this configuration however, both Y-bending and torsion modes were not excited and hence could not be accurately measured. The simple solution seemed to be to take two measurement sets in the first excitation configuration, and two additional measurement sets with the actuators rotated ninety degrees. While all modes were now clearly identifiable in the transfer functions, a new problem was observed. The inertia properties of the rectangular linear actuator's affected the measured response depending on their orientation, and thus a shifting of the modes resulted whenever the actuator position was changed. A compromise was achieved by using the two actuators atop two longerons diagonally from one another and mounted ninety degrees to one another. In this configuration each actuator was excited independently, one exciting X-bending and breathing, and the second exciting Y-bending and torsion. This still did not represent an ideal situation for the following reason. As one actuator was being excited, the other actuator's proof mass was fixed. This effectively changed the apparent inertia

properties atop either longeron, depending upon which actuator was being excited. Again, a small shift was observed in the measured frequencies, however, this was determined to be an acceptable compromise, not requiring actuator re-design. Note that the difficulties with the actuator excitation all arose as the result of using non-ground based excitation, which represented a significant mass at the tip of the cantilevered frame. For future space application studies, actuator design is an important consideration in obtaining accurate modal data.

Having finally determined the sensor and actuator positions, the modal extraction method using ERA was performed. Due to the closely spaced modes, an additional problem was encountered. Although the modal frequencies were easily identified, the extracted mode shapes were observed as linear combinations of one another for the closely spaced modes. This was especially troublesome during the identification of partial mode shapes for the damaged structure. Damage Case 2, as described in Section 8.3.4 was chosen to illustrate the problem. The measured modes along with the analytical modes for the eight sensor locations are depicted in Figure 8.13. As shown in the figure, there is considerable discrepancy in the data, particularly for the closely spaced fourth, fifth, and sixth modes. Additional testing using four independent excitations, where each mode was individually excited, yielded close results to the analytical shapes. However, when only two actuators were used, for the reasons expounded upon above, the modes appeared as linear combinations of one another. To determine the linear combination, a least squares solution was used to determine the coefficients required to best match the measured modes to the modes of the simulated damaged analytical model. Two coefficients were computed to separate modes 1 and 2, and three different coefficients were used to separate modes 3, 4, and 5. The de-coupled mode shapes are shown in Figure 8.14. The abscissa represents the eight sensor measurements numbered one through eight. A line is shown connecting the eight discrete points to aid in visualization. Note that this de-coupling method was only possible because of the known location of the damage for the simulation. In actual practice, a re-design of the input actuators would be required to correctly obtain the measured modes without resorting to the analytical model. This problem was not observed in the data on the NASA truss, which did not use non-ground based actuators, nor exhibit a breathing mode. In all cases, there was no trouble in obtaining the torsion shapes, which were clearly separated from the bending and breathing shapes. Additional research on determining partial mode shapes for closely spaced modes is recommended for future work.

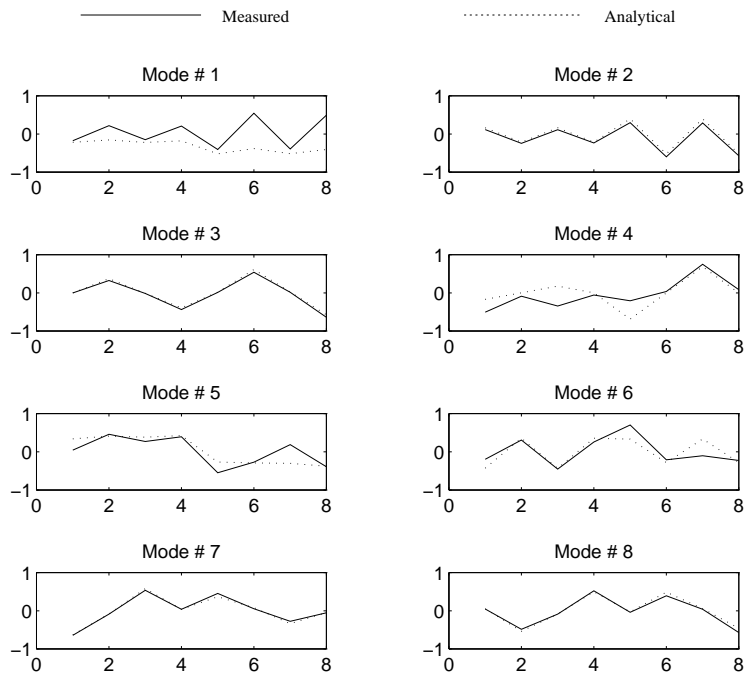


Figure 8.13 Analytical and measured mode shapes before de-coupling, Case 2.

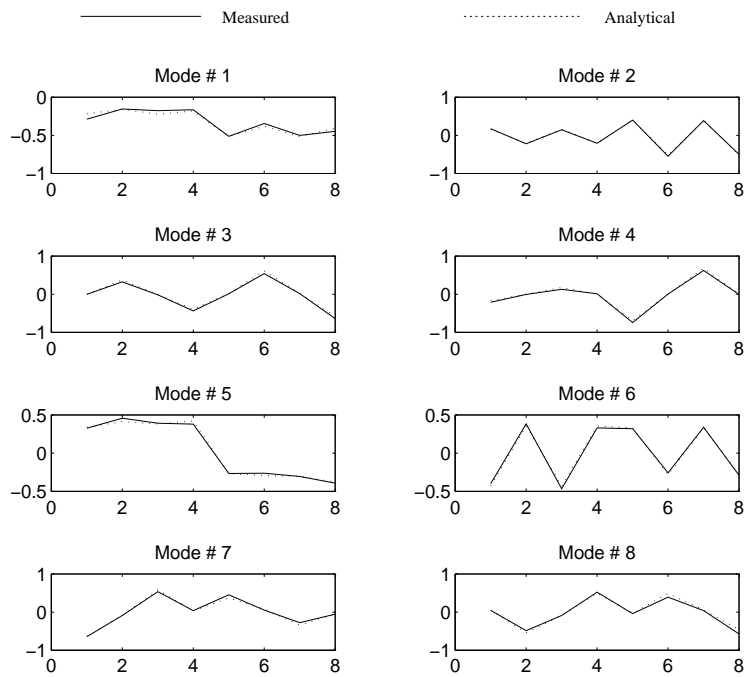


Figure 8.14 Analytical and measured mode shapes after de-coupling, Case 2.

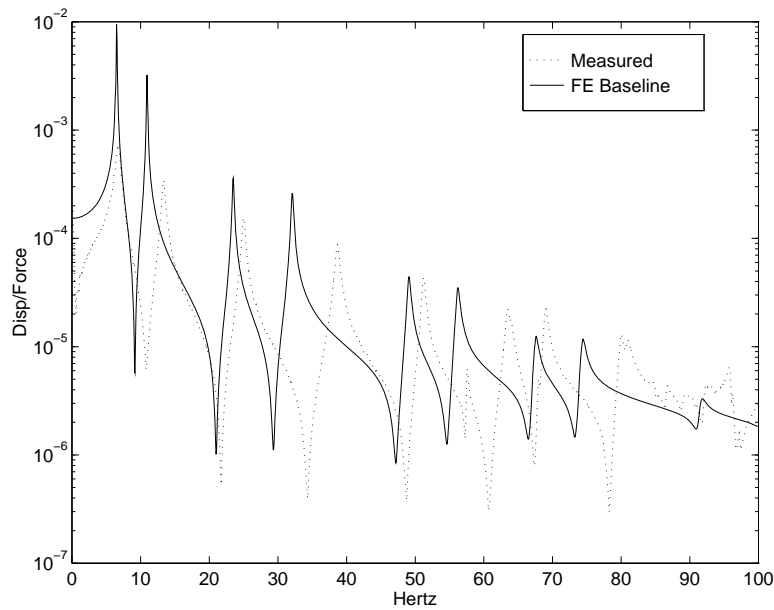


Figure 8.15 Comparison of initial analytical model and measured frequency response.

8.3.2.5 *Model Tuning Results.* Despite the effort expended in constructing the baseline finite element model of the FTE, it did not agree well with the measured data. The poor correlation between the baseline analytical and measured data is depicted in Figure 8.15, which shows the transfer function between a colocated sensor and actuator at the top of the FTE. Prior to computing the analytical transfer functions, damping was included in the model by assuming a value of one half of one percent of critical damping for all modes (a typical measured value). This was done only to avoid the unbounded resonant spikes due to an undamped model, and thus the height of the resonant peaks between analytical and measured data is insignificant. It is clear from Figure 8.15 that the baseline finite element model does not adequately represent the measured dynamic characteristics of the FTE and would hence benefit greatly from model tuning.

Using ASTROS-ID, the baseline finite element model was tuned to the measured data. For the tuning, the frequencies and shapes of the first eight modes were included in the objective function. Twenty three design variables were chosen for the tuning process. A description of the design variables as well as the tuned values, are given in Table 8.7. Values in the table are normalized, such that the initially assumed value for each design variable is unity. To account for the added stiffness in the

Table 8.7 Design variable values in the FTE finite element model.

DV #	Description	Tuned value [†]
1	battens (elastic modulus)	1.00
2	mid-battens(elastic modulus)	1.00
3	longerons (elastic modulus)	0.80 [‡]
4	diagonals (elastic modulus)	1.20 [‡]
5	top-battens (elastic modulus)	0.99
6	battens (I_1)	0.79
7	mid-battens (I_1)	0.67
8	longerons (I_1)	0.58
9	diagonals (I_1)	1.18
10	top-battens (I_1)	0.84
11	battens (I_2)	1.11
12	mid-battens (I_2)	1.14
13	longerons (I_2)	1.99
14	diagonals (I_2)	1.00
15	top-battens (I_2)	1.00
16	battens (mass)	1.51
17	mid-battens (mass)	1.26
18	longerons (mass)	0.42
19	diagonals (mass)	2.81
20	“K” brackets (mass)	0.50 [‡]
21	actuators (mass)	1.00
22	mid-plates (mass)	0.84
23	top-plates (mass)	1.28

[†]Values were normalized such that initial values are all unity.

[‡]Value on boundary of allowable excursion limit for this variable.

joints resulting from the welded assemblies, the bending stiffness of the elements was chosen as a design variable by allowing the I_1 and I_2 properties to vary in addition to the elastic modulus for each element. To account for the symmetry of the structure, all common elements were linked to a single design variable. The tuning process converged in six outer-loop iterations requiring 18 minutes of CPU time. Convergence was defined as a less than one half of one percent change in the objective function value between two consecutive outer-loop iterations. The results of this tuning are shown in Figure 8.16, depicted for the same actuator/sensor combination as used in Figure 8.15.

The results show excellent agreement over the 40 Hz frequency band spanned by the modes included in the objective function. The first four columns of Table 8.8 lists the frequencies for the first eight modes, comparing the measured data to the tuned finite element model. The objective

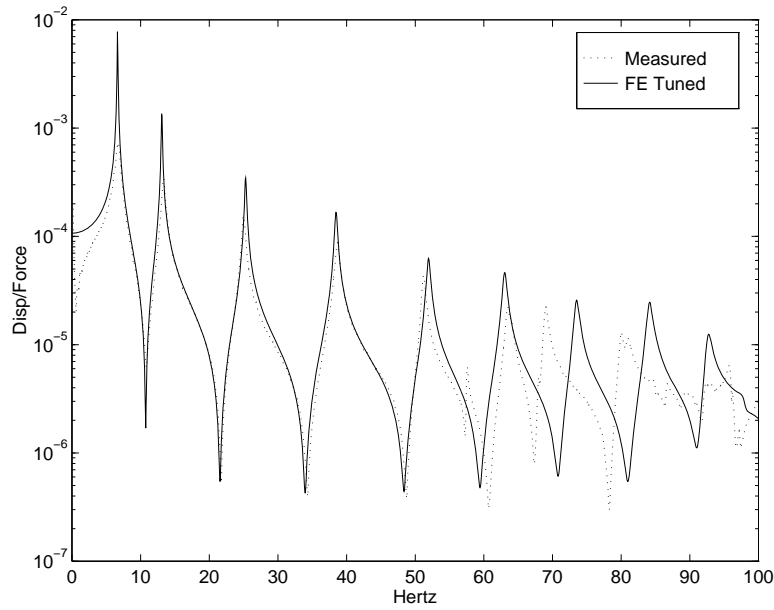


Figure 8.16 Comparison of the tuned analytical model and measured frequency response.

function, Equation (3.2), included the terms a_i and b_{ij} to weight individual contributions to the overall value. For the tuning, all a_i coefficients were set to 100 and all b_{ij} were set to unity. This represents equal confidence in the measurement data for all frequencies included in the objective function, with a stronger emphasis placed on tuning the modal frequencies than the shapes. In general, selection of the weighting coefficients is dependent upon the confidence with which each mode is measured, as well as the designer's desire to minimize a selected portion of the correlation error. For this case, emphasis was placed on minimizing the frequency correlation errors.

8.3.3 Damage Localization Analysis. Using the tuned analytical model, the damage localization method presented in Chapter VII was applied to the FTE. Based on repeatability of the measurement data, and the existing correlation errors between the finite element model and the measured data, the detectability threshold values were set at 10%. The threshold for S_λ was set at 7% and the S_ϕ threshold at 25%. This reflected the increased confidence in measuring the eigenvalues over the eigenvectors, reflecting the difficulty in measuring the closely spaced modes. Using the eight sensor locations chosen in Section 8.3.2.3 and the first eight modes, the extent to which damage can be

Table 8.8 Analytical and measured natural frequencies of the FTE.

Mode #	Description	Frequency (Hz)					
		Nominal		Damaged			
		FE tuned	measured	Case 1		Case 2	
FE	measured			FE	measured		
1	1st Y Bending	6.32	6.32	6.32	6.34	6.23	6.20
2	1st X Bending	6.33	6.33	5.85	5.86	6.32	6.30
3	1st Torsion	12.51	12.64	11.38	11.27	12.27	12.37
4	1st Breathing	22.26	22.29	22.26	23.31	22.26	22.10
5	2nd Y Bending	23.97	24.02	22.01	21.48	23.17	23.48
6	2nd X Bending	24.09	24.18	24.03	24.15	24.04	24.20
7	2nd Breathing	34.01	34.03	33.36	33.63	33.71	33.79
8	2nd Torsion	36.46	36.31	36.07	35.89	36.15	36.02

localized was determined by classifying the 96 elements using the U/S/I format. The results indicate that 26 elements cannot be identified, and the remaining 70 elements are arranged in 15 symmetric groups. The 26 undetectable elements were all batten elements. The remaining 15 symmetric groups consisted of either longerons, battens, or diagonal elements localized to either a single bay or adjacent bays. This analysis was used to define the initial search space for a damage identification algorithm using APE. The results of the damage localization analysis are given in Table 8.9. A description of the element numbering is contained in Table 8.10.

8.3.4 Damage Identification Results. For the APE method, the tuned elemental parameters of the finite element beam model were used to construct the matrix B according to Equation (6.13) along with the tuned mass and stiffness matrices M and K . The measured partial eigendata of modes 1 through 8 were then used to determine structural damage. Two damage configurations were tested. The first (Case 1) was the full removal of a diagonal strut in the sixth bay (as measured from the free end). The second (Case 2) damage configuration was the replacement of a diagonal strut in the seventh bay with one in which ≈ 50 percent of the strut's cross sectional area was removed. The analytical and measured natural frequencies for the first eight modes are contained in Table 8.8. Mismatches between the analytical and measured frequencies are the result of both measurement uncertainty as well as modeling errors.

Using the results of the damage localization analysis, the search space consisted of fifteen elements, one element from each APE symmetric group. Since no *a priori* knowledge of the damage

Table 8.9 Damage localization results for the FTE.

Element #	Equivalent Symmetric Elements
17	18, 19, 20
29	30, 31, 32
33	34, 35, 36
37	39
38	40, 42, 44
41	43, 46, 48
45	47, 49, 52
50	51, 53, 55
54	56, 57, 59
58	60, 62, 63
69	70, 71, 72, 73, 74, 75, 76
77	78, 79, 80
81	90, 95, 96
82	89, 94, 97
83	84, 85, 86, 87, 88, 91, 92, 93, 98, 99, 100
Undetectable Elements	5 - 16, 21 - 28, 61, 64 - 68

Table 8.10 Element numbering and descriptions for the FTE.

Bay [†] #	Description		
	Longeron	Diagonal	Batten
1	65, 66, 67, 68	85, 86, 91, 100	33, 34, 35, 36
2	61, 62, 63, 64	84, 87, 92, 99	29, 30, 31, 32
3	57, 58, 59, 60	83, 88, 93, 98	25, 26, 27, 28
4	53, 54, 55, 56	82, 89, 94, 97	21, 22, 23, 24
5	49, 50, 51, 52	81, 90, 95, 96	17, 18, 19, 20
6	45, 46, 47, 48	77, 78, 79, 80	13, 14, 15, 16
7	41, 42, 43, 44	73, 74, 75, 76	9, 10, 11, 12
8	37, 38, 39, 40	69, 70, 71, 72	5, 6, 7, 8

[†]Bays are numbered consecutively starting from the free end.

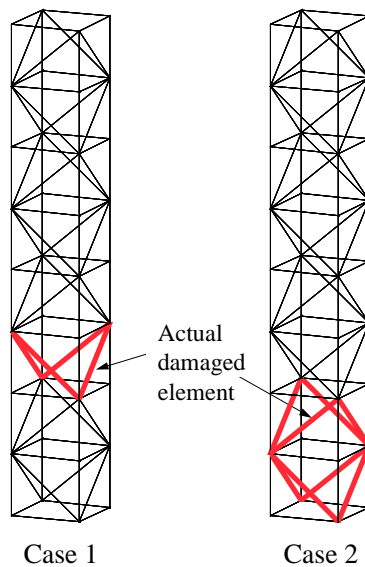


Figure 8.17 APE identified damage regions on the FTE.

Table 8.11 APE damage identification results on the FTE.

Test Case	True failed element #	APE identified element #s	APE symmetric element #s	cpu time (sec.)
1	77 - 100%	77 - 104%	78 79 80	530
2	75 - 50%	69 - 40%	70 71 72 73 74 75 76	543

location is assumed, and the measurement and model uncertainty for both test cases are identical, the search space for each test case is identical.

The results of the two test cases are presented in Table 8.11 and depicted in Figure 8.17. In each case, the damage was correctly localized to a small area of the truss containing the true damaged element. Further damage identification refinement to the exact element would require either additional measured data, or a closer correlation between measured data and the analytical model. Improving model correlation requires a higher fidelity model and/or less measurement uncertainty. In each test case, the correct element and exact amount of damage was determined when noise free analytical

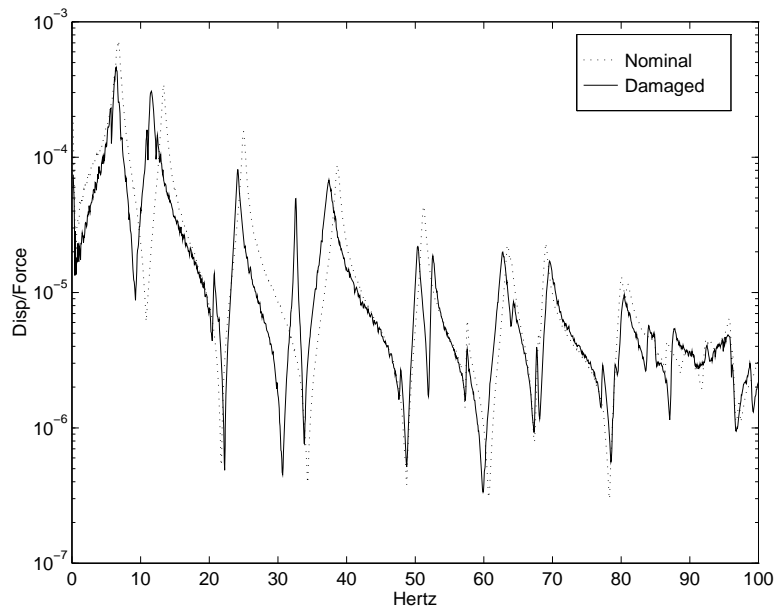


Figure 8.18 Effect of structural damage on the measured response.

simulated data was used in lieu of the measured data. A representative frequency response, showing the effect of damage (Case 1) is depicted in Figure 8.18.

8.4 Summary

The damage identification process was illustrated on two experimental structures and the results reported. The first was a cantilevered truss modeled with 104 rod elements with a total of 96 degrees-of-freedom. The measured data consisted of the first five flexible modal frequencies, and only eight components of the five corresponding eigenvectors. The second experiment was a cantilevered frame assembly modeled with 96 beam elements with a total of 192 degrees-of-freedom. The measured data consisted of the first eight flexible modal frequencies, and only eight components of the eight corresponding eigenvectors. In each test case, the structural damage could be localized to a small portion of the structure. The extent to which damage can be localized was limited by both model fidelity and accuracy of the measured modes.

IX. Conclusions and Recommendations

9.1 Research Conclusions

A method was presented to identify damaged structural elements from limited measurement data. The problem was broken into four distinct tasks: identification of modal parameters, model tuning, damage localization, and damage identification. The research showed that structural damage can be identified using only a small measured subset of the eigenstructure. Experimental tests were conducted on two separate structures. The first was a cantilevered truss modeled with 104 rod elements with a total of 96 degrees-of-freedom. The measured data consisted of the first five flexible modal frequencies, and only eight components of the five corresponding eigenvectors. The second experiment was a cantilevered frame assembly modeled with 96 beam elements with a total of 192 degrees-of-freedom. The measured data consisted of the first eight flexible modal frequencies, and only eight components of the eight corresponding eigenvectors. Two key factors in the ability to identify the damage are: the accuracy of the measured data, and the fidelity of the analytical model. In the case of perfect measurements and perfect model correlation, the exact damage can be identified. To account for imperfect measurements and model correlation errors, the concept of damage localization was introduced. In such cases, damage can be localized to a small sub-section of the structure.

Also investigated was the relation between increasing the number of sensors and increasing the number of measured modes. The results showed that more information on structural damage is gained from the ability to measure an additional modal frequency than from the ability to measure one more degree-of-freedom. Previous studies investigated which modes should be used in a damage identification algorithm by determining which modes change the most. In this research work, it was found that as many modes as can accurately be measured should be used. Modes which are unchanged from damage contain information on elements which are undamaged, and thus help further narrow down the search space.

For the case where structural damage is confined to changes in the stiffness of structural elements, it was shown that the resulting natural frequencies from damage can only decrease. Placing an upper limit on the target frequencies corresponding to the nominal frequency of the analytical model minimized the problem of mode switching during the iteration process and produced results which were closer to the true damage.

An objective function was introduced which represents the mismatch between the measured and analytical partial eigendata. Two methods were used to minimize this function: ASTROS-ID, and APE. A comparison of these two methods follows. Both solution methods use an iterative solution technique to minimize the same objective function and are suitable with partial measured modal data. (An iterative method is not required for the APE solution when perfect full length eigenvector measurements can be obtained.) For ASTROS-ID, design variables can be any elemental mass or stiffness values, whereas for APE the design variables are limited to changes in elemental stiffness. The advantage of the APE method is that it does not require an eigenanalysis and the computation of the sensitivity values to each design parameter at each outer-loop iteration step. APE however requires the decomposition of a large, sparse, possibly singular matrix, which requires sparse matrix techniques to make it computationally competitive. Both techniques benefit greatly from an initial sensitivity analysis to reduce the search space prior to initiating either method. Due to the algorithm percolation process used in the APE method, APE typically reduces the solution space to fewer elements than the ASTROS-ID method. As currently coded, the APE method is computationally an order of magnitude faster than ASTROS-ID. The success of either method is contingent upon accurate measured data and an analytical model which correlates well with the measured data for the nominal, as well as the damaged configuration. Neither method is guaranteed to converge to a global minimum.

9.2 Recommendations for Additional Research

During the course of any research investigation, additional understanding of the problem is always accompanied with additional questions. During the experimental portion of modal identification on the FTE, considerable difficulty was associated with extracting partial modal data for modes which are spaced very closely in frequency. The use of additional input/output relationships helped to minimize this problem, but may not be possible on orbit. Thus, it is recommended that additional research be conducted on extracting mode shapes for closely spaced modes using non-ground base actuators. For model tuning, several methods can be adopted to speed up the ASTROS-ID algorithm. Currently, the design variable sensitivity is performed through a finite-difference method. Since these sensitivities are known explicitly from the finite element formulation, the finite-difference method can be replaced with either an analytical method in the current version of ASTROS (12) or the use of the matrix operator P as used in APE. Additional research can be conducted in the percolation of either algorithm for damage

identification. For either method, an adaptive method to narrow the search space can be employed to speed the processing time. The ASTROS-ID search space currently is not reduced during the solution process, and hence requires the sensitivity calculation during each outer-loop iteration step for all design variables included in the initial search space. For the APE method, the search space is reduced during the iteration process by fixed initial tolerances on the damage fractions. A method of gradually tightening these tolerances as the solution progresses is desirable, and requires further investigation. With respect to damage localization and sensor prioritization, the results are dependent on the chosen thresholds for both detectability and colinearity. Although the threshold values are problem dependent, additional studies would enhance future selection of these design parameters. Both methods can be expanded to include structural damping in the formulation.

Lastly, the damage identification method presented in this study should be applied to other structural applications. This method is suitable to any modeled structure where practicality dictates that only a small portion of the eigenstructure can be measured. The method is ideally suited for remote monitoring where more conventional non-destructive testing methods, such as x-raying and acoustic emissions, cannot be employed.

Appendix A. ASTROS-ID Software Modules

A full description of the initial version of ASTROS-ID is contained in the work by Gibson.^[18] However, during the course of this research effort, several shortcomings of the software were discovered, requiring either modification or replacement of the original software code. The overall intent has not been altered from that originally proposed by Gibson. This section is intended only to provide a brief description of the software component modules used in ASTROS-ID that were modified or altered after the original work. Errors encountered using the original code included runtime errors when using non-consecutively numbered modes, as well as when using a different number of mode shapes than modal frequencies. Other problems encountered included gradient calculations that did not properly account for mode normalization and mode switches which were not identified, as well as errors in the reporting of results. Second-order eigenvalue gradient information was also included in the sensitivity calculations. Changes in the software are listed below which corrected these problems. The mathematical foundation was presented in Chapter V. This list should be used to supplement the original work. Information on the use of ASTROS can be obtained in Reference 55.

A.1 Modified Software Modules

1. *MAPOL-ID.SEQ* The mapol sequence was modified to incorporate the non-consecutive eigendata, correct for point normalization, and incorporate the use of second-order gradients.
2. *TUNE.FOR* This module was modified to incorporate the non-consecutive eigendata and incorporate the use of second-order gradients. Also included was the ability to set the optimization parameters from the input data deck, and incorporate the numerical optimizer Design Optimization Tools (DOT)^[13] for the inner-loop optimization.
3. *REPORT.FOR* This module was updated to correct numerous formatting errors when reporting results.
4. *Misc.* The original code included an unstructured data base entry called 'MTRACE' which kept track of the mapping between mode numbers during the iteration process. A simpler method of renumbering the stored input data whenever a mode switch occurred

was incorporated. As a result, most subroutines required a minor modification to remove the MTRACE reference.

A.2 *New Software Modules*

1. *ORTHTEST.FOR* This routine checks for mode switching by performing a matrix search on the modal correlation coefficient matrix, and updates the TSHAPE and TFREQ relational entities corresponding to switched modes. This routine replaced the previously used orthogonalization test.
2. *MTCHINDX.FOR* This routine matches mode numbers and index numbers between frequencies and shapes required when non-consecutive data is input.
3. *GETDLAM2.FOR* This routine retrieves entities required for the second-order gradient term calculations.
4. *DLAM2.FOR* This routine computes the second-order eigenvalue gradient terms.
5. *UTMCOPY.FOR* Matrix utility routine to copy a matrix entity in the data base.
6. *PUTSCAL.FOR* This routine allows multiple calls to put scalars into a matrix in the data base from within the same loop.
7. *NORMINDX.FOR* This routine determines the internal degree-of-freedom corresponding to the normalization point.
8. *NORMAL.FOR* This routine point normalizes the analytical eigenvectors such that the degree-of-freedom corresponding to the max measured degree-of-freedom from the input (TSHAPE) data is unity. A warning message is displayed (and the proper normalization performed) if the input mode shapes were not normalized to maximum entry equals one. Eigenvectors not used in the tuning process are mass normalized.

Appendix B. APEWARE: Damage Identification Integrated Software

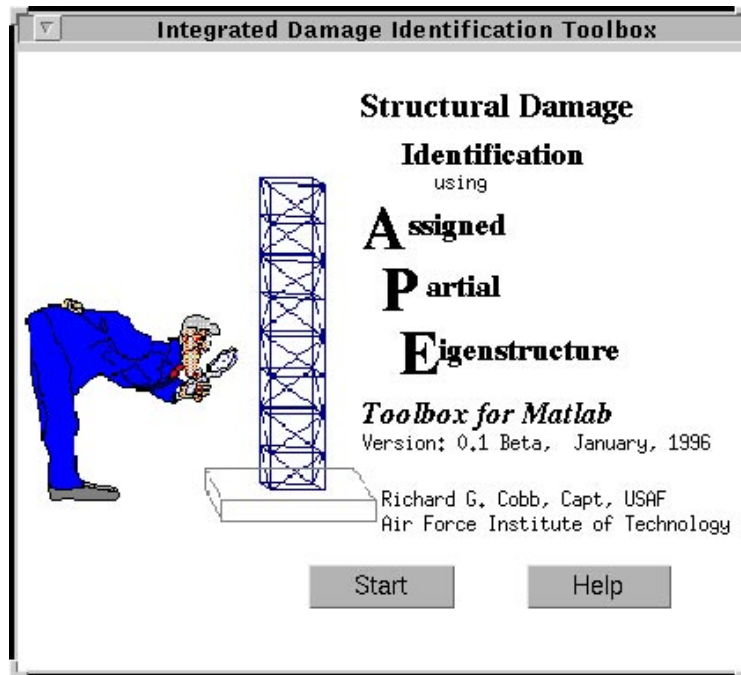


Figure B.1 Software opening menu.

The four tasks associated with damage identification were combined into an integrated software tool which was programmed in MATLAB[®]. This software package provides the design engineer an easy to use tool to aid in determining system identification requirements, sensor placement, damage localization studies, and damage identification using the assigned partial eigenstructure method. Also included is pre and post-processing routines for use with ASTROS-ID. This appendix is intended only to provide the reader with a brief introduction to the functionality and capabilities of the software package. The algorithms for each task are based on the work presented in the main text, and were briefly described under the software implementation section for each task. The specific algorithm descriptions are not provided. Familiarity with MATLAB[®] is assumed. Information on the use of MATLAB[®] is contained in Reference 52. The software was written and implemented on a Sun Sparc-10 workstation running under Unix/Sun4. While most routines are ascii '.m' format which can be run on any platform, routines related to the sparse matrix operations were written in FORTRAN and compiled as '.mex4' code. These routines must be re-compiled when changing to a different platform. The routines are **bspars.mex4**(bspars.f), **fillmat.mex4**(fillmat.f), and **spqrmex.mex4**(available from MATLAB[®] technical support).

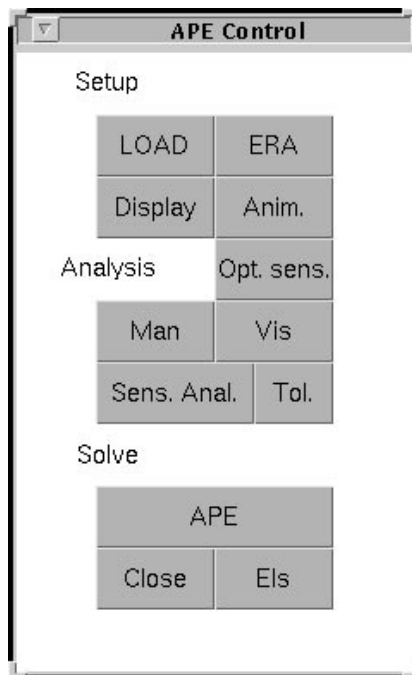


Figure B.2 APE control menu.

The program is initiated from the MATLAB[®] command line with the command ‘apeware’. Program control is facilitated through the main control panel as depicted in Figure B.2. Model files are loaded into the workspace by depressing the [**LOAD**] button. The model files consist of information on the finite element model matrices, grid data, and element connectivity data. A complete description of the required data in the model file along with a list of utilities which can be used to generate the data is included in Section B.5. The remaining buttons are described below.

[ERA.] Initiates the ERA submenu used for system identification as further defined in section B.1.

[Display.] Produces a wire frame drawing of the model, showing all instrumented degrees-of-freedom. A typical display is shown in Figure B.3.

[Anim.] Initiates the animation submenu used to display and animate deformed geometry for any mode contained in the model file. Modes may be produced either from the measured data using ERA, or from the results of an eigenanalysis on the FEM model. This feature is further described in Section B.2.

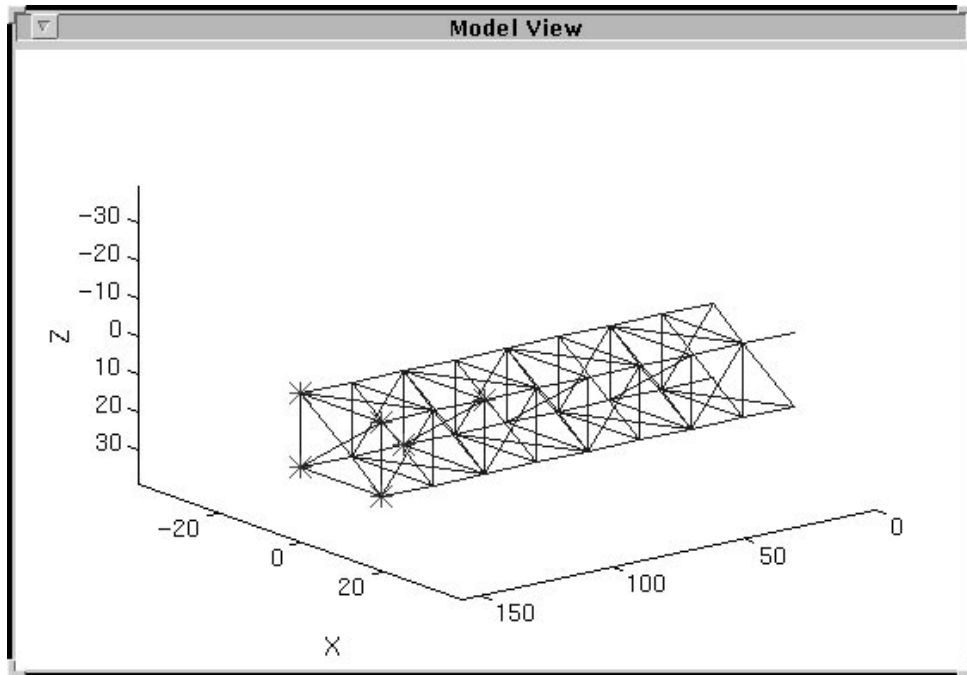


Figure B.3 Geometry display screen.

[Opt. sens.] Performs an analysis to prioritize the degrees-of-freedom to instrument based on the modes selected (using the **[Man]** selection) and the tolerances set in **[Tol]**. This feature is further discussed in Section B.3.

[Man.] Opens a dialogue box as shown in Figure B.4, allowing the user to input the measured modes, the instrumented degrees-of-freedom and the element numbers of the elements used for the APE method. The instrumented degrees-of-freedom and the element numbers are updated automatically when using the **[Vis]** and **[Sens. Anal.]** selections respectively, as discussed below.

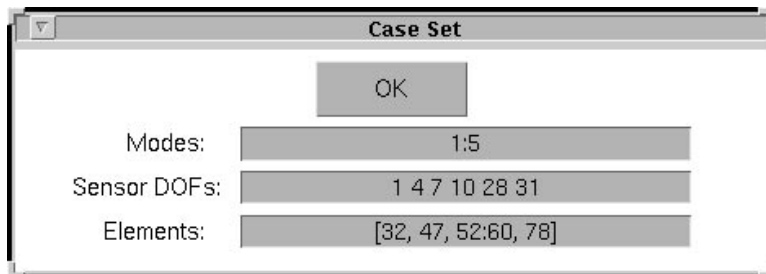


Figure B.4 Manual input dialogue box.

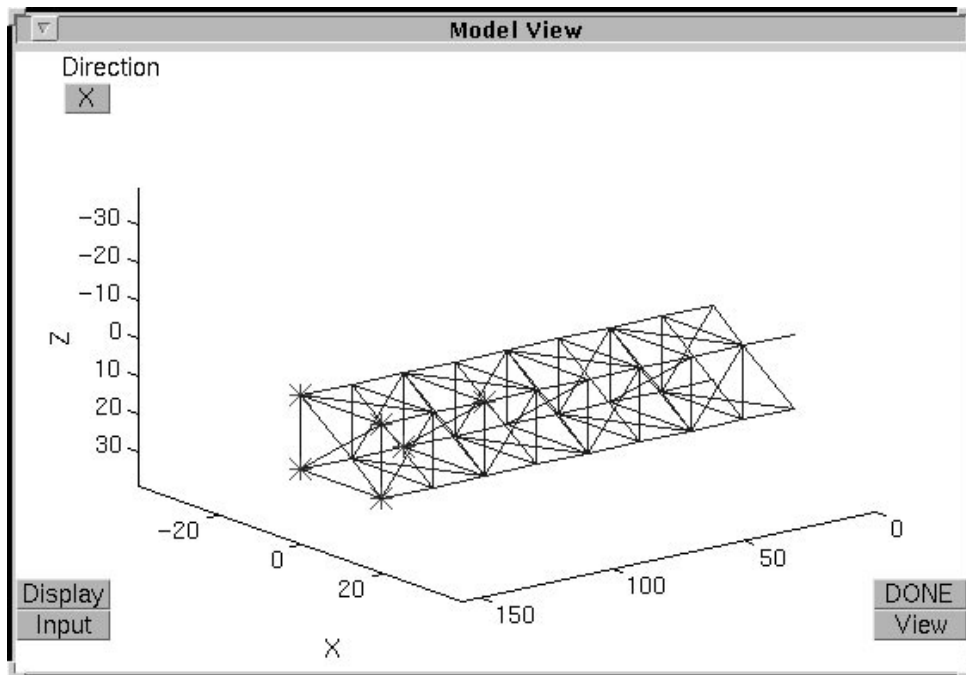


Figure B.5 Sample graphical sensor selection window.

[Vis.] Produces a wire-frame drawing of the model, and includes additional buttons which allow the user to select, via the pointing device, the degrees-of-freedom to instrument. The **[Direction]** button shows the current degree-of-freedom direction (X, Y, Z, Rx, Ry, Rz) corresponding only to the degrees-of-freedom included in the model. Repeatedly depressing this button toggles through the selections. Selecting the **[Input]** button allows the user to select degrees-of-freedom by clicking (right mouse button) on the node to instrument. Nodes which are selected can be deselected in a similar fashion. All selected nodes for the current degree-of-freedom direction are highlighted. The selection process is terminated by making the final selection with the left mouse button. The **[View]** button initiates the 3-D viewer, used to rotate the wire frame for ease of node selection. The **[DONE]** button terminates the **[Vis]** command. A typical screen display is depicted in Figure B.5. The 3-D viewer is shown in Figure B.6.

[Sens. Anal.] Initiates the sensitivity analysis for damage detectability and damage localization. This feature is described in Section B.3.

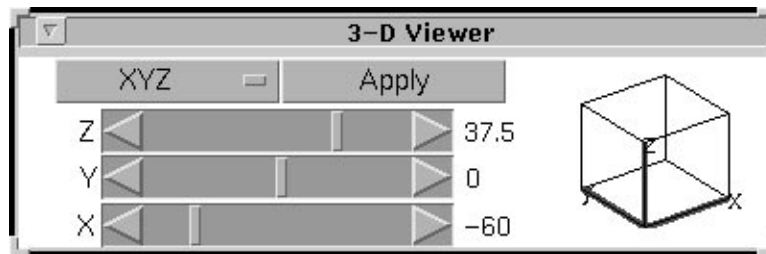


Figure B.6 Sample 3-D view selection control.

[Tol.] Initiates the tolerance menu containing the tolerance values for sensor prioritization, damage detectability, damage localization, and the APE method. The tolerance menu is depicted in Figure B.7.

[APE.] Performs the APE method for the search space defined in **[Man]** using the current tolerance values. Graphical results obtained using APE are described in section B.4.

[Els.] Opens a dialogue box which allows the user to key in element numbers. Depressing the **[SHOW]** button displays the keyed in elements on the wire-frame model in red.

[Close.] Terminates the software package.

B.1 System Identification

Identification of modal parameters from measured frequency response functions is fully automated using the apeware package. The process is initiated by depressing the **[ERA]** button from the main control panel, which displays the ERA control panel as shown in Figure B.8. If the measured transfer functions are not included in the model file, they can be loaded into the workspace either from the command line or through the **[LOAD]** button on the main control panel. Information on how the data was recorded, (sample rate, number of sample points, etc.) should be keyed in using the **[ERA specs]** button, which initiates the parameters control panel as shown in Figure B.9. An explanation on each parameter is obtained by depressing the **[HELP]** button. After setting the ERA parameters, the ERA method, including the inverse Fourier transforms to obtain the time domain data, is performed by depressing the **[ERA]** button. The state-space identified quadruple is contained in the workspace in the variables (aera,bera,cera,dera), in either continuous or discrete form as determined by the setting in the ERA parameters panel. If desired, a display of the singular values of the block Hankel matrix is

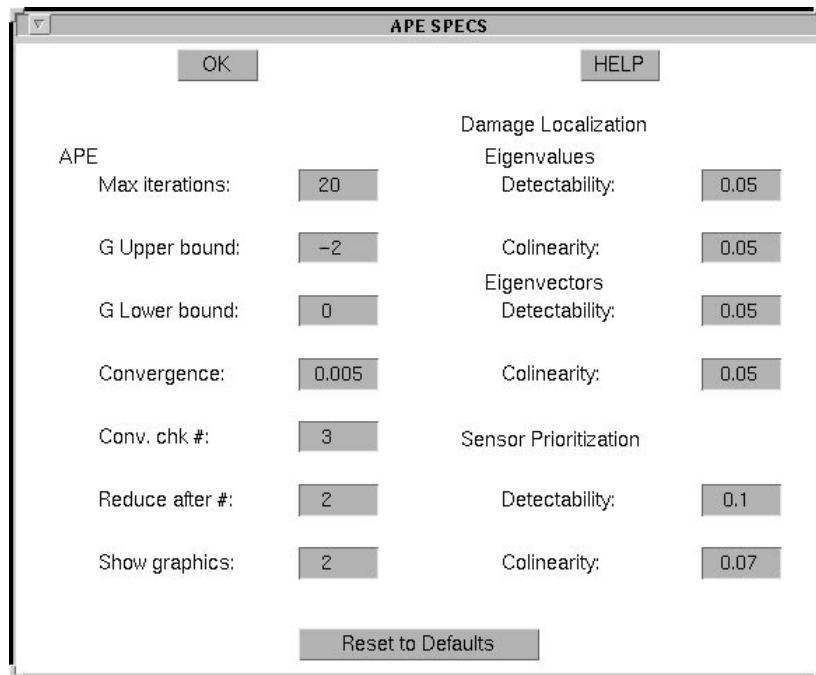


Figure B.7 Tolerance menu.

provided to allow the user to select the number of singular values to retain, using the pointing device. Simulated frequency response functions of the identified state-space quadruple can be computed and displayed according to the value entered in the **[plot fit]** parameter box. A comparison of a simulated frequency response function(s) of the identified model can then be obtained and displayed, as shown in Figure B.11. An additional option to include a low-pass filter on the measured data is also incorporated.

The extraction of the modal parameters (frequencies and shapes) from the measured data is performed using the **[Extract]** button. The resulting control screen is shown in Figure B.12. Modes are selected by using the pointing device to click on a modal peak in the displayed frequency response function(s). The eigenvalue of the model corresponding to the closest mouse pick is automatically determined, along with the partial eigenvector for this mode. The selected partial mode shape is displayed along with a polar plot indicating the phase of the identified eigenvector. When used on measured data of structures with minimal structural damping, the phase of the eigenvectors should lie along the abscissa (corresponding to real eigenvectors). The polar plot is used as a check on the identified eigenvector. If the phase is scattered off the abscissa, the mode was poorly identified. Each identified eigenvalue and eigenvector must be assigned a mode number. The software automatically

compares the identified partial eigenvector with the stored eigenvectors of the analytical model. A figure-of-merit (FOM) is listed on the display screen along with the mode number of the analytical model with the highest FOM. The FOM is a measure of the colinearity, with a maximum value for perfect colinearity at unity. Depressing the [**Store**] button saves the identified eigenvalue/eigenvector pair for future use. The mode numbers can be changed by changing the entry in the displayed mode number box. This pairing of the identified and analytical modes is performed to account for mode swaps occurring in the damaged structure. Note that when using only partial eigenvectors, no guarantee is made that the highest FOM corresponds to the correct mode number, and thus care must be exercised when assigning mode numbers. The [**Clear modes**] button can be used to clear the previously stored modes from the workspace. The currently stored modes are listed on the display screen, and is updated after each store operation. The mode selection process is repeated by depressing the [**Select again**] button for each mode desired. The [**Zoom**] button can be used to help the selection of closely spaced frequency peaks. A green circle is displayed on each peak selected to aid in the identification process. Modal peaks can be selected from any frequency response function. Because the frequency functions are all based on the same ERA identified model, they all contain the same modal information. However, some modes may not be visible from the selected transfer function. Different transfer functions are selected by changing the [**Input**] and [**Output**] numbers on the ERA control menu. Multiple transfer functions can be displayed by including several combinations in the Input/Output boxes. The [**clear**] button is used to clear the plotting window.

B.2 Model Tuning

Model tuning is performed using ASTROS-ID, a software package independent of the apeware package. ASTROS-ID however lacks a graphical pre and post-processor. Apeware partially accommodates this deficiency by providing an easy to use graphical interface to display deformed geometries and animate mode shapes. This information is useful in classifying mode shapes and correlating analytical and measured mode shapes. This feature is initiated using the [**Anim**] button (animation) on the main control panel. The mode view control panel is depicted in Figure B.13. Several types of displayed results are possible. Deformed geometries using the wire-frame model can be displayed for any stored mode, from either the analytical data as in Figure B.14, measured data, or both. Additionally, mode shapes can be animated at fifteen frames per second to aid in the classification process. Alternatively,

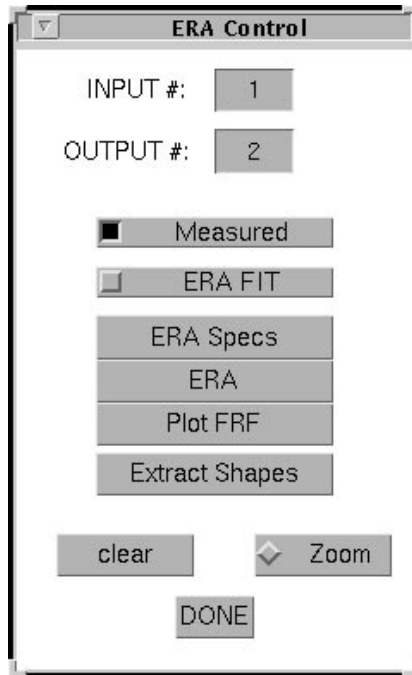


Figure B.8 ERA control menu.

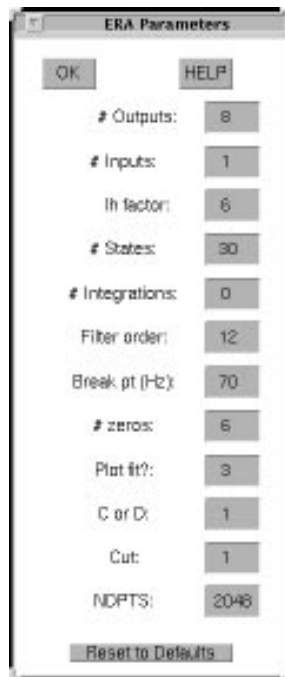


Figure B.9 ERA parameters control panel.

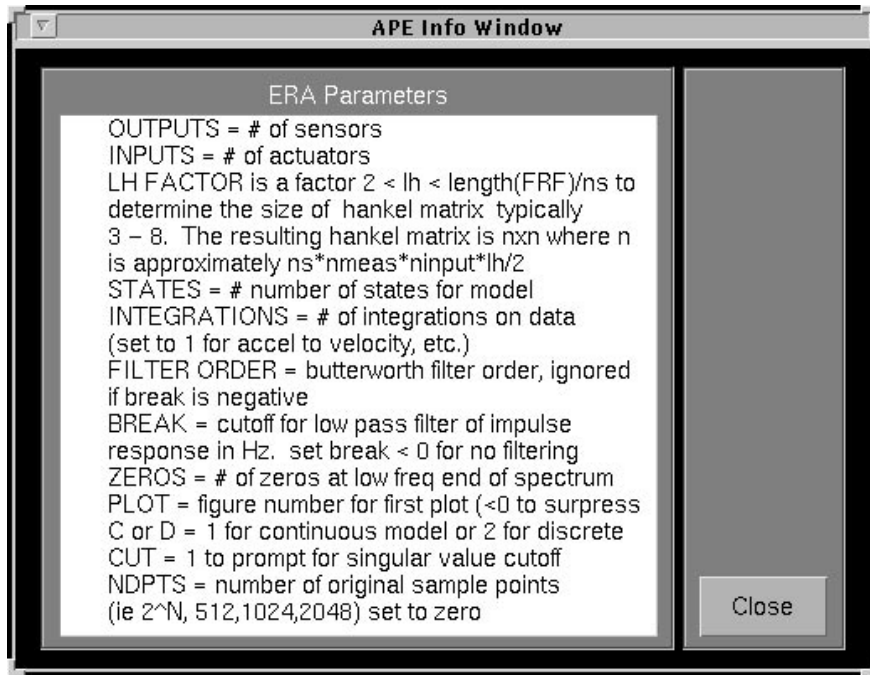


Figure B.10 ERA help menu dialogue box.

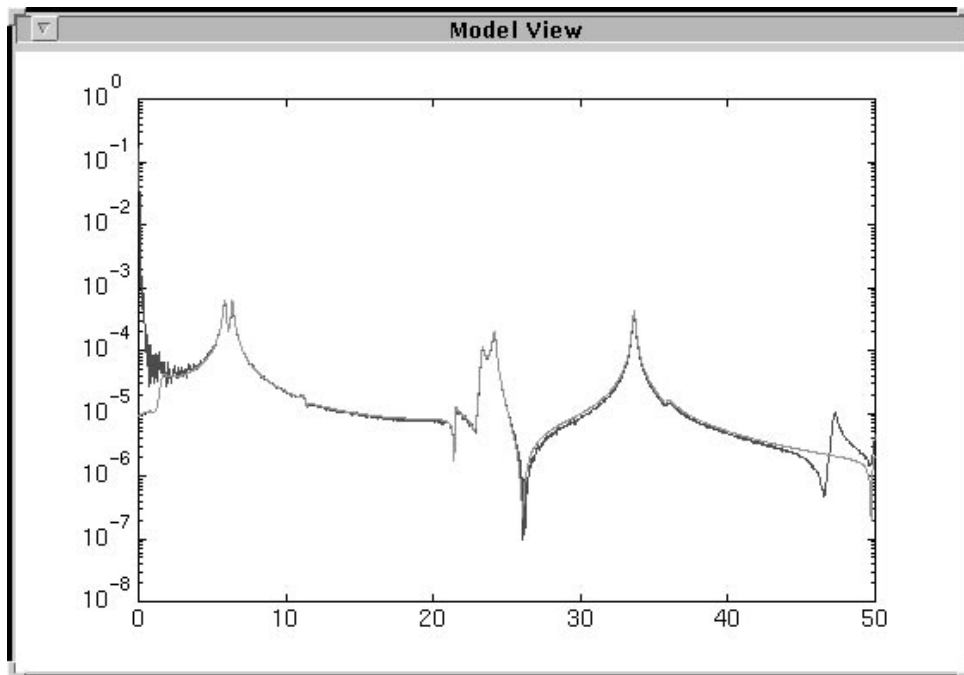


Figure B.11 Sample frequency response showing measured data and simulated data from an ERA identified model.

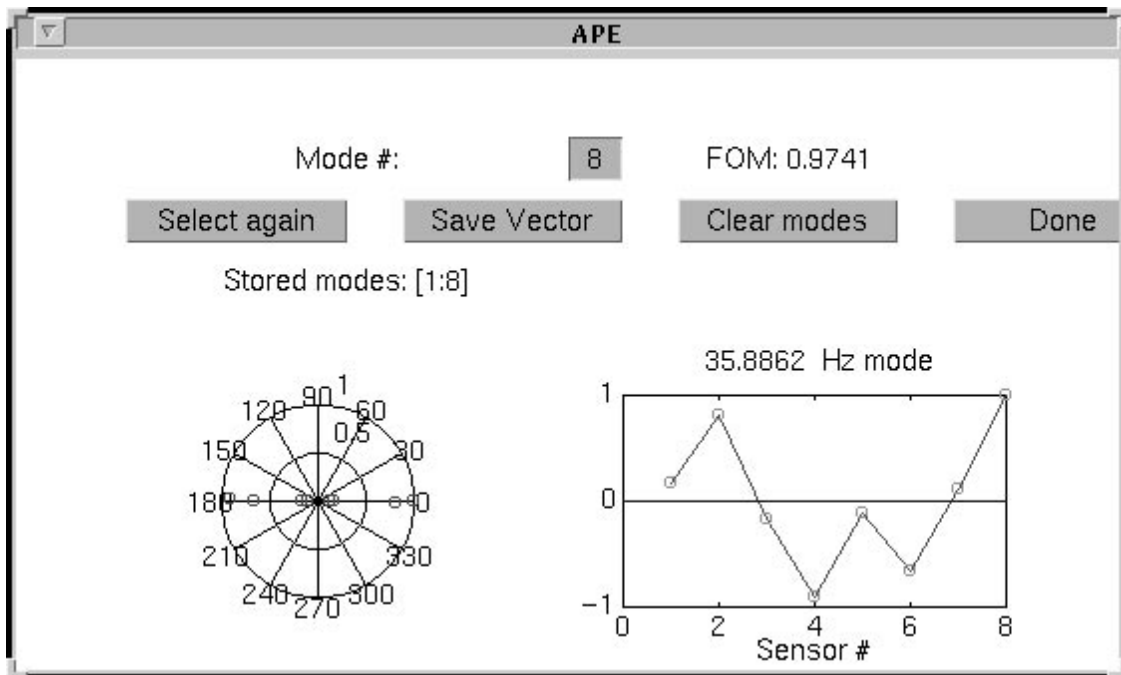


Figure B.12 Control panel to extract measured modes.

the mode shapes can be viewed using a line plot format, using either the full length eigenvectors as in Figure B.16, or the partial eigenvectors corresponding to the instrumented degrees-of-freedom as in Figure B.15. Vector normalization and sign convention are automatically accounted for in the displayed results.

Interactive compiled FORTRAN routines (**db2mate**, **db2xyz**, **db2dvs**) can be used to extract the eigenvalues and eigenvectors, the finite element model, and the tuned design variables from the ASTROS data base. The results are stored in MATLAB[®] binary format for use with apeware. Additionally, the MATLAB[®] routines **wrtshape** and **wrtfreq** can be used to generate the TSHAPE and TFREQ data cards from the identified data, for use in ASTROS-ID.

B.3 Sensitivity Analysis

The sensitivity analysis is performed using the stored analytical model. The analysis is performed on the modes keyed in using the **[Man]** button on the main control panel. Parameters for both the damage localization and the sensor prioritization are determined from the keyed in entries on the tolerance menu obtained using the **[Tol]** button. The sensor prioritization is performed by depressing

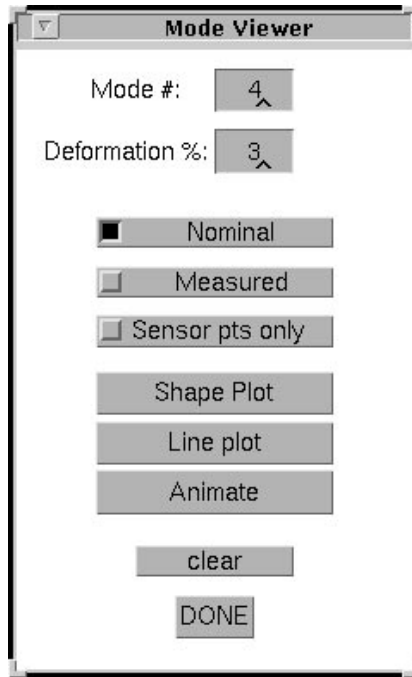


Figure B.13 Mode viewer control panel.

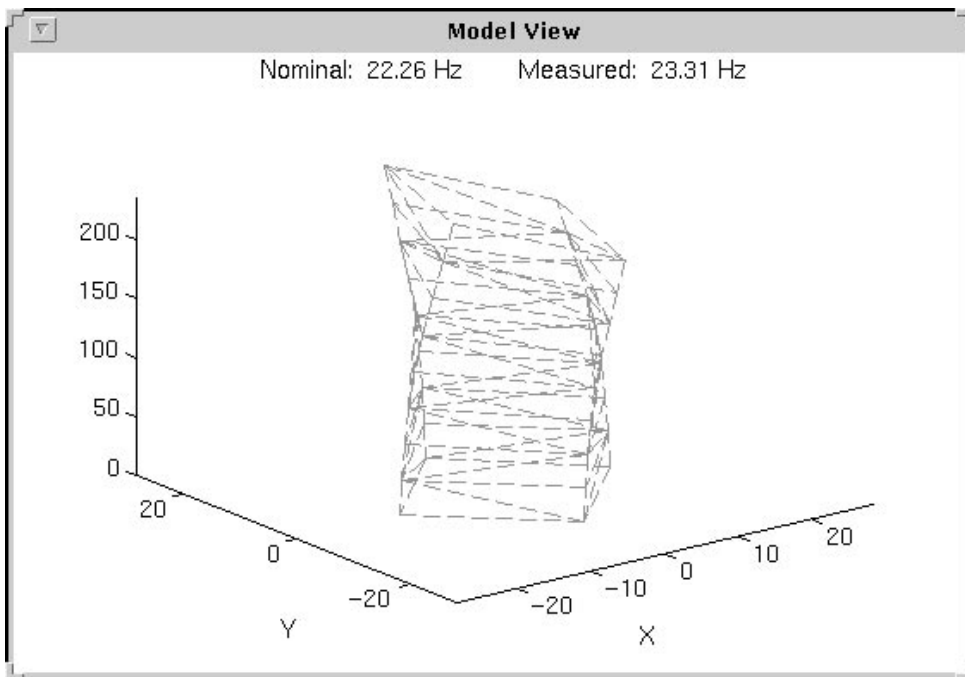


Figure B.14 Sample display of deformed geometry.

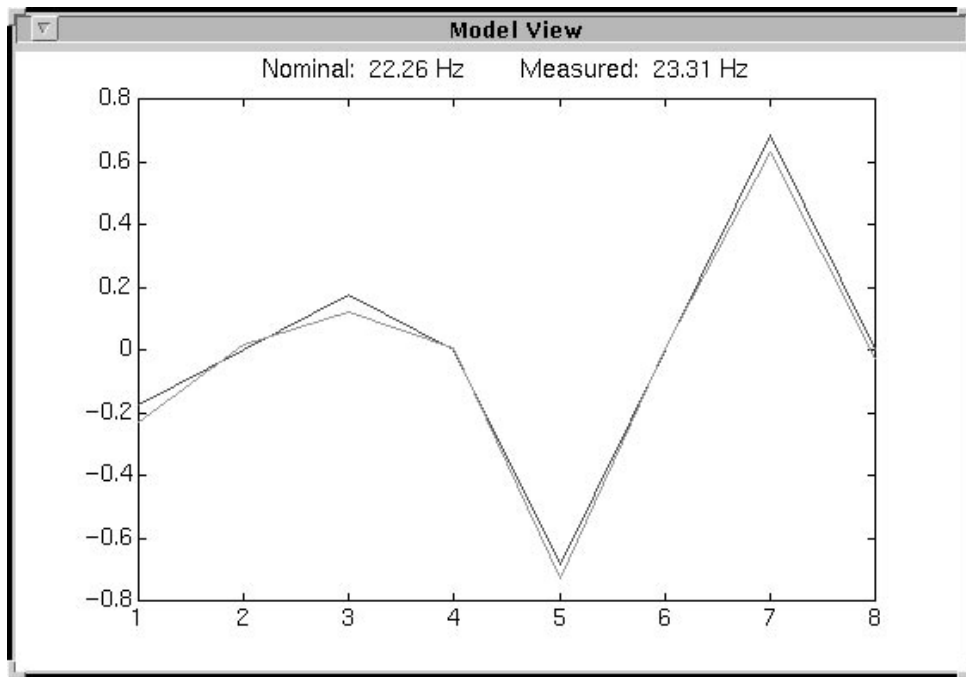


Figure B.15 Sample line plot of a partial measured eigenvector corresponding to the sensor points only.

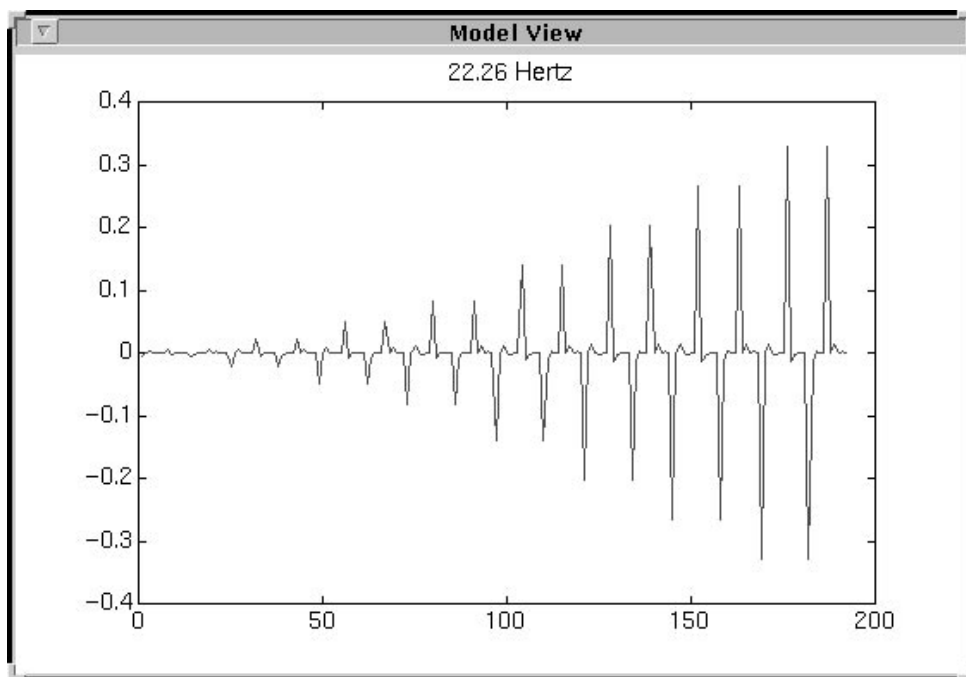


Figure B.16 Sample line plot of a full eigenvector.

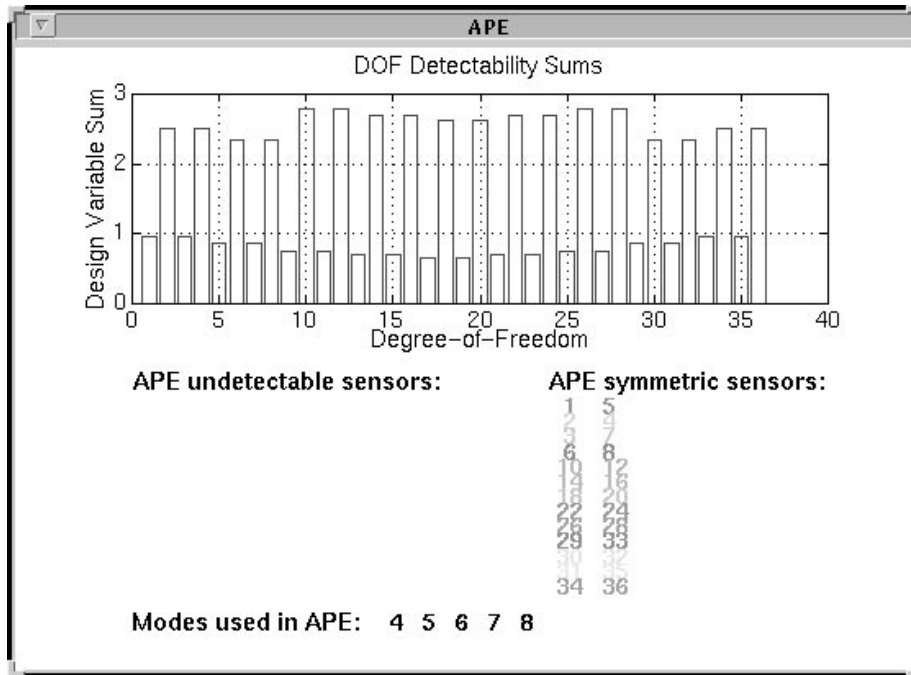


Figure B.17 Sample sensor location gradient information.

the **[Opt. Sens.]** button. The results of the sensor prioritization are shown in two separate display windows. The first is the gradient information, depicting the values of D_ϕ for each sensor location as shown in Figure B.17. Also listed are the degrees-of-freedom with values of D_ϕ below the detectability threshold level, and degrees-of-freedom within the colinearity S_ϕ threshold level. A second figure lists the prioritized locations in order, starting from the upper left, as shown in Figure B.18.

Damage localization is performed by depressing the **[Sens. Anal.]** button on the main control panel. The results are displayed in two separate figures. Eigenvalue and eigenvector gradient information contained in D_λ and D_ϕ is displayed as shown in Figure B.19. The colinearity analysis results are displayed as shown in Figure B.20, which lists the symmetric elements as well as the undetectable elements. Element numbers are color coded, with each symmetric set assigned to a distinct color. For reference, a wire-frame model is also displayed with the elements color coded according to the displayed information. Bright green elements are classified as undetectable and white elements correspond to elements which can be uniquely identified.



Figure B.18 Sample sensor location prioritized list.

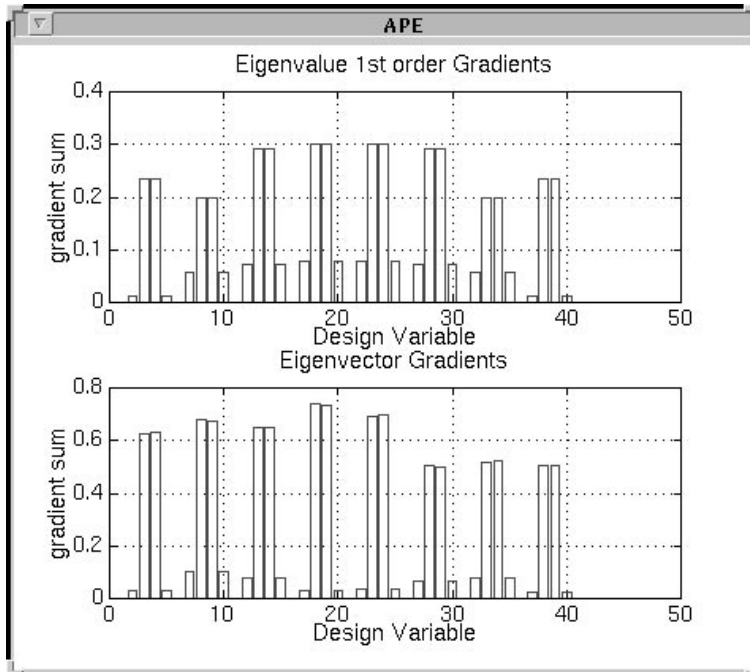


Figure B.19 Sample damage localization gradient results.

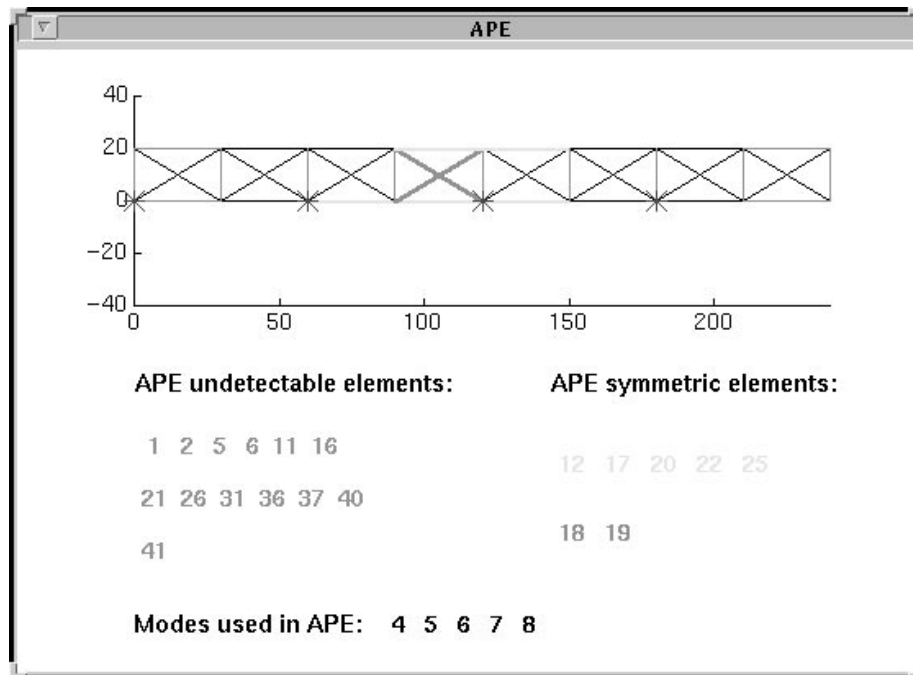


Figure B.20 Sample damage localization analysis results.

B.4 Damage Identification

Damage identification using APE is performed using the **[APE]** button on the main control panel. The APE iteration proceeds according to the parameters set in the tolerance menu as shown in Figure B.7. The iteration tolerance values are explained using the **[HELP]** button. The numerical results of the APE method are displayed as shown in Figure B.21. If the **[show graphics]** box is set to 1, the results are also shown in graphical format as depicted in Figure B.22, with the identified damaged elements color coded according to the percent damage identified. If **[show graphics]** is set to 2, the intermediate results for each iteration step are displayed.

B.5 Model File Requirements

The following is a list of variables and their descriptions, which must be contained in a MATLAB[®] binary file. This file must be loaded into the workspace after initiating the apeware program. The existing workspace is purged when the program is initiated. Note also that MATLAB[®] is case sensitive.

Ape Results		
Element #	% Damage	Symmetric with
7	50.08	
18	30.02	19

Figure B.21 Sample damage identification numerical results.

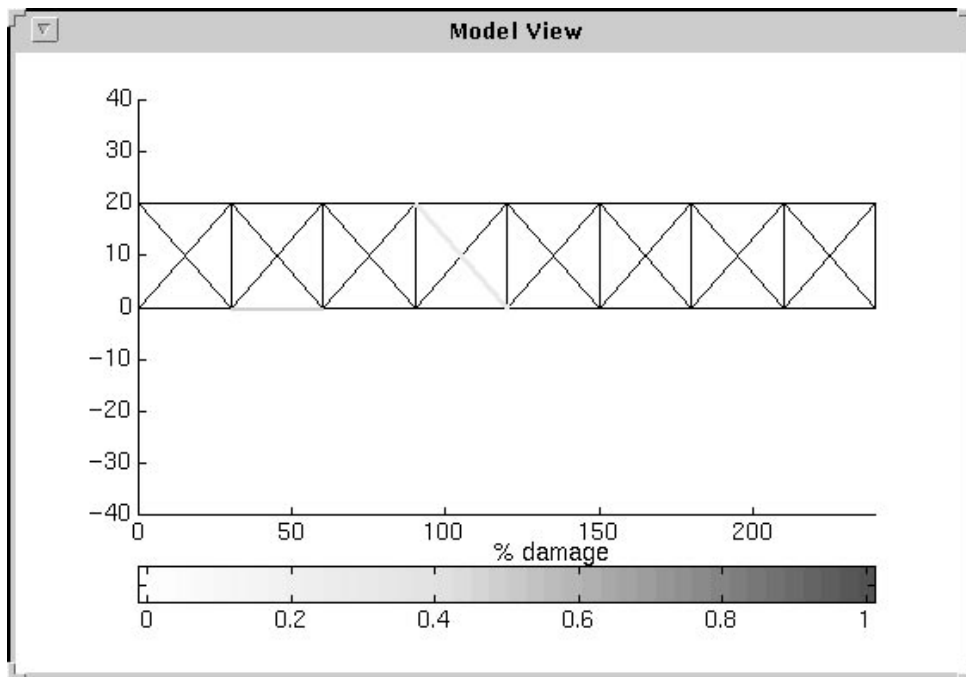


Figure B.22 Sample damage identification graphical results.

1. M Finite element mass matrix.
2. K Finite element stiffness matrix.
3. C Identity matrix the size of M .
4. **eol** Sorted eigenvalues of M, K .
5. **vol** Sorted eigenvectors of M, K .
6. B Matrix as defined in Equation (6.10) or (6.13) such that $K_i = B_i B_i^T$.
7. **nb** Number of columns in B corresponding to a single element (scalar).
8. **DOFTYPE** Number of degrees of freedom per node (scalar).
9. **xyz** Matrix containing the grid point coordinates, one (x,y,z) triplet for each node. Matrix size is (# of nodes x 3).
10. **con** Matrix whose i^{th} row points to the row of grid points in **xyz** for the i^{th} element. Matrix size is (# of elements x 2).
11. **CONINDEX** Vector which points to rows in **con** that have columns in B (# of design variables).
12. **connodes** Vector listing nodes which are constrained.
13. **DOFSTR** String vector of degree-of-freedom labels, ('X', 'Y', 'Z', 'Rx', 'Ry', 'Rz'), used in the model.

B.5.1 Utilities. To aid in construction of some of the model file requirements, the following utilities are available.

1. **db2mate** Executable routine to extract the mass, stiffness, circular frequencies, and eigenvectors from an ASTROS data base.
2. **db2xyz** Executable routine to extract the **xyz** and **con** matrices from an ASTROS data base.
3. **db2dvs** Executable routine to extract the tuned design variables and elemental properties from an ASTROS data base.

4. **bildbeam** MATLAB[®].m file to construct the B matrix for beam elements from the elemental properties.
5. **bildrod** MATLAB[®].m file to construct the B matrix for rod elements from the elemental properties.
6. **eigsrt** MATLAB[®].m file to construct the sorted eigenvalue (**eol**) and eigenvectors (**vol**) matrices from M and K .

Bibliography

1. Akers, J. C. and D. S. Bernstein. "Measurement Noise Error Bounds for Eigensystem Realization Algorithm." In *The 36th Structures, Structural Dynamics, and Materials Conference*, pages 1198–1208, AIAA, 1995.
2. Alfriend, K. T. and D. L. Lewis. "Estimation of the Low Earth Orbit Space Object Population Using a Non-Vertical Staring Radar." In *First European Conference on Space Debris*, pages 329–336, 1993.
3. Alvin, K.F. and K.C. Park. "A Second-Order Structural Identification Procedure Via State-Space Based System Identification." In *AIAA Guidance, Navigation, and Control Conference*, pages 1600–1611, AIAA, 1992.
4. Andry, A.N. and others. "Eigenstructure Assignment for Linear Systems," *IEEE Transactions on Aerospace and Electronic Systems*, 19(5):711–728 (September 1983).
5. Baruch, M. "Optimal Correction of Mass and Stiffness Matrices Using Measured Modes," *AIAA Journal*, 20(11):1623–1626 (November 1982).
6. Baruch, M. and I.Y. Bar Itzhack. "Optimal Weighted Orthogonalization of Measured Modes," *AIAA Journal*, 16(4):346–351 (1978).
7. Berman, A. and E.J. Nagy. "Improvement of a Large Analytical Model Using Test Data," *AIAA Journal*, 21(8):1168–1173 (August 1983).
8. Brock, J.E. "Optimal Matrices Describing Linear Systems," *AIAA Journal*, 6(7):1292–1296 (1968).
9. Chen, J.C. and J.A. Garba. "Analytical Model Improvement Using Modal Test Results," *AIAA Journal*, 18:684 (June 1980).
10. Chen, J.C. and J.A. Garba. "On-Orbit Damage Assessment for Large Space Structures," *AIAA Journal*, 26(9):1119–1126 (1988).
11. Cobb, R. G., R. A. Canfield and B. S. Liebst. "Finite Element Model Tuning Using Automated Structural Optimization System Software," *AIAA Journal*, 34(2):392–399 (February 1996).
12. Crassidis, J.L. and others. "Robust Identification and Vibration Suppression of a Flexible Structure." In *AIAA Guidance, Navigation, and Control Conference*, pages 1560–1570, AIAA, 1993.
13. "Design Optimization Tools." VMA Engineering, Version 4.00, 1994.
14. Doebling, S.W. and others. "Selection of Experimental Modal Data sets for Damage Detection Via Model Update." In *The 34th Structures, Structural Dynamics, and Materials Conference*, pages 1506–1517, AIAA, 1993.
15. Fainakis, Y.E. and others. "Computing Bounds for a Simple Fault Detection Scheme," *American Control Conference*, 3:2638–2642 (July 1994).
16. Fox, R.L. and M.P. Kapoor. "Rates of Change of Eigenvalues and Eigenvectors," *AIAA Journal*, 6(12):2426–2429 (December 1968).
17. Franklin, G. F., et al. *Digital Control of Dynamic Systems* (Second Edition). Addison–Wesley, 1990.

18. Gibson, W. C. "ASTROS-ID: Software for System Identification Using Mathematical Programming," *WL-TR-91-3101* (September 1992).
19. Golub, G.H. and C.F. Van Loan. *Matrix Computations* (First Edition). Maryland: The John Hopkins University Press, 1983.
20. Gordon, R. W. "The Twelve-Meter Truss Active Control Experiment Design, Analysis & Open Loop Testing," *WL-TR-92-3012* (April 1992).
21. Grossman, D.T. "An Automated Technique for Improving Modal Test/Analysis Correlation," *AIAA Paper*, 82-0604 (May 1982).
22. Gustafson, J.A. and P.S. Maybeck. "Control of a Large Flexible Space Structure with Moving-Bank Multiple Model Adaptive Algorithms." In *Proceedings of the IEEE Conference on Decision and Control*, pages 1273–1278, 1992.
23. Haftka, R. T. and Z. Gurdal. *Elements of Structural Optimization* (Third Edition). Kluwer Academic Publishers, 1992.
24. Hemez, F. and C. Farhat. "Locating and Identifying Structural Damage Using a Sensitivity-Based Model Updating Methodology." In *The 34th Structures, Structural Dynamics, and Materials Conference*, pages 2641–2653, AIAA, 1993.
25. Hemez, F. and C. Farhat. "Comparing Mode Shape Expansion Methods for Test-Analysis Correlation." In *12th International Modal Analysis Conference*, pages 1560–1567, 1994.
26. Hollkamp, J.J. "Multi-Input, Multi-Output Time-Series Models from Short Data Records," *AIAA Journal of Guidance, Control, and Dynamics*, 16(3):549–556 (June 1993).
27. "International Space Station Alpha." Retrieved from world wide web site: <http://integra.jsc.nasa.gov/WWW/Images>.
28. "International Space Station Alpha's solar array sub-assembly." Retrieved from world wide web site: <http://integra.jsc.nasa.gov/WWW/Images/Parts>.
29. Imregun, M. and D. J. Ewins. "An Investigation into Mode Shape Expansion Techniques." In *11th International Modal Analysis Conference*, pages 168–175, 1994.
30. Isermann, R. "Process Fault Detection Based on Modeling and Estimation Methods- A Survey," *Automatica*, 20(4):387–404 (1984).
31. Isermann, R. "Robust Fault Detection: the Effect of Model Error," *American Control Conference*, pages 1094–1096 (June 1989).
32. Juang, J. and R.S. Pappa. "An Eigensystem Realization Algorithm for Modal Parameter Identification and Model Reduction," *AIAA Journal of Guidance, Control, and Dynamics*, 8(5):620–627 (1985).
33. Juang, J. and R.S. Pappa. "Effects of Noise on Modal Parameters Identified by the Eigensystem Realization Algorithm," *AIAA Journal of Guidance, Control, and Dynamics*, 9(3):294–303 (1986).
34. Juang, J.N. and M. Phan. "Linear System Identification via Backward-time Observer Models," *NASA TM-107632* (May 1992).
35. Kabe, A. "Stiffness Matrix Adjustment Using Mode Data," *AIAA Journal*, 23(9):1431–1436 (September 1985).

36. Kammer, D. C. "Sensor Placement for On-Orbit Modal Identification and Correlation of Large Space Structures," *AIAA Journal of Guidance, Control, and Dynamics*, 14(9):251–259 (1991).
37. Kammer, Daniel C. "Optimum Approximation for Residual Stiffness in Linear System Identification," *AIAA Journal*, 26(1):104–112 (1988).
38. Kaouk, M. and D. C. Zimmerman. "Evaluation of the Minimum Rank Update in Damage Detection: An Experimental Study." In *11th International Modal Analysis Conference*, pages 1061–1068, 1994.
39. Kaouk, M. and D.C. Zimmerman. "Structural Damage Assesment Using Generalized Minimum Rank Perturbation Theory." In *The 34th Structures, Structural Dynamics, and Materials Conference*, pages 1529–1538, AIAA, 1993.
40. Kashangaki, T. "Ground Vibration Tests of a High Fidelity Truss for Verification of On Orbit Damage Location Techniques," *NASA-TM-107626* (May 1992).
41. Kashangaki, T. "Mode Selection for Damage Detection Using the Modal Sensitivity Parameter." In *The 33rd Structures, Structural Dynamics, and Materials Conference*, pages 1535–1542, AIAA, 1995.
42. Kashangaki, T. and others. "Underlying Modal Data Issues for Detecting Damage in Truss Structures." In *The 33rd Structures, Structural Dynamics, and Materials Conference*, pages 1437–1446, AIAA, 1992.
43. Kim, H.M. and T.J. Bartkowicz. "Damage Detection and Health Monitoring of Large Space Structures," *Sound and Vibration*, pages 12–17 (1993).
44. Kinard, W. H. and R. L. O'Neal. "Long Duration Exposure Facility (LDEF) Results," *AIAA Paper, 91-0096* (January 1991).
45. Liebst, B.S. and W.L. Garrard. "Application of Eigenspace Techniques to Design of Aircraft Control Systems," *Proceedings of the American Control Conference*, 1:475–480 (June 1985).
46. Lim, K. B. "A Method for Optimal Actuator and Sensor Placement for Large Flexible Space Structures." In *AIAA Guidance, Navigation, and Control Conference*, pages 1352–1356, AIAA, 1990.
47. Lindner, D.K. and others. "Damage Detection, Location, and Estimation for Large Truss Structures." In *The 34th Structures, Structural Dynamics, and Materials Conference*, pages 1539–1548, AIAA, 1993.
48. Liu, C. and F. A. Tasker. "Sensor Placement for Multi-Input Multi-Output Dynamic Identification." In *The 36th Structures, Structural Dynamics, and Materials Conference*, pages 3327–3337, AIAA, 1995.
49. Ljung, L. *System Identification, Theory for the User* (Second Edition). New York: John Wiley & Sons, 1990.
50. Ljung, L. and T. Glad. *Modeling of Dynamic Systems*. New Jersey: Prentice-Hall, 1994.
51. Lou, X. and R. V. Grandhi. "ASTROS for Reliability-based Multidisciplinary Structural Analysis and Optimization," *The 36th Structures, Structural Dynamics, and Materials Conference*, pages 93–102 (1995).

52. "MATLAB[®]: High Performance Numeric Computation and Visualization Software." The Math Works, Inc., Natick MA, 1994.
53. Maybeck, P.S. *Stochastic Models, Estimation and Control, Volume 2*. New York: Academic Press, 1979.
54. Mook, D.J. and J.L. Junkins. "Minimum Model Error Estimation for Poorly Modeled Dynamic Systems," *AIAA Journal of Guidance, Control, and Dynamics*, 11(3):256–261 (June 1988).
55. Neill, D. J. and E.J. Johnson and R. Canfield. "ASTROS—A Multidisciplinary Automated Structural Design Tool," *AIAA Journal of Aircraft*, 27(12):1021–1027 (December 1990).
56. Nelson, R.B. "Simplified Calculation of Eigenvector Derivatives," *AIAA Journal*, 14(9):1201–1205 (September 1976).
57. Newland, D.E. *An Introduction to Random Vibrations and Spectral Analysis* (Second Edition). New York: Longman Inc., 1984.
58. Niell, D.J. and D.L. Herendeen. "ASTROS User's Manual," *WL-TR-93-3025* (March 1993).
59. Ojalvo, I.U. and D. Pilon. "Diagnostics for Geometrically Locating Structural Math Model Errors From Modal Test Data." In *The 29th Structures, Structural Dynamics, and Materials Conference*, pages 1174–1186, AIAA, 1988.
60. Peterson, L.D. and others. "Damage Detection Using Experimentally Measured Mass and Stiffness Matrices." In *The 34th Structures, Structural Dynamics, and Materials Conference*, pages 1518–1528, AIAA, 1993.
61. Plaut, R.H. and K. Huseyin. "Derivatives of Eigenvalues and Eigenvectors in Non-Self-Adjoint Systems," *AIAA Journal*, 11(2):250–251 (February 1973).
62. Reid, J.G. *Linear System Fundamentals, Continuous and Discrete, Classic and Modern*. New York: McGraw Hill, 1983.
63. Roy, N. A., et al. "Expansion of Experimental Mode Shapes - An Improvement of the Projection Technique." In *11th International Modal Analysis Conference*, pages 152–158, 1994.
64. Smith, S.W. and C.A. Beattie. "Secant-Method Adjustment for Structural Models," *AIAA Journal*, 29(1):119–126 (1991).
65. Srinathkumar, S. "Eigenvalue/Eigenvector Assignment Using Output Feedback," *IEEE Transactions on Automatic Control*, 23(1):79–81 (1978).
66. Stiles, P.A. and J.B. Kosmatka. "Comparison of Model Refinement Techniques." In *The 30th Structures, Structural Dynamics and Materials Conference*, pages 1052–1061, AIAA, 1989.
67. Venkayya, V. B. "Optimality Criteria: A Basis for Multidisciplinary Optimization," *Computational Mechanics*, 5:1–21 (1989).
68. Willsky, A.S. "A Survey of Design Methods for Failure Detection in Dynamic Systems," *Automatica*, 12:601–611 (1976).
69. Woods, R. D., B. S. Liebst and R. G. Cobb. "A State-Space Model of a Large, Lightly Damped Space Structure." In *AIAA Guidance, Navigation, and Control Conference*, pages 345–355, AIAA, 1995.
70. Zimmerman, D.C. and M. Widengren. "Correcting Finite Element Models Using a Symmetric Eigenstructure Assignment Technique," *AIAA Journal*, 28(9):1670–1676 (September 1990).

Vita

Captain Richard G. Cobb [REDACTED]. He enlisted in the Air Force in September 1981. While serving as a weapons control system specialist on F4-D aircraft at Homestead AFB, he was selected for the Airman Education and Commissioning Program. He graduated top of his class from the Pennsylvania State University's Aerospace Engineering Department in May, 1988. After commissioning, he served as the Global Positioning System's (GPS) launch operations officer at Cape Canaveral AFS where he managed daily operations leading to the successful launch of the first ten Block II GPS satellites. Captain Cobb entered the Air Force Institute of Technology (AFIT), Graduate School of Engineering in June 1991. He was a distinguished graduate and earned a Master of Science degree in Astronautical Engineering. Captain Cobb remained at AFIT to begin the Doctoral program in January 1992. He married Lisa Cordeiro in September of 1982, and has two sons, Gregory and Ryan.

Permanent address: [REDACTED]
[REDACTED]

REPORT DOCUMENTATION PAGE

Form Approved
OMB No. 0704-0188

Public reporting burden for this collection of information is estimated to average 1 hour per response, including the time for reviewing instructions, searching existing data sources, gathering and maintaining the data needed, and completing and reviewing the collection of information. Send comments regarding this burden estimate or any other aspect of this collection of information, including suggestions for reducing this burden, to Washington Headquarters Services, Directorate for Information Operations and Reports, 1215 Jefferson Davis Highway, Suite 1204, Arlington, VA 22202-4302, and to the Office of Management and Budget, Paperwork Reduction Project (0704-0188), Washington, DC 20503.

1. AGENCY USE ONLY (Leave blank)	2. REPORT DATE March 1996	3. REPORT TYPE AND DATES COVERED Doctoral Dissertation	
4. TITLE AND SUBTITLE STRUCTURAL DAMAGE IDENTIFICATION FROM LIMITED MEASUREMENT DATA			5. FUNDING NUMBERS
6. AUTHOR(S) Richard G. Cobb Captain, USAF			
7. PERFORMING ORGANIZATION NAME(S) AND ADDRESS(ES) Air Force Institute of Technology Wright Patterson AFB OH 45433-6583			8. PERFORMING ORGANIZATION REPORT NUMBER AFIT/DS/ENY/96-3
9. SPONSORING/MONITORING AGENCY NAME(S) AND ADDRESS(ES) Kevin Slimak PL/VTS Kirtland AFB NM 87117-5776			10. SPONSORING/MONITORING AGENCY REPORT NUMBER
11. SUPPLEMENTARY NOTES			
12a. DISTRIBUTION / AVAILABILITY STATEMENT Approved For Public Release; Distribution Unlimited			12b. DISTRIBUTION CODE
13. ABSTRACT (Maximum 200 words) A new method was developed to identify damaged structural elements from large flexible space structures on-orbit, using limited measured modal data. The research was decomposed into four specific tasks: (1) identification of partial modal properties from measured data, (2) finite element model tuning, (3) sensitivity analysis to determine sensor placement and damage localization, and (4) damage identification using an assigned partial eigenstructure method. Identification of the modal parameters was accomplished using the Eigensystem Realization Algorithm, adopted for use with averaged measured frequency response functions. Model tuning was performed using ASTROS-ID software. Sensor prioritization and damage localization was performed using an eigenvalue and eigenvector sensitivity based approach. Damage identification was performed using an assigned partial eigenstructure method, which determines required stiffness changes consistent with the finite element formulation to achieve the measured data. Two experimental demonstrations were performed and the results reported. The research showed that in each test case, the structural damage could successfully be localized to a small portion of the structure with relatively low cpu requirements. The extent to which damage can be localized was limited by both model fidelity and accuracy of the measured modes.			
14. SUBJECT TERMS Large Flexible Space Structures, Damage Identification, System Identification, Model Tuning, Eigenstructure Assignment, Sensor Determination			15. NUMBER OF PAGES 149
			16. PRICE CODE
17. SECURITY CLASSIFICATION OF REPORT UNCLASSIFIED	18. SECURITY CLASSIFICATION OF THIS PAGE UNCLASSIFIED	19. SECURITY CLASSIFICATION OF ABSTRACT UNCLASSIFIED	20. LIMITATION OF ABSTRACT UL